

UNIVERSITY OF NAPLES “FEDERICO II”
DEPARTMENT OF AGRICULTURAL SCIENCE



Doctor of Philosophy in “Agricultural and Food Science”
(XXIX cycle)

Exploitation of Lignocellulosic Biowastes in the Production of Bio-Composites

Tutors

Prof. Alessandro Piccolo

Dr. Gennaro Scarinzi

Candidate

Stefania Angelini

Portici, 2016/2017

Vola alto o in basso,
veloce o piano,
sul mare o sulla
terra... ma
sempre e solo con
le tue ali.

Vola alto o in basso, veloce o piano,
sul mare o sulla terra...
ma sempre e solo con le tue ali.”

[“Fly up or down, fast or slowly,
on the sea or on land...
but always and only with your wings”].

Cosimo Angelini

Contents

Page

ABSTRACT	i
INTRODUCTION	1
Plant cell wall	1
Lignocellulosic Biomass	2
Exploitation of Lignocellulosic Biomass	6
Synthetic Composites with Man-Made Fillers or Lignocellulosic Biowastes.....	9
Bio-Composites Containing Man-Made Fillers or Lignocellulosic Biowastes	11
Lignocellulosic-Based Composites and Blends Applications	14
Aim of the Thesis	16
Publications	18
References	19

CHAPTER 1

Lignocellulosic Biomass from Biorefinery

Prologue.....	27
1.1 Experimental Section	27
1.1.1 Materials.....	27
1.1.2 Methods of Characterization	28
1.2 Results and Discussions	29
1.2.1 Morphological, Chemical and Thermal Characterization of Lignocellulosic Biomass	29
1.3 Conclusions	33
References	35

CHAPTER 2

Poly(3-hydroxybutyrate)/Lignocellulosic Biomass Blends and Bio-Composites

Prologue.....	36
2.1 Experimental Section	36
2.1.1 Materials.....	36
2.1.2 Methods of Preparation and Characterization.....	36
2.2 Results and Discussions	40
2.2.1 Processability and Thermal Properties of PHB and PHB-based Blends ...	40
2.2.2 Morphological, Chemical and Mechanical Characterization of PHB and PHB-based Bio-Composites	47
2.2.3 Soil Degradation of PHB and PHB-based Bio-Composites	51
2.3 Conclusions	53
References	55

CHAPTER 3

Extraction and Fractionation of Lignocellulosic Biomass

Prologue.....	57
3.1 Experimental Section	57
3.1.1 Materials.....	57
3.1.2 Methods of Characterization	58
3.2 Results and Discussions	60
3.2.1 Morphological, Chemical and Thermal Characterization of Lignocellulosic Biomass Derivatives	60
3.3 Conclusions	67
References	70

CHAPTER 4

Poly(3-hydroxybutyrate)/Lignocellulosic Derivatives Blends and Bio-Composites

Prologue.....	72
---------------	----

4.1 Experimental Section	72
4.1.1 Materials.....	72
4.1.2 Methods of Preparation and Characterization.....	73
4.2 Results and Discussions	75
4.2.1 Processability and Thermal Stability of PHB and PHB-Lignocellulosic Derivatives Blends	75
4.2.2 Crystallization of PHB and PHB-Lignocellulosic Derivatives Blends	84
4.2.3 Crystallization of PHB/Sonicated Holocellulose Bio-Composites.....	87
4.2.4 Mechanical and Morphological Characterization of PHB and PHB- Lignocellulosic Derivatives Bio-Composites	94
4.3 Conclusions	97
References	98

CHAPTER 5

Lignosulfonates from Paper Mill and Their Use in Wood Flour-Based Particleboard

Prologue.....	100
5.1 Experimental Section	100
5.1.1 Materials.....	100
5.1.2 Lignosulfonates Purification and Characterization.....	101
5.1.3 Particleboards Preparation and Characterization	101
5.2 Results and Discussion.....	103
5.2.1 Characterization of Lignosulfonates	103
5.2.2 Fire Reaction Evaluation of Wood Flour Particleboards Through Cone Calorimeter Tests	109
5.2.3 Thermal Stability.....	119
5.2.4 Mechanical Properties and Morphological Analysis	121
5.3 Conclusions	123
References	125

CONCLUSIONS AND FUTURE PERSPECTIVES	127
LIST OF FIGURES	130
LIST OF TABLES	134
RINGRAZIAMENTI	136
ACKNOWLEDGEMENTS	138

Abstract

This Ph.D. thesis deals with the exploitation of lignocellulosic industrial biowastes as potential reinforcing agents and flame retardants in sustainable polymer matrices, with the aim of obtaining bio-composites with improved properties and reduced production costs.

The work is based on two main activities, the first one involved a lignocellulosic biowaste (LC) from a second generation bioethanol production process, while lignosulfonates (LS) from pulp and paper industry were used in the second one.

In the first activity, LC was submitted to a thorough morphological, chemical and thermal characterization. Afterwards, it was used as a filler in a biodegradable microbial polymer, poly(3-hydroxybutyrate) (PHB). Blends and compression-moulded bio-composites were prepared. Their rheological, thermal, mechanical properties were studied, along with the biodegradation rate in soil.

In order to identify which of the LC components was responsible for the effects recorded on PHB properties, the biomass was further processed and fractionated to isolate its lignin and polysaccharide constituents. Acid-insoluble lignin (IL) and holocellulose (HC), along with polar and apolar extractive-free solid residues (W, TE) were obtained from the parent LC and used as fillers in PHB in order to prepare bio-based blends and composites. The rheological, thermal, mechanical and crystallization properties of the resulting materials were investigated. This study showed that the use of LC and particularly of IL and HC derivatives, produced a remarkable improvement of PHB processability and crystallization. Such outcomes were relevant in the perspective of replacing oil-based composites with bio-based materials to be exploited in agriculture or packaging.

In the second activity, waste lignosulfonates from pulping process were purified through dialysis in order to remove most of sugar contaminants. Plain and dialysed lignosulfonates were characterized through morphological, chemical and thermal analysis, then used as additives in the production of wood-flour based particleboards (WFP). Their potential fire retardant effect was investigated, and compared to reference WFP containing different amounts of a commercial flame retardant, namely ammonium polyphosphate. The flame retardancy, thermal stability and mechanical performance of the obtained WFP were studied, in order to investigate the effect of lignosulfonates along with their potential synergistic role with ammonium polyphosphate. This activity provided proof of evidence of the possibility to reduce the amount of commercial

expensive and toxic flame retardants by partially replacing them with cheap and sustainable lignocellulosic-based biowastes for applications in construction field.

Introduction

Plant cell wall

Plants are one of the few eukaryotes along with algae and fungi endowed with cell walls that are located outside the plasma membrane. Type and composition of cell wall vary according to the botanical species and developmental stage of cell.

Plant cells capable to grow and differentiate are surrounded by a polysaccharide-rich layer, referred to as primary cell wall. The primary wall is predominantly composed of polysaccharides (cellulose, hemicellulose, pectins) together with lower amounts of structural glycoproteins, phenolic esters, ionically and covalently bound minerals, and proteins with structural and enzymatic functions. Such composition confers specific properties to the cell wall, such as flexibility and extensibility [McCann, 1990]. Throughout cell growth, primary wall forms, which provides structural and mechanical support. Moreover, it helps cells to keep their shape by controlling direction and rate of growth, and to withstand the internal osmotic pressure that is several times higher than the atmospheric one. Because of its location, primary cell wall plays an important role in plant-microorganisms interactions including defence responses against potential pathogens, in the chemical intercellular communication, as well as in regulating diffusion of materials through the apoplast, that corresponds to the area between plasma membrane and plant external cuticle [Cosgrove, 2001]. Moreover, it is a polysaccharide storage structure; not surprisingly, it represents one of the edible components of food plants.

When cells stop growing, they can differentiate and adopt a well-defined role in the physiology of the plant. Differentiated cells, as tracheids and sclereids with vessel function, are surrounded by another layer referred to as secondary wall. The latter represents an adaptation of plants to live on land and get more nutrients. The secondary wall, in fact, helps water and nutrients to be transported from the bottom to the top of the plant and allows extensive upright growth [Keegstra, 2010].

The role of secondary wall is strictly dependent on its composition. Apart from minor components, it is characterized by three structural macromolecules, cellulose, lignin and hemicelluloses, that collectively are called lignocellulosic biomass (LB) [Sanderson, 2011]. A schematic representation of the supramolecular arrangement of LB in the plant is illustrated in Figure 1.

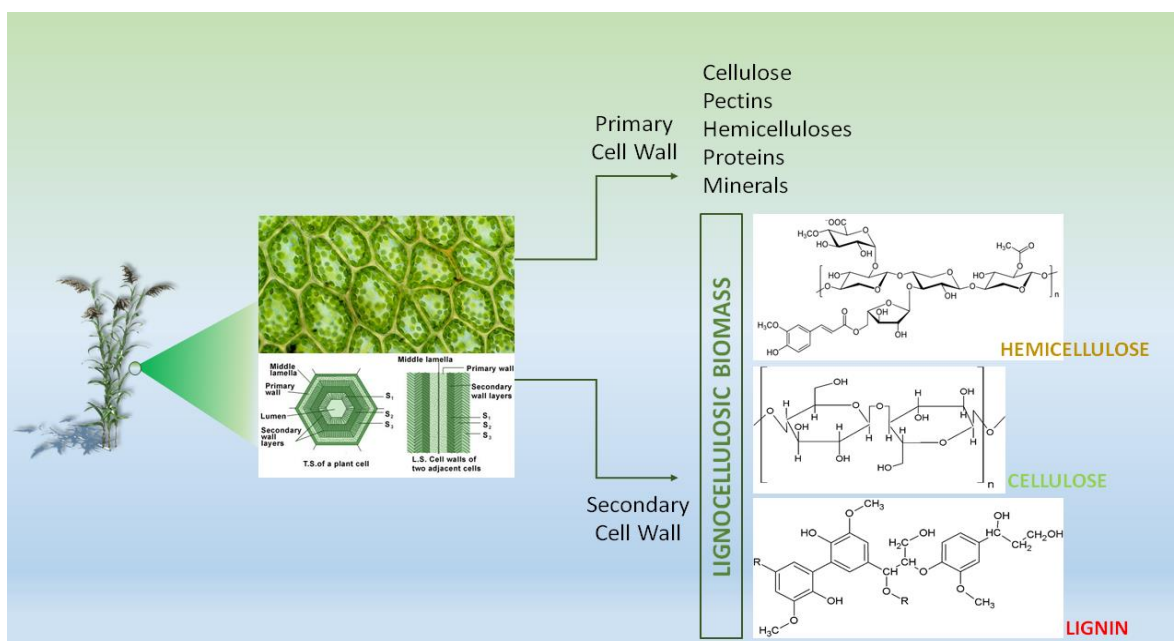


Figure 1: From plant to cell wall: schematic representation of inner structure.

Lignocellulosic Biomass

The lignocellulosic biomass is the most abundant material among the organic substances on earth. It is estimated that more than 40 million tonnes of inedible lignocellulosic-based materials are produced yearly [Sanderson, 2011].

There are several types of lignocellulosic biomasses, that can be divided into virgin and waste LB according to the source. In particular, virgin LB includes all naturally-occurring land plants, from wood to grass [Lin and Huber, 2009]. On the other hand, the term waste LB encompasses all lignocellulosic-based materials produced as by-products of primary and secondary sectors [Iqbal et al., 2013]. Most of waste LB is generated from agriculture as corn stover, rice husk, sugarcane bagasse, wheat/barley/oat/rice straw, nut shell, banana leaf, olive pit [Sánchez, 2009], by forestry (saw mill, wood flour) [Rönqvist, 2003] and by pulp and paper industry (lignosulfonates, lignin-based products) [Abdelaziz and Hultberg, 2016]. Another stream of lignocellulosic materials is from municipalities as residues of food or green areas maintenance [Taherzadeh and Karimi, 2008]. A further way to produce LB involves energy crops as sorghum, miscanthus, reed or jatropha, which are low-cost plantations, harvested to exploit their energy content in terms of heat or electricity, or to produce bio-fuels [Kumar et al., 2008; Anwar et al., 2014]. LB, in fact, is used

in the so-called lignocellulosic biorefineries as a feed in the production of second-generation bio-fuels. This definition refers to the use of an inedible substrate that does not interfere with food industry [Carriquiry et al., 2011]. At the same time, these biorefineries produce low-cost and degraded lignocellulosic wastes as streams of the process.

All the above-mentioned lignocellulosic biowastes are very interesting materials that can be exploited and valorised because they can still contain variable amounts of the three main components of virgin LB structure, cellulose, hemicellulose and lignin.

Cellulose is a linear homopolysaccharide made up of β -(1 \rightarrow 4)-D-glucopyranose units. The chemical structure of cellulose is reported in Figure 2.

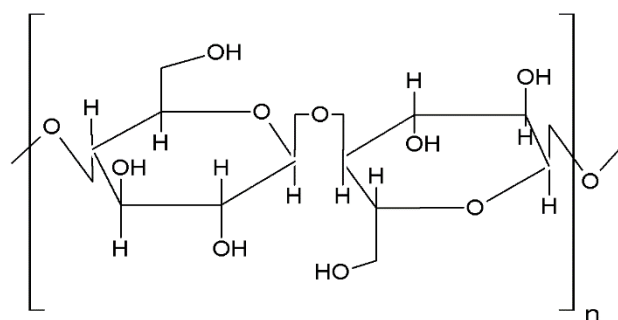


Figure 2: Cellulose structure.

In plant cell wall, cellulose is organized in form of microfibrils. The cellulose chains are aligned parallel to the microfibril axis, and closely associated through hydrogen bonds. This structural organization exhibits a high crystalline texture and represents the primary reinforcing element of the lignocellulosic biomass, providing strength to the material and water insolubility.

The occurrence of several different crystalline structures of cellulose is known and defined as polymorphisms. The latter vary according to the position of hydrogen bonds between and within strands. Natural cellulose is of I type, with structures I α and I β . Bacteria and algae are enriched in I α , while plants mainly in I β . Other cellulose forms are II, III and IV. The conversion from I to II type is irreversible, suggesting that cellulose I is less stable than II type [Wada et al., 2004]. Some parts of the microfibrils have a less ordered, non-crystalline structure referred to as amorphous regions [Vignon et al., 2004].

In the lignocellulosic biomass, cellulose microfibrils and lignin matrix are connected by hemicelluloses, that act as interfacial coupling agents.

Hemicelluloses are branched heteropolysaccharides of pentose and hexose sugars as D-xylose, L-arabinose, D-mannose, D-glucose, D-galactose and D-glucuronic acid. The xylan-type hemicelluloses are characterized by a linear chain of xylopyranose units that can be acetylated or not, and can present branching of uronic acids or carbohydrates in the furanose form [Carpita and Gibeaut, 1993]. While the cellulose content does not vary greatly in quantity between normal hardwoods and softwoods, there are characteristic differences between composition and structure of the hemicelluloses present in the two types of wood. In softwoods, O-acetyl-galactoglucomannan is the principal hemicellulose component, accounting for around 20% of dry weight [Lundqvist et al., 2003]. The glucose to mannose ratio is about 1:3, whereas the ratio of galactose to glucose can vary from 1:1 to 1:10 [Hakkila, 1989].

Conversely, the major group of hemicelluloses found in hardwoods are the glucuronoxylans. Specifically, these xylans are based on O-acetyl-(4-O-methylglucurono)- β -D-xylan units whose content typically ranges between 15 and 30% by weight in hardwood [Sjostrom, 1981]. The chemical structure of a xylan-type hemicellulose is reported in Figure 3.

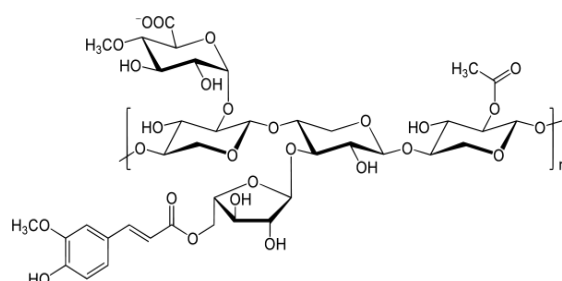


Figure 3: Typical xylan-type hemicellulose structure [Wang, 2008].

In plant cells hemicelluloses play carbon storage functions and structural roles by dictating wall extensibility rate during their growth [Fry, 1989]. In LB, the presence of hemicelluloses is responsible for a high water uptake, along with major susceptibility to biodegradation and a low thermal stability [Saha, 2003]. Hemicellulose is closely associated to cellulose microfibrils and interacts by covalent linkages with lignin [Åkerölm and Salmén, 2001].

Lignin is a complex cross-linked aromatic macromolecule, whose structure depends on botanical origin, anatomical part and age of the plant [Mathews et al., 2015]. Lignin derives from radical polymerization of three phenolic monolignols, namely sinapyl, coniferyl and *p*-coumaryl alcohols that arrange into syringyl, guaiacyl and *p*-hydroxyphenyl units, respectively (Figure 4).

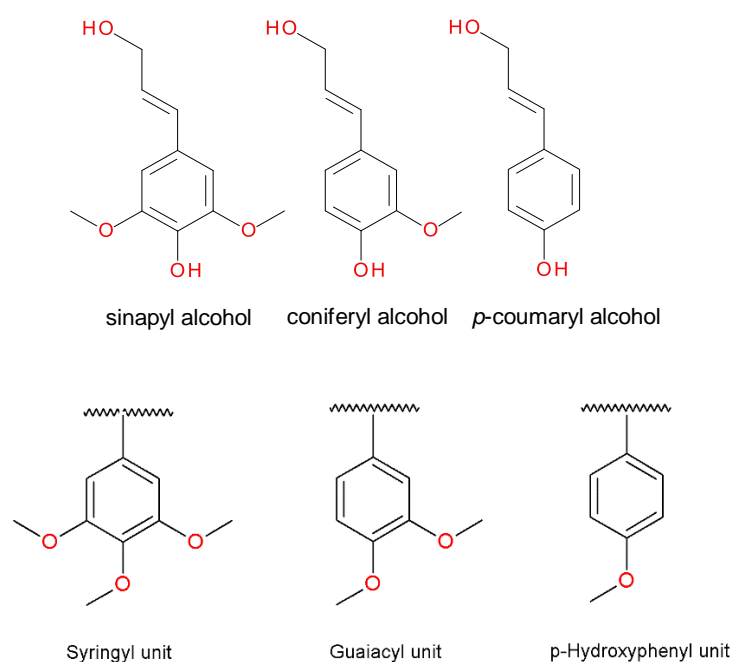


Figure 4: Lignin monolignols.

The latter units are tightly linked by aryl ether or conjugated and non-conjugated carbon-carbon bonds. This entails that substructure repetition in the lignin network is highly variable.

In the cell, lignin mainly acts as a structural component, allowing upright plant growth and conferring stability and protection towards microbial attacks. Moreover, lignin is present in those parts of the plants where cells differentiate and acquire the role of nutrients and lifeblood channels. Therefore, it is also responsible for hydraulic communications in plants. In the lignocellulosic biomass, the lignin network provides thermal stability, hydrophobicity and stiffness [Boudet et al., 2003].

Exploitation of Lignocellulosic Biomass

Virgin LB has been extensively used for construction, production of weapons, furniture, decorative objects, tool handles, toys, sport equipment and so on [Rowell, 2013].

Among historical usages of virgin LB, there is the production of pulp [Jiménez et al., 2008 (a)]. The latter can be obtained by means of mechanical, thermomechanical, chemical pulping processes [Jiménez et al., 2006 (b)]. The obtained pulp is composed of a lignocellulosic fibrous material, mainly containing cellulose fibres, that can be further bleached in order to produce white paper products [Eriksson, 1990]. Over time, pulping and bleaching processes have been upgraded, and papers of different qualities, thickness, and roughness can be obtained according to different treatments [Roncero et al., 2003]. Virgin LB is also used as animal feed. Hay, for example, is an herbaceous lignocellulosic material that is cultivated and harvested for this purposes.

LB wastes from agriculture and forestry represents, in the same way, a noticeable source of lignocellulosic materials that are used as animal fodder. In this case, the LB waste nutritional level can be increased by means of microbial conversion procedures [Villas-Boas et al., 2002]. Over time, LB agricultural wastes as straws or sugarcane bagasse have been also exploited to improve soil fertility [Barreveld, 1989], as substrates for several species of *Pleurotus* mushroom cultivations [Yildiz et al., 2002] or as biofertilizers, being a good source of nitrogen and organic matter [Malik et al., 2001]. Biotechnological applications of LB wastes have been also developed. Among them, it can be accounted the production of ligninolytic enzymes. The latter can be generated from soluble sugars and enzyme synthesis inducers present in lignocellulosic wastes streams [Iqbal et al., 2013].

Apart from these applications, both virgin and waste LB have been always exploited as fuel since the time humans learned to control fire [Iqbal et al., 2013]. In this regard, combustion represents the most common way to discard biomass worldwide [McKendry, 2002]. With an energy content ranging between 17 and 21 MJ/kg, LB remains the most typical source of heat. Regrettably, the practice of burning has an alarming environmental and health impact due to the polluting gas and fine particle emissions [Bølling et al., 2009]. The latter represents an environmental concern when a contaminated lignocellulosic biomass is burnt as in the case of wastes from municipalities or industries. In addition, this practice does not allow to exploit some valuable LB properties, such as renewability, large availability and high content in chemical functional groups. Nonetheless combustion is still widespread, so as to represent a global issue.

Due to these environmental and economic concerns, lignocellulosic biomass greener exploitation is encouraged. Nowadays, this issue is particularly important because fossil fuels floating costs, greenhouse gas effects and air pollution have risen an environmental awareness targeted to a greener and eco-friendly world. This new awareness has led to the establishment of provisions as those included in the climate and energy package 20 20 20, issued by European Union [Tol, 2012]. The latter is aimed to reduce green-house emissions, increase the consumption of renewable resources and promote energy saving to 20 % within 2020. In these provisions, the use of biomasses and in particular of lignocellulosic wastes for the production of biofuels is strongly required. In this frame, from an industrial point of view, biorefineries are developing novel processes targeted to the production of second-generation biofuels as biomethane or bioethanol from energy crops or agricultural/forestry LB wastes [Menon and Rao, 2012]. The definition “second generation” refers to the use of fermentable substrates not interfering with food industry [Sims et al., 2010]. One of the first Italian companies able to develop a plant for the production of bioethanol was Biochemtex in 2006, by implementing the so-called “PROESATM” technology. This plant was designed to produce approximately 20 million gallons of bioethanol from a combination of agricultural residues as straw and energy crops as reed [Gray, 2014].

In the lignocellulosic biorefineries the feed is pre-treated by a physical-chemical process, as steam explosion, with the aim of opening up the tight LB macromolecular network. Then, cellulases are used to attack cellulose by breaking ether bonds between D-glucopyranose units. The residual hydrolysed monosaccharides are then fermented to ethanol by yeasts. Eventually, ethanol is distilled, and large amounts of black liquors containing lignocellulosic residues are recovered at the bottom of the distillation column.

The amount of LB waste streams is estimated to increase due to the increasingly higher production of biofuels. For this reason, in the frame of circular economy, several academic and industrial efforts are ongoing to convert these LB wastes (particularly polysaccharide and lignin components) into new value-added products or conventional materials generally produced from fossil-fuel resources. [Percival Zhang, 2008]. Biochemtex, for example, has invested in a new project targeted to depolymerize lignin extracted from lignocellulosic biowaste streams, in order to recover aromatic hydrocarbons as benzene, toluene and xylene.

Novamont, one of the European market leader in biodegradable plastics from renewable resources, is pursuing extraction of monosaccharides from cellulose and hemicellulose of LB biowastes, in

order to convert them into chemicals of industrial interest as xylitol, sorbitol, furfural, succinic acid or poly(hydroxyalkanoates) [Kumar et al., 2008; Su et al., 2009].

In the academic world, on the other hand, scientists are studying LB chemical modifications able to produce renewable polymeric materials [Sadeghifar et al., 2012; Saito et al., 2012; Laurichesse et al., 2014; Buono et al., 2017].

Another activity producing huge amounts of LB wastes is the pulp and paper industry. Among paper wastes, for example, lignosulfonates (LS) are a class of sulfonated water-soluble materials [Soltani et al., 2002]. The most common are calcium, ammonium or sodium LS, according to the sulphite salt used during the chemical pulping process. From a structural point of view, lignosulfonates are characterized by highly polar functional sulfonic groups on a hydrophobic skeleton, which confer them solubility in water and surface-active properties [Lemes et al., 2010]. LS contain different amounts of carbohydrates that should be removed to allow and optimize their exploitation [Yan et al., 2008]. Purified lignosulfonates are commonly used as dispersants [Yang et al., 2007; Matsushita and Yasuda, 2005], emulsion stabilizers [Gundersen and Sjöblom, 1999], and solid suspensions deflocculating agents [Browning, 1975]. In the perspective of exploiting them in a sustainable way, lignosulfonates have been used to produce low molecular weight aromatic chemicals of industrial interest as vanillin [Santos et al., 2011], dimethyl sulfide and dimethylsulfoxide [Hocking, 1997; Calvo-Flores and Dobado, 2010], methyl mercaptan, or catechol [Browning, 1975].

Apart from these exploitations, one of the more pursued route to use LB wastes has been in composite materials. In particular, LB can be used as reinforcing agent or thermo-oxidative stabilizer in polymer matrices [Kim et al., 2004; Le Digabel et al., 2004; Imam et al., 2005; Avérous and Le Digabel, 2006; Ludueña et al., 2012]. According to this approach, the use of wastes can decrease production costs of composites and confer unique and improved properties to the final materials, due to their potential biodegradability, stiffness and reinforcement features [Satyanarayana et al., 2009]. The potential applications of LB wastes in polymers are discussed in detail below.

Synthetic Composites with Man-Made Fillers or Lignocellulosic Biowastes

Composites are multiphase materials made of a matrix and a reinforcement. The latter ones, despite constituting two separate phases, work together and, according to the kind of reinforcement used, confer unique features such as lightness, improved mechanical, thermal and actuation properties to the final materials.

Polymers, either synthetic or bio-based, thermoplastic or thermoset, generally constitute the matrix [Zadorecki and Michell, 1989]. The reinforcement is composed of stiff, strong material, frequently of fibrous nature as man-made glass, aramid, nylon and carbon or natural bio-based fibres [Papirer et al., 1988; Li et al., 2007]. Synthetic polymers as polyolefins, polyurethanes or thermosetting resins are produced from oil-based resources and their use is widespread in several fields as medicine, food packaging, agriculture, cosmetics, furniture, composites, etc [Gunatillake and Adhikari, 2003; Feldman and Barbalata, 2006; Kasirajan and Ngouajio, 2012]. Several of these applications require the use of synthetic composites based on fossil-fuel polymers and man-made carbonaceous reinforcements [Bhattacharyya et al., 2003; McNally et al., 2005; Gunes et al., 2009].

In the past few years, man-made reinforcements are increasingly being replaced by natural lignocellulosic biomasses. These latter materials are more appealing because they are renewable, biodegradable, nonabrasive, and available all over the world. Moreover, low cost and high performance make them interesting for industrial applications. In this regard, both virgin and waste LB, as jute [Rahman et al., 2008], coconut [Lai et al., 2005], pineapple leaf [George et al., 1998], banana fibres [Ibrahim et al., 2010] have been used as fillers in synthetic polymers, particularly polyolefin such as polyethylene or polypropylene. The obtained materials have been defined as wood plastic composites (WPCs) [Markarian, 2008]. Such term was introduced in Italy in 1970s and was referred to any thermoset or thermoplastic synthetic polymer composite filled with a natural lignocellulosic reinforcement [Ashori, 2008]. Many types of natural LB fibres have been used, largely depending on local availability and economics. Researchers have found success in processing LB as nut shells [Girdis et al., 2016] or straws [Chaudhary et al., 2012]. Commercially, however, low-cost wood flour remains the most widely used LB for the preparation of WPCs both in North America and Europe [Markarian, 2008].

One of the major disadvantages encountered during the incorporation of natural lignocellulosic materials into synthetic polymers is the poor compatibility between LB fibre and polymer matrix [Ashori, 2008]. The lack of good interfacial adhesion between the two components has often resulted in poor properties of the final material [Sreekala et al., 1997]. This happens because the polar hydroxyl groups on the surface of the lignocellulosic materials are not able to strongly interact with polymer matrix, that in some cases is non-polar. Furthermore, the incorporation of lignocellulosic materials in a synthetic polymer has been often associated with non-uniform fibre dispersion and agglomeration, due to the tendency of the fillers to aggregate through hydrogen bonds. Due to the incompatibility and poor adhesion between polymers and lignocellulosic fillers, a worsening of composites mechanical properties has been recorded by several scientists [Karmarkar et al., 2007; Ayrimis et al., 2013]. Therefore, filler or polymer modification by chemical treatments, such as acetylation and chemical grafting [Rana et al., 1997, Ichazo et al., 2001], have been attempted with the aim to increase compatibility between polymer and fibre surface. A schematic representation of chemical modifications that can be performed on LB or on polymer matrix is illustrated in Figure 5.

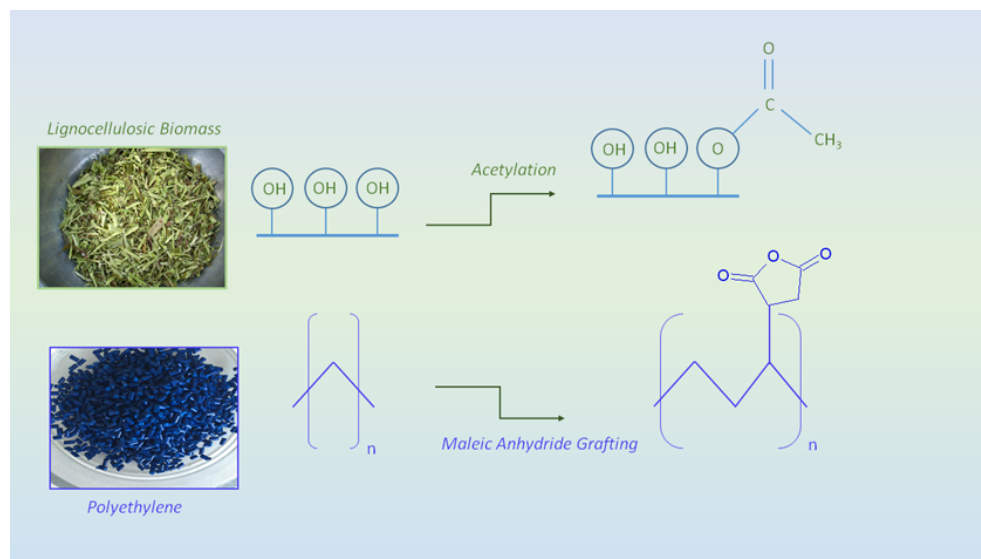


Figure 5: Potential chemical modifications carried out on lignocellulosic biomass and polymer.

Alternatively, some researchers have tried to enhance WPCs performances by using more polar thermoplastic polymers such as poly(vinylchloride) (PVC) or polyacrylates (PAA) [Mohanty et al., 2000; Avella et al., 2000], which are more compatible with lignocellulosic fillers.

Another research approach is based on the use of compatibilizers or coupling agents, which are usually made of a polymeric matrix grafted with anhydride moieties, such as maleic anhydride [Sathe et al., 1994; Wu, 2003]. These components are compatible with the polymeric matrix, as well as with the hydroxyl groups of the fibres, owing to the establishment of strong interactions or even covalent bonds between them (Figure 6).

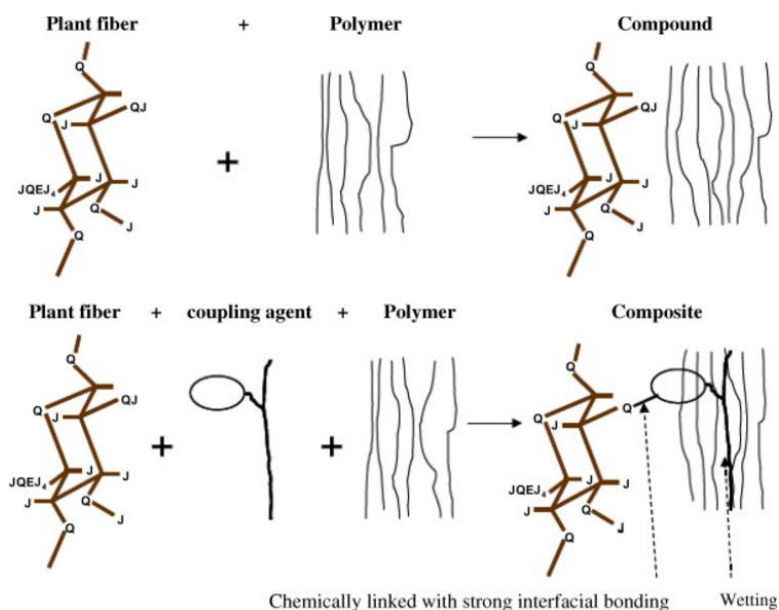


Figure 6: Natural fibre-polymer composites and mechanism of interaction with coupling agent as reported by Ashori, 2008. Reprinted with permission from Elsevier.

Considerable enhancement of composites mechanical and physical properties have been recorded by adopting these strategies, and several examples are reported in literature [Khalil et al., 2001; Rout et al., 2001, Hon and Ren, 2003; Abdelaal et al., 2012].

Bio-Composites Containing Man-Made Fillers or Lignocellulosic Biowastes

Main features of synthetic polymers as durability, toughness and elasticity have provided great benefits to modern society but have also raised significant economic and ecological issues. Indeed, most composites exhibit a remarkable resistance to biodegradation once landfill disposed and, in

some cases, their recycling is not economically sustainable [Dintcheva and La Mantia, 1999; Kim et al., 2001; Guo et al., 2009].

Hence, due to the rising environmental awareness, an increase of interest towards the development of novel and sustainable polymers based on renewable resources has been observed [Scott, 2000]. Bio-based polymers are a class of materials that derive from naturally occurring supplies [Niaounakis, 2013]. This definition refers to a heterogeneous group of bio-based, mostly biodegradable polymers. Among the more common bio-based polymers we can list polysaccharides (alginate, chitin, starch and starch-based blends such as Mater-Bi® or Solanyl®) [Franz, 1989; Kuciel et al., 2010], vegetable and animal proteins [Hunt and Grover, 2010], nucleic acids and lipids [Voet et al., 1999], polylactic acids (PLAs) [Van de Velde and Kiekens, 2002], polyhydroxyalkanoates (PHAs) [Tan et al., 2014].

PHAs represents an aliphatic polyester family, produced by microorganisms and accumulated in cytoplasm as energy storage materials [Bugnicourt et al., 2014]. A deeply studied member of PHAs is poly(3-hydroxybutyrate) (PHB), that is a linear polyester, homopolymer of 3-hydroxybutyrate. PHB is a thermoplastic polymer that shows biodegradability in compost and in different environments, such as marine water [Volova et al., 2010]. Due to its mechanical and barrier characteristics, which are similar to those of oil-based polymers such as polypropylene, this material can be proposed as a substitute for petroleum derived plastics.

Despite the comparable features with synthetic polymers, PHB exploitation is limited due to its high stiffness, brittleness and narrow processability window. Most of bio-based polymers suffer from these shortcomings to such an extent that their diffusion as commodity materials has been limited to niche applications [Lendlein and Langer, 2002].

Driven by the necessity to overcome these issues, attempts to improve bio-based polymer properties have been carried out and blending for the production of composites has been extensively experimented. For example, studies on the effect of carbon nanotubes [Kuan et al., 2008; Yun et al., 2008], organoclay minerals [Ozkoc and Kemaloglu, 2015; Bordes et al., 2008], graphene [Bouazak et al., 2015; Barrett et al., 2014] on mechanical and electrical properties of bio-based polymers as polylactic acid (PLA) and poly(hydroxyalkanoates) (PHAs) to obtain nanocomposites have been performed. As a matter of fact, polymer nanocomposites exhibited markedly improved properties when compared to the pure polymers.

Nanocomposites have been incorporated into consumer products, however, the increasing awareness towards their negative effects on the environment and human health has pushed for obtaining fully sustainable and harmless composites. In this regard, the strategy of blending bio-based polymers with renewable and cheap LB wastes has been considered as a promising way to obtain bio-composites with enhanced mechanical properties and decreased costs [Tserki et al., 2003 (a); Avérous and Boquillon, 2004]. The attention has been focused on the use of natural resources such as agricultural/forestry or industrial LB wastes to be included as fillers in bio-based polymers [Bledzki and Gassan, 1999; Albano et al., 2001; Georgopoulos et al., 2005; Yang et al., 2006; Azeredo et al., 2010]. As an example, Dufresne et al. [2003] reported the effects of some lignocellulosic biowastes as spruce and olive stones flours on the properties of poly(3-hydroxybutyrate-co-valerate) (PHBV). The authors blended lignocellulosic wastes with PHBV, with the aim to reduce the price of the final product and improve the polymer mechanical properties, while preserving biodegradability. In spite of the nucleating effect of LB on the polymer, a poor interfacial adhesion between filler and matrix was recorded.

Due to the problems of incompatibility, other researchers have exploited the chemical modification procedure and the use of compatibilizers to improve the interfacial adhesion between phases. In particular, Tserki et al. [2006 (b)] used acetylated and propionylated lignocellulosic forestry, agricultural and industrial wastes as spruce, olive husk and paper flour as fillers in two polyester copolymers of succinic and adipic dimethyl esters with 1,4 butanediol. The main results of the study evidenced that the acetic/propionic anhydride treatment of the lignocellulosic flours did not improve materials mechanical properties. Conversely, when added a compatibilizer, they recorded a significant improvement of the composites tensile strength and all the others mechanical properties.

Apart from the agricultural residues, by-products from biorefineries and pulp and paper industries can be used as fillers in bio-based polymers for the production of fully sustainable bio-composites [Arancon et al., 2013]. Lastly, several papers have been published on the use of lignosulfonates as fillers in bio-based polymers, such as soy protein [Huang et al., 2003] or thermoplastic starch [Morais et al., 2005]. Calcium lignosulfonates have been selected as natural fillers to improve the performances of a poly(butylene succinate) (PBS)-based material [Lin et al., 2011]. Because of their availability, low cost, and the presence of several chemical functionalities, the introduction of lignosulfonates is expected to enhance rigidity, as well as improve crystallinity and thermal

behaviour of the PBS matrix. Compared with neat PBS, the blends filled with lignosulfonates effectively showed enhanced elastic modulus, increased hydrophilicity and higher values of water uptake at equilibrium [Lin et al., 2011].

Another research approach that has been preliminarily investigated in bio-composites is based on the use of lignosulfonates as flame retardant fillers. Studies on flame performance of chemically modified lignosulfonates have been performed historically [Struszczyk, 1986]. Recently, the attention has shifted towards the use of plain lignosulfonates as flame retardants in polymers as PBS. A decrease in material flammability has been proved [Grexa et al., 2003]. This outcome has been attributed to the aromatic nature of lignosulfonates, that is responsible for a high charring tendency and a low heat release during combustion [Li et al., 2002; Chapple and Anandjiwala, 2010].

Lignocellulosic-Based Composites and Blends Applications

Lignocellulosic-based composites can be exploited as structural materials in several fields, from construction to automotive to production of consumer goods.

About 400,000 tons of Wood Plastic Composites (WPCs) are produced in Europe every year. The main sector of WPCs has always been construction and building for indoor and outdoor applications (decks, furniture, fences, plywoods, roofs) [Olakanmi and Strydom, 2016]. WPCs have been also used as replacement of timber and other materials, then helping to preserve forests and green areas in the planet [Markarian, 2008].

WPCs have also been increasingly used in automotive industry as a result of their enhanced mechanical strength and acoustic performance, lightness for interiors components, lower production cost, improved passenger safety and improved biodegradability [Ashori, 2008]. Furthermore, flute, toys, cups, trays, watchcases and pencils are among the lignocellulosic-based consumer goods which have been manufactured [Li, 2015]. The end products have good mechanical properties, but above all appeal to consumers due to a refined natural look and nice feel [Partanen and Carus, 2016].

Alongside these structural applications, lignocellulosic-based blends in form of films can be used for mulching in agriculture. Mulch films cover soils by forming a physical barrier that limits soil

water evaporation and protects crops from weeds and contaminants. Traditionally, mulch films are manufactured from petroleum-based synthetic polymers as polyethylene, and have been causing considerable waste disposal problems [Halley et al., 2001]. Current technologies are aimed to replace traditional mulch films with bio-based and biodegradable polymers. Biodegradable mulch films based on aliphatic polyesters, e.g. poly(hydroxybutyrate) (PHB) or polylactic acid (PLA) or starch-polymer blends have been investigated for over twenty years [Scarascia-Mugnozza et al., 2006]. However, the high cost of these films constitutes an important disadvantage. To circumvent this issue, current research has focused on the production of bio-based mulch films based on organic wastes as straws, husks, leaves [Sekhon et al., 2005; Singh and Singh, 2012] or blends with low-cost additives as starch [Halley et al., 2001] or lignocellulosic materials [Finkenstadt and Tisserat, 2010]. In this sector, the use of lignocelluloses is interesting because they contain lignin, which confers a dark brown colour to the final product, that allows to control soil temperature and solarisation. The presence of lignin in lignocellulosic-based composites can also modulate the biodegradability of the film, due to the well-known antimicrobial properties [Dizhbite et al., 2004]. In this way, it is possible to obtain mulch films with increased durability.

Some examples of manufactures obtained with lignocellulosic-based composites for construction, automotive, agriculture and consumer goods applications are reported in Figure 7.



Figure 7: Applications of lignocellulosic-based composites and films.

Aim of the Thesis

As mentioned above, combustion is the conventional and widespread way to dispose of lignocellulosic biomass and biowastes. However, this procedure is not economically attractive [Baumberger et al., 1997] and, as in the case of lignosulfonates from pulp and paper industry, it is technically difficult to pursue and polluting. Moreover, the potentialities of lignocellulosic biomass are not exploited. Hence, there is the need to find economically worthwhile outlets to lignocellulosic biowastes.

In this thesis, an attempt to find an alternative application of lignocellulosic industrial by-products is proposed with the aim to convert them into resources.

In particular, two lignocellulosic materials, biowastes of biorefinery and pulp and paper industry, were used as fillers and additives in renewable bio-based polymers. The lignocellulosic biowastes used in this thesis are listed below:

- Lignocellulosic biomass from biorefinery (LC);
- Calcium lignosulfonates from pulp and paper mill (LS).

They differ in industrial origin, chemical composition and solvent solubility.

Lignocellulosic biomass from biorefinery (LC) was obtained as a biowaste from a second generation bioethanol production process, in which *Arundo donax* giant reed stems constituted the inlet feed. LC was received as a brownish fine powder, resulting from the typical bioethanol production phases of pre-treatment, hydrolysis, fermentation and distillation [Sarkar et al., 2012]. LC is insoluble in most of organic solvents, and is composed of lignin and a not negligible amount of polysaccharide contaminants.

Calcium lignosulfonates, usually defined as technical lignins, were provided by a paper mill. They are amorphous aromatic polymers in form of fine powder, available from the paper industry as water-soluble by-products of the pulping process [Fredheim, 2003].

The main objective of the thesis was the valorisation of the aforementioned lignocellulosic biowastes by producing low cost WPCs-type bio-composites. The main properties of the obtained bio-composites were analysed in the perspective of using them in agriculture or building applications.

The results obtained from LC are discussed in Chapters 1-4. In particular, Chapter 1 deals with LC morphological, chemical and thermal characterization analyses and their comparison with those

of a commercial lignin, extracted by an alkaline standard method. Next, Chapter 2 concerns the use of LC as a filler in poly(3-hydroxybutyrate) (PHB) for the production of renewable bio-composites. The preparation of blends and bio-composites, along with the discussion of their morphological, rheological, thermal, calorimetric properties are reported. Moreover, a focus on the effect of LC on biodegradation of PHB in soil is also included.

Chapter 3 regards the extraction and fractionation of LC, with the aim to isolate its main components. A detailed characterization of the isolated fractions is provided. In Chapter 4, the LC derivatives, obtained and discussed in the previous section, were used for the preparation of bio-composites with PHB as matrix. The morphological, rheological and thermal properties of the obtained bio-composites are examined. In addition, the effect of the polysaccharidic fraction of LC on the crystallization properties of PHB is analysed and discussed in detail.

In Chapter 5, the work performed on the use of calcium lignosulfonates as additives in wood-flour particleboards is dealt with. LS were purified through a dialysis treatment in order to reduce the sugar content. Plain and dialysed lignosulfonates were characterized in depth from a morphological, chemical and thermal point of view. Then, both plain and purified LS were used as additives to produce wood-flour-based particleboards. The effect of the lignosulfonates on the particleboards flame performances were investigated through cone calorimeter tests. Formulations with a commercial flame retardant, ammonium polyphosphate (APP), were also prepared and tested. The potential synergistic effects of lignosulfonates with APP were evaluated. Finally, the thermo-degradative and mechanical properties of the obtained particleboards were analysed in order to assess their potential applicability in building and construction.

Publications

Part of the activity carried out in this Ph.D. activity was accounted in several papers published on peer-reviewed international journals, books and conferences as listed below:

Papers:

1. S. Angelini, P. Cerruti, B. Immirzi, G. Santagata, G. Scarinzi, M. Malinconico, *Int. J. Biol. Macromol.* 71 (2014) 163-173.
2. S. Angelini, P. Cerruti, B. Immirzi, G. Scarinzi, M. Malinconico, *Eur. Polym. J.* 76 (2016) 63-76.
3. S. Angelini, P. Cerruti, B. Immirzi, G. Scarinzi, M. Malinconico, *Cellul. Chem. Technol.* 50 (2016) 429-437.
4. S. Angelini, D. Ingles, M. Gelosia, P. Cerruti, E. Pompili, G. Scarinzi, G. Cavalaglio, F. Cotana, M. Malinconico, *J. Clean. Prod.* 151 (2017) 152-162.

Book Chapters:

1. S. Angelini, P. Cerruti, B. Immirzi, G. Santagata, M. Poskovic, G. Scarinzi, M. Malinconico, (2015). *Microbial Factories: Biodiversity, Biofuels, Biopolymers, Bioactive Molecules and Waste Treatment – From microbial biopolymers to bioplastics: sustainable additives for PHB processing and stabilization.* (V. C. Kalia, ed.) Springer India, Chapter 10, Volume 2, pp. 139-160.

Proceedings:

1. M. Auriemma, A. Piscitelli, R. Pasquino, P. Cerruti, S. Angelini, G. Scarinzi, M. Malinconico, N. Grizzuti, *AIP Conference Proceedings* 1695 (2015) 020016-1/020016-6.

References

- M. Y. Abdelaal, E. H. Elmoallami, S. O. S. Bahaffi, *American J. Polym. Sci.* 2 (2012) 102-108.
- O. Y. Abdelaziz and C. P. Hulteborg, *Waste Biomass Valor.* (2016) 1-11 DOI 10.1007/s12649-016-9643-9.
- M. Åkerölm and L. Salmén 42 (2001) 963-969.
- C. Albano, M. Ichazo, J. González, M. Delgado, R. Poleo, *Materials Research Innovations* 4 (2001) 284-293.
- Z. Anwar, M. Gulfranz, M. Irshad, *J. Radiation Research Appl. Sci.* 7 (2014) 163-173.
- R. A. D. Arancon, C. S. K. Lin, K. M. Chan, T. H. Kwan, R. Luque, *Energy Sci. Eng.* 1 (2013) 53-71.
- A. Ashori, *Bioresource Technol.* 99 (2008) 4661–4667.
- M. Avella, G. La Rota, E. Martuscelli, M. Raimo, P. Sadocco, et al., *J. Mater. Sci.* 35 (2000) 829-836.
- L. Avérous and F. Le Digabel, *Carbohydrate Polym.* 66 (2006) 480-493.
- L. Avérous and N. Boquillon, *Carbohydrate Polym.* 56 (2004) 111-122.
- N. Ayrilmisa, A. Kaymakcia, T. Akbuluta, G. Mertoglu Elmasb, *Composites Part B: Engineering* 47 (2013) 150-154.
- H. M. C. Azeredo, L. H. C. Mattoso, R. J. Avena-Bustillos, G. Ceotto Filho, et al., 75 (2010) N1-N7.
- N. Ayrilmis, *Composites B: Engineering* 44 (2013) 745-749.
- J. S. F. Barrett, A. A. Abdala, F. Srienc, *Macromol.* 47 (2014) 3926-3941.
- W. H. Barreveld, *Rural Use of Lignocellulosic Residues* (1989) FAO Agricultural Services Bulletin.
- S. Baumberger, C. Lapierre, B. Monties, D. Lourdin, P. Colonna, *Ind. Crops Prod.* 6 (1997) 253-258.

A. R. Bhattacharyya, T. V. Sreekumara, T. Liua, S. Kumara, L. M. Ericsonb, et al., *Polym.* 44 (2003) 2373-2377.

A. K. Bledzki and J. Gassan, *Progress in Polym Sci.* 24 (1999) 221-274.

A. K. Bølling, J. Pagels, K. E. Yttri, L. Barregard, G. Sallsten, *Particle Fibre Tox.* 6:29 (2009) 1-20.

P. Bordes, E. Pollet, S. Bourbigot, L. Avérous, *Macrol. Chem. Physics* 209 (2008) 1473-1484.

B. S. Bouakaz, I. Pillin, A. Habi, Y. Grohens, *Appl Clay Sci.* 116-117 (2015) 69-77.

A. M. Boudet, S. Kajita, J. Grima-Pettenati, D. Goffner, *Trends Plant Sci.* 8 (2003) 576-581.

W. C. Browning, *Appl. Polym. Symposia* (1975) Editor: T. E. Timell.

E. Bugnicourt, P. Cinelli, A. Lazzeri, V. A. Alvarez, *Express Polym. Letters* 8 (2014) 791-808.

P. Buono, A. Duval, L. Avérous, Y. Habibi, *ChemSusChem* (2017) doi:10.1002/cssc.201601738.

F. G. Calvo-Flores and J. A. Dobado, *ChemSusChem* 3 (2010) 1227-1235.

N. Carpita and D. M. Gibeaut, *The Plant J.* 3 (1993) 1-30.

M. A. Carriquiry, X. Du, G. R. Timilsina, *Energy Policy* 39 (2011) 4222-4234.

S. Chapple and R. Anandjiwala, *J. Thermo. Composite Mat.* 23 (2010) 871-893.

A. K. Chaudhary, V. K. Singh, M. Tewari, *Indian Research J. Extens. Educ.* 1 (2012) 89-92.

D. J. Cosgrove, *Plant Physiol.* 125 (2001) 131-134.

N. T. Dintcheva and F. P. La Mantia, *Polym. Adv. Technol.* 10 (1999) 607-614.

T. Dizhbite, G. Telysheva, V. Jurkjane, U. Viesturs, *Bioresource Technol.* 95 (2004) 309-317.

A. Dufresne, D. Dupeyre, M. Paillet, *J. Appl. Polym.* 87 (2003) 1302-1315.

K. E. L. Eriksson, *Wood Sci. Technol.* 24 (1990) 79-101.

G. Franz, *Planta Medica* 55 (1989) 493-497.

G. E. Fredheim, *Biomacromol.* 4 (2003) 232-239.

- S. C. Fry, *J. Exp. Botany* 40 (1989) 1-11.
- P. A. Gunatillake and R. Adhikari, *Europ Cells Mat.* 5 (2003) 1-16.
- J. George, S. S. Bhagawan, S. Thomas, *Composites Sci. Technol.* 58 (1998) 1471-1485.
- S. T. Georgopoulos, P. A. Tarantili, E. Avgerinos, A. G. Andreopoulos, *Polym. Degrad. Stab.* 90 (2005) 303-312.
- J. Girdis, L. Gaudion, G. Proust, S. Löscke, A. Dong, *JOM* (2016) 1-5 doi:10.1007/s11837-016-2213-6.
- K. Gray, *Symposium on Biotechnology for Fuels and Chemicals*, (2014) Clearwater Beach, FL.
- O. Grexa (2003), F. Poutch, D. Manikova, H. Martvonova, A. Bartekova, *Polym. Degrad. Stab.* 82 (2003) 373-377.
- S. A. Gundersen and J. Sjöblom, *Colloid Polym. Sci.* 277 (1999) 462-468.
- I. S. Gunes, G. A. Jimenez, S. C. Jana, *Carbon* 47 (2009) 981-997.
- J. Guo and Z. Xu, *J. Hazard Mater.* 168 (2009) 567-590.
- P. Hakkila, *Utilisation of Residual Forest Biomass* (1989) Berlin, Springer-Verlag.
- P. Halley, R. Rutgers, S. Coombs, J. Kettels, J. Gralton, G. Christie, M. Jenkins, *Starch* 53 (2001) 362-367.
- M. L. Hassan and A.A. M. A. Nada, *J. Appl. Polym. Sci.* 87 (2003) 653-660.
- M. B. Hocking, *J. Chem. Ed.* 74 (1997) 1055-1059.
- D. N. S. Hon and S. Ren, *J. Reinforced Plastics Compos.* 22 (2003) 957-971.
- J. Huang, L. Zhang, F. Chen, *J. Appl. Polym. Sci.* 88 (2003) 3284-3290.
- N. C. Hunt and L. M. Grover, *Biotechnol. Letters* 32 (2010) 733-742.
- M. M. Ibrahim, A. Dufresne, W. K. El-Zawawy, F. A. Agblevor, *Carbohydrate Polym.* 81 (2010) 811-819.
- M. N. Ichazo, C. Albano, J. Gonzalez, R. Perera, M. V. Candal, *Compos. Struct.* 54 (2001) 207-214.

- S. H. Imam, P. Cinelli, S. H. Gordon, E. Chiellini, *J. Polym. Environ.* 13 (2005) 47-55.
- H. M. N. Iqbal, G. Kyazze, T. Keshavarz, *BioResources* 8 (2013) 3157-3176.
- L. Jiménez (a), A. Rodríguez, A. Pérez, A. Moral, L. Serrano, *Ind. Crops Prod.* 28 (2008) 11-16.
- L. Jiménez (b), V. Angulo, E. Ramos, M. J. De la Torre, J. L. Ferrer, *Ind. Crops Prod.* 23 (2006) 122-130.
- A. Karmarkar, S. S. Chauhan, J. M. Modak, M. Chanda, *Composites Part A: Appl. Sci. Manufact.* 38 (2007) 227-233.
- S. Kasirajan and M. Ngouajio, *Agron. Sustain. Develop.* 32 (2012) 501-529.
- K. Keegstra, *Plant Physiol.* 154 (2010) 483-486.
- H. P. S. A. Khalil, H. Ismail, H. D. Rozman, M. N. Ahmad, *Europ. Polym. J.* 37 (2001) 1037-1045.
- H. S. Kim, H. S. Yang, H. J. Kim, H. J. Park, *J. Therm. Analysis Calorim.* 76 (2004) 395-404.
- B. K. Kim, G. C. Hwang, S. Y. Bae, S. C. Yi, H. Kumazawa, *J. Appl. Polym. Sci.* 81(2001) 2102-2108.
- C. F. Kuan, H. C. Kuan, C. C. M. Ma, C. H. Chen, *J. Phys. Chem. Solids* 69 (2008) 1395-1398.
- S. Kuciel, P. Kuźniar, A. Liber-Kneć, *Archives Foundry Engin.* 10 (2010) 53-56.
- R. Kumar, S. Singh, O. M. Singh, *J. Ind. Microbiol. Biotechnol.* 35 (2008) 377-391.
- S. Laurichesse and L. Avérous, *Progress in Polym. Sci* 39 (2014) 1266-1290.
- C. Y. Lai, S. M. Sapuan, M. Ahmad, N. Yahya, K. Z. H. M. Dahlan, *Polym Plastics Technol. Engineering* 44 (2005) 619-632.
- F. Le Digabel, N. Boquillon, P. Dole, B. Monties, L. Avérous, *J. Appl. Polym. Sci* 93 (2004) 428-436.
- C. M. Lee, A. Mittal, A. L. Barnette, K. Kafle, Y. B. Purk, H. Shin, et al., *Cellulose* 20 (2013) 991-1000.
- A. Lendlein and R. Langer, *Science* 296 (2002) 1673-1676.

- A. P. Lemes, M. A. Soto-Oviedo, W. R. Waldman, L. H. Innocentini-Mei, N. Duràn, *J. Polym. Environ.* 18 (2010) 250–259.
- X. Li, L. G. Tabil, S. Panigrahi, *J. Polym. Environ.* 15 (2007) 25-33.
- B. Li, X. Zhang, R. Su, *Polym. Degrad. Stab.* 75 (2002) 35-44.
- Y. Li, Wood polymer composites, in P. Tesinova (Ed.), *Advances in Composite Materials - Analysis of Natural and Man-Made Materials*, ISBN: 978-953-307-449-8 (2015) InTech.
- Y. C. Lin and G. W. Huber, *Energy Environ. Sci.* 2 (2009) 68-80.
- N. Lin, D. Fan, P. R. Chang, J. Xu, X. Cheng, J. Huang, *J. Appl. Polym. Sci.* 121 (2011) 1717-1724.
- L. Ludueña, A. Vázquez, V. Alvarez, *Carbohydrate Polym.* 87 (2012) 411-421.
- J. Lundqvist, A. Jacobs, M. Palm, G. Zacchi, O. Dahlman, H. Stålbrand, *Carbohydrate Polym.* 51 (2003) 203-211.
- F. R. Malik, S. Ahmed, Y. M. Rizki, *Pakistan J. Biol. Sci.* 4 (2001) 1217-1220.
- J. Markarian, *Plastics, Additives and Compounding* 7 (2008) 20-26.
- S. L. Mathews, J. Pawlak, A. M. Grunden *Appl. Microbiol. Biotechnol.* 99 (2015) 2939-2954.
- Y. Matsushita and S. Yasuda, *Bioresour. Technol.* 96 (2005) 465-470.
- M. C. McCann, B. Wells, K. Roberts, *J. Cell Sci.* 96 (1990) 323-334.
- T. McNally, P. Pötschke, P. Halley, M. Murphy, D. martin, et al., *Polym.* 46 (2005) 8222-8232.
- P. McKendry, *Bioresource Technol.* 83 (2002) 37–46.
- V. Menon and M. Rao, *Progress in Energy and Combustion Sci.* 38 (2012) 522-550.
- A. K. Mohanty, M. A. Khan, G. Hinrichsen, *Compos. Part A: Appl. Sci. Manufact.* 31 (2000) 143-150.
- L. C. Morais , A. A. S. Curvelo, M. D. Zambon, *Carbohydrate Polym.* 62 (2005) 104-112.
- M. Niaounakis *Biopolymers: Reuse, Recycling, and Disposal.* (2013) PDL Handbook Series William Andrew Inc, Norwich, NY, USA.

- E. O. Olakanmi and M. J. Strydom, *Materials Chem. Physic.* 171 (2016) 290-302.
- G. Ozkoc and S. Kemaloglu, *J. Appl. Polym. Sci.* 114 (2009) 2481-2487.
- E. Papirer, H. Balard, A. Vidal, *Europ. Polym. J.* 24 (1988) 783-790.
- Y. H. Percival Zhang, *J. Ind. Microbiol. Biotechnol.* 35 (2008) 367–375.
- R. Rahman, M. Huque, N. Islam, M. Hasan, *Composites Part A: Appl. Sci Manufact.* 39 (2008) 1739-1747.
- A. K. Rana, R. K. Basak, B. C. Mitra, M. Lawther, A. N. Banerjee, *J. Appl. Polym. Sci.* 64 (1997) 1517-1523.
- M. B. Roncero, A. L. Torres, J. F. Colom, T. Vidal, *Bioresource Technol.* 87 (2003) 305-314.
- M. Rönqvist, *Math. Progr.* 97 (2003) 267-284.
- J. Rout, M. Misra, S. S. Tripathy, S. K. Nayak, A. K. Mohanty, *Composit. Sci. Technol.* 61 (2001) 1303-1310.
- R. M. Rowell, *Handbook of Wood Chemistry and Wood Composites Second Edition*, (2013) CRC Press Taylor & Francis Group.
- H. Sadeghifar, C. Cui, D. S. Argyropoulos, *Ind. Eng. Chem.* 51 (2012) 16713-16720.
- B. C. Saha, *J. Ind. Microbiol. Biotechnol.* 30 (2003) 279-291.
- T. Saito, R. H. Brown, M. A. Hunt, D. L. Pickel, J. M. Pickel, J. M. Messman, F. S. Baker, et al., *Green Chem.* 14 (2012) 3295-3303.
- C. Sánchez, *Biotechnol. Advances* 27 (2009) 185-194.
- K. Sanderson, *Nature* 474 (2011) S12-S14.
- S. G. Santos, A. P. Marques, D. L. D. Lima, D. V. Evtuguin, *Ind. Eng. Chem. Res.* 50 (2011) 291-298.
- N. Sarkar, S. Kumar Ghosh, S. Bannerjee, K. Aikat, *Renew. Energy* 37 (2012) 19-27.
- S. N. Sathe, G. S. S. Rao, S. Devi, *J. Appl. Polym. Sci.* 53 (1994) 239-243.
- K. G. Satyanarayana, G. G. C. Arizaga, F. Wypych, *Progress Polym. Sci.* 34 (2009) 982-1021.

- G. Scarascia-Mugnozza, E. Schettini, G. Vox, M. Malinconico, B. Immirzi, et al., *Polym. Degrad. Stab.* 91 (2006) 2801-2808.
- G. Scott, *Polym. Degrad. Stab.* 68 (2000) 1-7.
- N. K. Sekhon, G. S. Hira, A. S. Sidhu, S. S. Thind, *Soil Use Manag.* 21 (2005) 422-426.
- R. E. H. Sims, W. Mabee, J. N. Saddler, M. Taylor, *Bioresource Technol.*, 101 (2010) 1570-1580.
- M. Singh and J. Singh, *Int. J. Electronics Eng.* 4 (2012) 163-166.
- E. Sjostrom, *Wood Chemistry: Fundamentals and Applications*. London (1981) UK, Academic Press, Inc.
- N. Soltani, K. L. Conn, P. A. Abbasi, G. Lazarovits, *Canadian J. Plant Pathol.* 24 (2002).
- M. S. Sreekala, M. G. Kumaran, S. Thomas, *J. Appl. Polym. Sci.* 66 (1997) 821-835.
- H. Struszczyk and J. Macromol. *Sci.: Part A - Chem.* 23 (1986) 973-992.
- Y. Su, H. M. Brown, X. Huang, X.-dong Zhou, J. E. Amonette, et al., *Applied Catalysis A: General* 361 (2009) 117-122.
- M. J. Taherzadeh and K. Karimi, *Int. J. Mol. Sci.* 9 (2008) 1621-1651.
- G. Y. A. Tan, C. L. Chen, L. Li, L. Ge, L. Wang, et al., *Polym.* 6 (2014) 706-754.
- R. S. J. Tol, *Energy Policy* 49 (2012) 288-295.
- V. Tserki (a), P. Matzinos, C. Panayiotou, *J. Appl. Polym.* 88 (2003) 1825-1835.
- V. Tserki (b), P. Matzinos, C. Panayiotou, *Composit. Part A Appl. Sci. Manufact.* 37 (2006) 1231-1238.
- K. van de Velde and P. Kiekens, *Polym. Tes.* 21 (2002) 433-442.
- M. R. Vignon, L. Heux, M. E. Malainine, M. Mahrouz, *Carbohydrate Research* 339 (2004) 123-131.
- S. G. Villas-Boas, E. Esposito, D. A. Mitchell, *Animal Feed Sci. Technol.* 98 (2002) 1-12.
- D. Voet, J. G. Voet, C. W. Pratt, *Fundamental of Biochemistry (Fourth Edition)* (1999) Wiley.

- T. G. Volova, A. N. Boyandin, A. D. Vasiliev, V. A. Karpov, S. V. Prudnikova, et al., *Polym. Degrad. Stab.* 95 (2010) 2350-2359.
- M. F. Yan, X. Q. Qiu, D. J. Yang, W. L. Hu, *Chem J. Chinese Universities* (2008).
- H. S. Yang, H. J. Kim, H. J. Park, B. J. Lee, et al., *Composites Structures* 72 (2006) 429-437.
- D. J. Yang, X. Q. Qiu, M. S. Zhou, H. M. Lou, *Energy Convers. Manage.* 48 (2007) 2433-2438.
- S. Yildiz, U. C. Yildiz, E. D. Gezer, A. Temiz, *Process Biochem.* 38 (2002) 301-306.
- S. I. Yun, G. E. Gadd, B. A. Latella, V. Lo, R. A. Russell, P. J. Holden, *Polymer Bulletin* 61 (2008) 267-275.
- M. Wada, L. Heux, J. Sugiyama, *Biomacromol.* 5 (2004) 1385-1391.
- B. Y. Wang, *Environmental Biodegradation Research Focus* (Wang BY, ed.), Nova Science Publishers Inc (2008), ISBN 978-1600219047.
- C. S. Wu, *Polym. Degrad. Stab.* 80 (2003) 127-134.
- P. Zadorecki and A. J. Michell, *Polym. Composites* 10 (1989) 69-77.

Chapter 1

Lignocellulosic Biomass from Biorefinery

Prologue

In this chapter, the outcomes acquired on the morphological, chemical and thermal characterization of a lignocellulosic biomass, biowaste of a second generation bioethanol production process, are reported. The investigated properties are compared with those of a commercial lignin used as reference.

1.1 Experimental Section

1.1.1 Materials

Lignocellulosic biomass (LC) was kindly provided as a dark brown powder by the Biomass Research Centre (CRB) of the University of Perugia, Italy.

LC was obtained as biowaste from biorefinery, and in particular from a second generation bioethanol production process using humid *Arundo donax* biomass as inlet feed. Such feedstock was processed through a steam explosion pre-treatment in order to open up the lignocellulosic frame and make cellulose more accessible to enzyme action. The enzymatic hydrolysis released simple sugars that were fermented to ethanol by yeasts. At the bottom of distillation column, a black liquor containing LC was recovered, filtrated and dried. LC was mostly insoluble in water and in common organic solvents.

Alkali lignin with low sulfonate content (AL, $M_w \sim 10000 \text{ g mol}^{-1}$) was purchased from Sigma-Aldrich and used as lignin reference.

1.1.2 Methods of Characterization

Morphological analysis: The morphological analysis of LC and AL was performed by means of a FEI Quanta 200 FEG scanning electron microscopy (SEM). Before the observation, the surfaces were coated with Au–Pd alloy by means of a sputtering device (MED 020, Bal-Tec AG). The coating provided the entire sample surfaces with a homogeneous layer of metal of 18 ± 0.2 nm.

Chemical characterization: FTIR-ATR spectroscopy was carried out on LC and AL by means of a Perkin Elmer Spectrum 100 spectrometer, equipped with a Universal ATR diamond crystal sampling accessory. Spectra were recorded as an average of 64 scans in the range $4000\text{--}480\text{ cm}^{-1}$, with a resolution of 4 cm^{-1} . Prior to measurements, the samples were dried at $60\text{ }^{\circ}\text{C}$ under vacuum for 24 h.

Solid-state ^{13}C CP MAS-NMR measurements were performed on dried LC and AL. Measurements were carried out using a Bruker Avance II 400 spectrometer operating at 100.47 MHz. Samples were spun at 10 kHz in 4 mm zirconium oxide rotors. Spectra were collected using a single pulse excitation sequence with a ^{13}C 90° pulse width of 3.2 μs , a recycle delay of 2 s, a contact time of 2 ms, by averaging 16,384 scans.

Thermal analysis: Thermogravimetric analysis (TGA) was performed under nitrogen (flow rate 30 mL min^{-1}) on 10 ± 2 mg of LC and AL samples, using a Mettler-Toledo TG-SDTA 851 thermobalance equipped with a differential thermal analyzer. The measurements were carried out heating the samples from 30 to $800\text{ }^{\circ}\text{C}$ at $10\text{ }^{\circ}\text{C min}^{-1}$. All the measurements were performed in duplicate.

Differential Scanning Calorimetric measurements (DSC) were performed on around 6 mg of LC and AL by a TA DSC-Q2000 instrument under a 50 mL min^{-1} nitrogen flow. LC and AL were first heated from 30 to $150\text{ }^{\circ}\text{C}$ at $20\text{ }^{\circ}\text{C min}^{-1}$, then cooled up to $30\text{ }^{\circ}\text{C}$ at $20\text{ }^{\circ}\text{C min}^{-1}$, and re-heated up to $200\text{ }^{\circ}\text{C}$ at $10\text{ }^{\circ}\text{C min}^{-1}$.

1.2 Results and Discussions

1.2.1 Morphological, Chemical and Thermal Characterization of Lignocellulosic Biomass

LC was a dark brown and fine powder insoluble in water and scarcely soluble in common organic solvents. The commercial lignin AL used as reference was a brown powder, slightly soluble in polar organic solvents. It was soluble in water, yielding a distinctly alkaline solution (pH = 10.5).

SEM characterization of LC and AL showed that the biomass morphology was significantly affected by the type of vegetal source, chemical treatment and extraction route. As shown in Figure 1.1a, AL featured regular spherical particles with large size dispersity, ranging from few to hundreds of micrometers. Many open volumes were also visible inside the particles. Such morphology was attributed to the low-pressure concentration process of lignin from black liquors, which caused the particles to take a spherical form due to their surface tension [Fierro et al., 2006; Pua et al., 2011]. The micrograph relative to LC, reported in Figure 1.1b, showed a heterogeneous morphology with many irregularly shaped lignin particles along with some fibrous material, of likely polysaccharide nature.

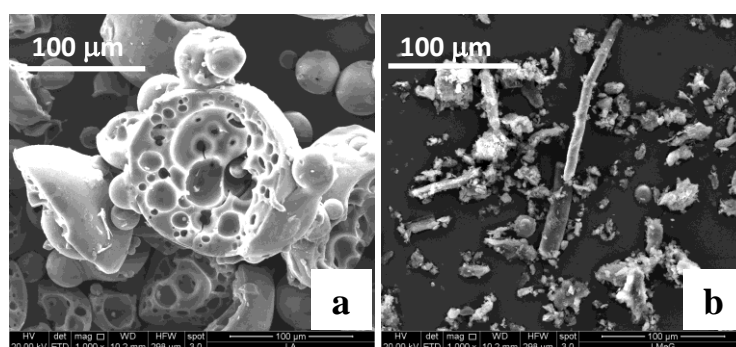


Figure 1.1: a) SEM micrographs of AL and b) LC.

Further evidence of the complex composition of LC came from the FTIR-ATR and ^{13}C P MAS-NMR investigations. The spectra are reported in Figure 1.2

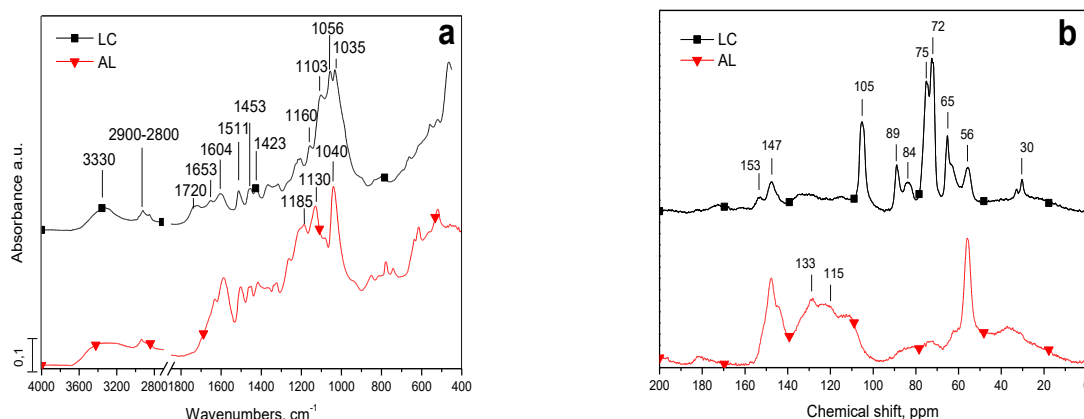


Figure 1.2: a) FTIR-ATR and b) ^{13}C P MAS-NMR spectra of AL and LC.

The FTIR-ATR spectrum of LC sample was reported in Figure 1.2a and compared to that of AL. The latter exhibited a broad band centered at about 3300 cm^{-1} connected to the stretching vibration of -OH linkages from alcoholic and phenolic groups. The absorption of C-H bonds, coming from the aliphatic portion of the material was visible in the range between $2900\text{-}2800\text{ cm}^{-1}$ [Zhang et al., 2010; Derkacheva and Sukhov, 2008]. In the carbonyl region, a weak band at 1653 cm^{-1} was indicative of the presence of conjugated carbonyls. This peak appeared overlapped with a stronger one centered at 1604 cm^{-1} generated from the skeleton vibration of aromatic moieties. At lower frequencies, the absorption at 1511 cm^{-1} shares the same origin, while the C-H of methoxyl groups were present with two bands at 1453 and 1423 cm^{-1} [Schwanninger et al., 2004]. For the 1453 cm^{-1} frequency, a contribution from the aromatic skeleton vibration cannot be excluded [Zhang et al., 2010]. At lower frequencies, the AL sample showed some intense bands at 1185 , 1130 and 1040 cm^{-1} . These absorptions were indicative of phenolic C-O vibrations and aromatic C-H in-plane deformation of syringyl and guaiacyl-type moieties, respectively [Zhang et al., 2010; Derkacheva and Sukhov, 2008].

In the LC spectrum, from a comparison with the AL sample, some typical features of lignin materials were come upon by the presence of the signals at 1653 , 1604 , 1511 , 1453 and 1423 cm^{-1} . These signals, as mentioned above, are relative to the conjugated carbonyls on lignin aliphatic chains, to the aromatic skeleton vibrations and to the methoxy groups.

Besides the bands previously described, the LC spectrum showed some features that were attributed to polysaccharides at 1160, 1103, 1056 and 1035 cm^{-1} . These peaks are associated to C–O stretching vibration from secondary alcohols and β -(1-4) linkages between cellulose monomers [Schwanninger et al., 2004]. Moreover, the 1720 cm^{-1} absorption is likely generated by the stretching vibration of acetyl groups of hemicellulose or by the carbonyl groups present on cellulose backbone. Nevertheless, it is not sure the polysaccharide origin of this signal because it could be also due to un-conjugated carbonyl groups present in the lignin aliphatic chains.

The structure and composition of the lignocellulosic biomass was also investigated by solid-state ^{13}C CP MAS-NMR. The NMR spectrum of LC was displayed in Figure 1.2b, along with the NMR spectrum of the reference alkali lignin AL. A comparison of AL and LC spectra confirmed that the latter contained both lignin and polysaccharide moieties. This outcome was indicated by typical sharp cellulose signals of C–1 at 105.2 ppm, C–2,3,5 at 72.5 and 75.1 ppm; C–4 at 84.0 and 89.0 ppm; C–6 at 63.5 and 65.2 ppm [Freitas et al., 2011]. A characteristic resonance visible in LC spectrum appeared at 32 and 30 ppm as a sharp doublet peak. This signal is likely due to carbons linked to C1 in the aliphatic chain of the monolignols and to waxes. The presence of the typical constituting lignin units in LC was demonstrated by the peaks at 153 and 147 ppm attributed to etherified and free phenolic carbon atoms, by the broad resonance around 133 and 115 ppm, assigned to the C1 in both syringyl and guaiacyl monomers and C5 in guaiacyl units, and the peak at 56 ppm due to carbon in methoxy groups [Jung and Himmelsbach, 1989; Kolodziejwski et al., 1982]. All these signals were also detected in the spectrum of AL and, in some cases, they appeared sharper.

Overall, apart from the substantial lignin component, LC sample exhibited a high polysaccharide content that was ascribed to the processing route the biomass underwent during the bioethanol production process. As a matter of fact, LC is produced by means of a steam explosion pretreatment of the *Arundo donax* lignocellulosic substrate, followed by the enzymatic hydrolysis and the fermentative step. It is very likely that the conditions used are not suitable to afford complete demolition of the highly crystalline cellulose fraction. Indeed, the recalcitrance of crystalline cellulose domains towards enzymatic hydrolysis results in the presence of a significant polysaccharide fraction in LC

The thermal stability of LC and AL was investigated through TGA. From the analysis of the TGA/DTG thermograms (Figure 1.3), it was noticed that both samples showed a rapid weight loss

starting above 250 °C. Compared to LC, AL showed slower degradation kinetics, along with higher amount of residual char at 800 °C. The above-described results are summarized in Table 1.1, which lists 5 wt.% loss temperature ($T_{5\%}$), maximum decomposition rate temperature (T_{max}), and char yield at 800 °C ($Char_{800}$).

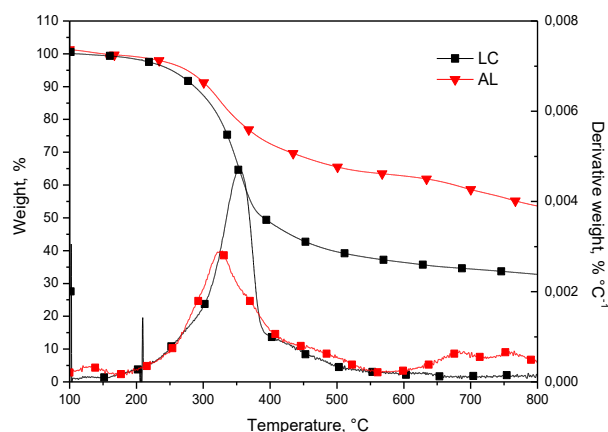


Figure 1.3: TGA/DTG thermograms of AL and LC.

Table 1.1: Thermal parameters obtained from TGA and DSC for LC and AL.

Sample	$T_{5\%}$ (°C)	T_{max} (°C)	$Char_{800} \cdot c$ (%)	T_g (°C)
LC	253 ± 0.9	344 ± 1.1	35 ± 0.7	113
AL	307 ± 1.2	327 ± 0.5	54 ± 1.3	112

Based on the TGA mass loss, the LC sample showed anticipated decomposition and lower char yield with respect to AL. These phenomena were attributed to the presence in LC of a cellulose fraction. The lower starting decomposition temperature of this material was related to the occurrence of cellulose dehydration processes, which are predominant at temperatures lower than 300 °C [Soares et al., 1995]. In this temperature range, lignin decomposition is slower due to its reduced content of free hydroxyls.

At higher temperatures faster radical degradation mechanisms are triggered, which cause extensive depolymerization through fast cleavage of the cellulose alkyl backbone bonds [Cerruti et al., 2008]. This effect is reflected in the lower char content of the LC sample.

DSC analysis performed on LC and AL (not shown in this chapter) did not display any signals due to melting, while a very broad endotherm step ascribed to glass transition was visible at temperature higher than 100 °C. Since the glass transition temperatures were not clearly appreciable, their values (Table 1.1) were assessed using the first derivative of the DSC traces [Gordobil et al., 2014]. By means of this procedure, T_g values of 112 and 113 °C were obtained for AL and LC, respectively.

1.3 Conclusions

Lignocellulosic biomass (LC) was a complex material composed of lignin particles and polysaccharides fibres as SEM, FTIR-ATR and ^{13}C CP MAS-NMR analysis evidenced. The presence of polysaccharides was also testified by the TGA analysis. LC showed anticipated decomposition and lower char yield with respect to the commercial alkali lignin (AL). The lower starting decomposition temperature of LC was related to the occurrence of cellulose dehydration processes. Cellulose is thermally less stable than lignin and starts to decompose at lower temperatures. This finding showed that the pretreatment used in the second generation bioethanol production process aimed at opening up the lignocellulosic network in order to get cellulose more accessible to enzymatic hydrolysis was not completely effective. Therefore, it is supposed that the complete demolition of the highly crystalline cellulose fraction does not occur due to the not suitable pretreatment conditions or to the presence of covalent linkages between lignin and polysaccharides. Thus, at the end of the entire process, a by-product still containing a remarkable amount of cellulose is recovered.

The exploitation and conversion of such a lignocellulosic biowaste into a bioresource can bring several benefits, as helping biorefineries to dispose of biowastes, avoiding polluting and harmful combustion procedures. Moreover, the renewability, fibrous nature, stiffness and abundance in hydroxyl groups of LC makes it a suitable filler for thermoplastic polyester matrices. The use of a waste as filler into a polymer matrix can provide a final composite product with improved

performances and reduced production costs. The preparation and the characterization of polymer blends and bio-composites with LC as filler will be discussed in the next “chapter”.

References

- P. Cerruti, V. Ambrogio, A. Postiglione, J. Rychl'ý, L. Matisová-Rychlá, C. Carfagna, *Biomacromol.* 9 (2008) 3004-3013.
- O. Derkacheva, D. Sukhov, *Macromol. Symp.* 265 (2008) 61-68.
- V. Fierro, V. Torné-Fernández, A. Celzard, *Microporous Mesoporous Mater.* 92 (2006) 243-250.
- J. C. C. Freitas, T. J. Bonagamba, F. G. Emmerich, *Carbon* 39 (2001) 535-545.
- O. Gordobil, I. Egüés, R. Llano-Ponte, J. Labidi, *Polym. Degrad. Stab.* 108 (2014) 330-338.
- H. J. G. Jung and D. S. Himmelsbach, *J. Agric. Food Chem.* 37 (1989) 81-87.
- W. Kolodziejcki, J. S. Frye, G. E. Maclell, *Anal. Chem.* 54 (1982) 1419-1424.
- F. L. Pua, Z. Fang, S. Zakaria, C. H. Chia, F. Guo, *Biotechnol. Biofuels* 4 (2011) 56-64.
- M. Schwanninger, J. C. Rodrigues, H. Pereira, B. Hinterstoisser, *Vib. Spectrosc.* 36 (2004) 23-40.
- S. Soares, G. Caminot, S. Levchik, *Polym. Degrad. Stab.* 49 (1995) 275-283.
- J. Zhang, H. Deng, L. Lin, Y. Sun, C. Pan, S. Liu, *Bioresour. Technol.* 101 (2010) 2311-2316.

Chapter 2

Poly(3-hydroxybutyrate)/Lignocellulosic Biomass Blends and Bio-Composites

Prologue

In this chapter the use of the lignocellulosic biomass from biorefinery as filler in a thermoplastic biodegradable polyester is reported. The effect of the filler content on rheological, thermal and crystallization properties of the polymer matrix is studied in depth. This activity has been carried out in the perspective of tailoring polymer thermal stability and processability for verifying its upgrade in technological applications.

2.1 Experimental Section

2.1.1 Materials

A non-commercial, additive-free poly(3-hydroxybutyrate) (PHB) (lot T19, $M_w = 223$ kDa, $T_m = 175 \pm 0.3$ °C, $M_w/M_n = 1.23$), was supplied by Biomer (Germany).

Methanol and HPLC grade chloroform were purchased from Romil.

A lignocellulosic biomass (LC), biowaste from a second generation bioethanol production process was provided by the Biomass Research Centre (CRB) of the University of Perugia, Italy. Alkali lignin with low sulfonate content (AL, $M_w \sim 10000$ g mol⁻¹) was supplied by Sigma-Aldrich and used as lignin reference. LC and AL features are discussed in Chapter 1.

All materials were used as supplied after a drying cycle for 48 h at 60 °C under vacuum.

2.1.2 Methods of Preparation and Characterization

PHB-based blends and bio-composites preparation: PHB-based blends containing 5wt.% AL (coded PHB/5AL) or 5, 15 and 30 wt.% LC (coded PHB/5LC, PHB/15LC and PHB/30LC,

respectively) were prepared. In order to get homogeneous mixing, the blends were prepared by a solvent-assisted method. 10 g of PHB powder were added either to a 20 mL solution of 0.52 g AL in distilled water, or to a 20 mL dispersion of 0.52, 1.76 or 4.28 g LC in methanol. The resulting solution and dispersions were kept under stirring at 190 rpm for 30 min at 50 °C to allow a slow solvent evaporation. The obtained blends were dried for 48-72 h at 60 °C under vacuum, until constant weight.

Once dried, the blends were ground in a mortar to a fine powder.

Compression molded films (average thickness 150 μm) were obtained by pressing 1.5 g of the above mentioned blends at 180 °C and 100 bar for 2 min by a Collin P200E bench-top press.

Compression molded plates were prepared using the same equipment, by pressing 20 ± 2 g of powder at 185 °C for 10 min at atmospheric pressure, then at 185 °C and 100 bar for 2 min, using a 10 cm wide, 10 cm long, 0.3 cm thick steel frame. It was not possible to get composite samples for PHB/5AL due to massive thermal degradation of the sample.

Rheological analysis: Rheological measurements were carried out on PHB and PHB-based blends powders by means of a Thermo Fisher RS6000 stress controlled rotational rheometer in the dynamic flow field, using parallel plate geometry with a plate diameter of 20 mm. The gap size between plates was set at 0.5 mm for all samples except for PHB/30LC. For the latter sample a gap of 1 mm was chosen as the large amount of filler prevented obtaining reliable rheological measurements at lower distance. Since one of the objectives of this work was to study the effect of high temperature and time on the stability of the PHB-based blends, special attention was paid in defining a standard protocol for sample loading and rheological characterization. In all experiments the samples in form of powder were directly loaded into the rheometer at the desired test temperature, under a nitrogen flow. The plates were rapidly approached to a gap size of 2.5 mm, then the gap was stepwisely reduced in about 150 s to the measurement value. After 220 s the normal force relaxed and the rheological tests started. PHB/30LC was an exception, since this sample did not show complete normal force relaxation; therefore in this case the rheological measurements started after 270 s, which was the time required to achieve force relaxation for pure PHB at a gap of 1 mm. In these conditions, the values of the residual normal stress for PHB/30LC was about 15 N, while when the gap was set at 0.5 mm a force of about 9 N was measured. All samples showed a linear viscoelastic response at strains $< 1\%$. *Dynamic Time Sweep* test was

performed at 190 °C, at the angular frequency (ω) of 10 rad s⁻¹, for 7200 s. *Dynamic Frequency Sweep* was performed at 190 °C, over the range of 200-0.1 rad s⁻¹ from high to low frequency. Strain values were chosen after having performed a *Dynamic Amplitude Sweep* and were lower than 0.3%.

Gel Permeation Chromatography essay: Average molecular weights of PHB and PHB-based blends, collected at different experimental times during the oscillatory *Time Sweep* test, were measured by a Waters 150 C gel permeation chromatography system (GPC). The instrument was equipped with a Polymer Laboratories Evaporative Light Scattering detector, at 30 °C, using two consecutive Polymer Laboratories PolyPore 5M 300 x 7.5 mm mixed columns. PHB-based samples were dissolved in chloroform (1 mg mL⁻¹), under stirring at 50 °C for 48 h. Then, 0.1 mL of the solutions were injected. Chloroform was used as eluent (1 mL min⁻¹). The calibration curves for GPC analysis were obtained using ten polystyrene standards having molecular weights from 5.0 × 10² to 3.0 × 10⁶ g mol⁻¹.

Thermal analysis: Thermogravimetric analysis (TGA) was performed under nitrogen (flow rate 30 mL min⁻¹) on 10 ± 2 mg of PHB and PHB-based blend powders, using a Mettler-Toledo TG-SDTA 851 thermobalance equipped with a differential thermal analyzer. The measurements were carried out in isothermal conditions for 20000 s at 190 °C, which is about the processing temperature of PHB, until the polymer complete volatilization was observed.

Differential Scanning Calorimetric measurements (DSC) were performed by a TA DSC-Q2000 instrument under a 50 mL min⁻¹ nitrogen flow. Approximately 6 mg of PHB and PHB-based blend powders were first heated from -50 to 200 °C at 10 °C min⁻¹, then rapidly cooled to -50 °C at 50 °C min⁻¹ and reheated to 220 °C at 10 °C min⁻¹. DSC cooling rate for the blends was selected having in mind the typical cooling rates attained during plate preparation by means of a water chilled conventional platen press.

Soil degradation test: Soil degradation behaviour of PHB and PHB/30LC bio-composites films (length = 40 mm, thickness = 0.10 mm and width = 20 mm) was evaluated by placing the samples in close-mesh plastic jackets, which were buried 15 cm deep in garden soil in Pozzuoli (40° 85'N, 14° 07'E, about 2 km from the sea) for 10, 20 and 80 days, with constant irrigation. After the time buried in soil, the samples were washed and ultrasonicated in distilled water by means of an ultrasonic processor (Sonics Vibracell, 500 W, 20 kHz, Sonics & Materials, Newtown, CT, USA)

at room temperature for 30 min alternating ON/OFF cycles lasting 40 and 30 s, respectively, with an amplitude of 30%.

Soil analysis: Soil sample was collected from the ground at a depth of 15 cm. The sample was dried in oven under vacuum at 80 °C for 5 h. The gravimetric moisture content of the sample was then computed as the ratio between the masses of the soil before and after drying. The pH of the soil was measured by means of a Crison Titromatic 1S pH meter. The organic carbon present in the soil was determined by means of Walkley-Black method [Schumacher, 2002] and the analysis was performed in duplicate. The conductivity of an aqueous suspension of soil was measured through Crison GLP 31 conductivity meter.

Morphological analysis: The morphological analysis of the cryogenic fracture surfaces of PHB, PHB/5LC and PHB/30LC bio-composite films, and the observation of the surface of soil buried samples were performed by means of a FEI Quanta 200 FEG scanning electron microscopy (SEM). Before the observation, the surfaces were coated with Au-Pd alloy by means of a sputtering device (MED 020, Bal-Tec AG). The coating provided the entire sample surfaces with a homogeneous layer of metal of 18 ± 0.2 nm.

Chemical analysis: FTIR-ATR experiments were carried out on cross-sections cut from PHB, PHB/15LC and PHB/30LC bio-composites plates by means of a Perkin Elmer Spectrum 100 spectrometer, equipped with a Universal ATR diamond crystal sampling accessory. Spectra were recorded as an average of 64 scans in the range $4000-480$ cm^{-1} , with a resolution of 4 cm^{-1} . Prior to measurements, the samples were kept for 24 h at 60 °C under vacuum. The carbonyl stretching region ($1800-1640$ cm^{-1}) of PHB was deconvoluted using the Origin 8.5 software program, assuming Lorentzian bandshapes.

Mechanical tests: Tensile tests were performed by means of a Instron model 5564 dynamometer, equipped with a 1 kN load cell. Dumbbell-shaped films of PHB and PHB-based bio-composites (average thickness = 0.150 mm, width = 4 mm, length = 50 mm) were used. Before the test, the samples were conditioned in an environmental chamber at 25 °C and 50% relative humidity for 48 h prior to testing. The tests were performed with a 2 mm min^{-1} clamp separation rate. The reported data are the average values of 11 determinations.

Impact tests were performed by means of a Ceast M197 Charpy pendulum on PHB and PHB-based bio-composites (length = 60 mm, thickness = 3 mm and width = 9 mm) cut from plates. The

tests were performed with a 1 m s^{-1} impact speed, using an impact energy of 3.6 J. The experimental data are averaged on five determinations.

Flexural tests were performed on PHB and PHB-based bio-composites (length = 70 mm, thickness = 3 mm and width = 6 mm) cut from plates by means of a Instron model 4505 dynamometer, at a deformation speed of 1 mm min^{-1} with a span of 48 mm; the experimental data are averaged on five determinations.

2.2 Results and Discussions

2.2.1 Processability and Thermal Properties of PHB and PHB-based Blends

Rheological analysis represents a useful tool in determining the experimental conditions for polymers processing and viscoelastic response [Persico et al., 2012; Mousavioun et al., 2013 (c); Yamaguchi et al., 2006]. A rheological characterization was carried out on the blends in order to evaluate the effect of AL and LC on viscoelastic properties and thermal stability of PHB. Shear storage modulus G' and loss modulus G'' of PHB and PHB-based unprocessed blends were measured as a function of the residence time and angular frequency in a rotational rheometer at $190 \text{ }^\circ\text{C}$. *Dynamic Time Sweep* tests were performed by applying a constant frequency in order to monitor the viscoelastic response of the polymer as a function of time to get information on the thermal stability of the melt. The results obtained are reported in Figure 2.1a, which displays the time evolution of G' for pure PHB and its blends. Samples that underwent *Dynamic Time Sweep* test were collected at different times as indicated in the Figure 2.1a, and their molecular weight was measured by means of GPC (Figure 2.1b).

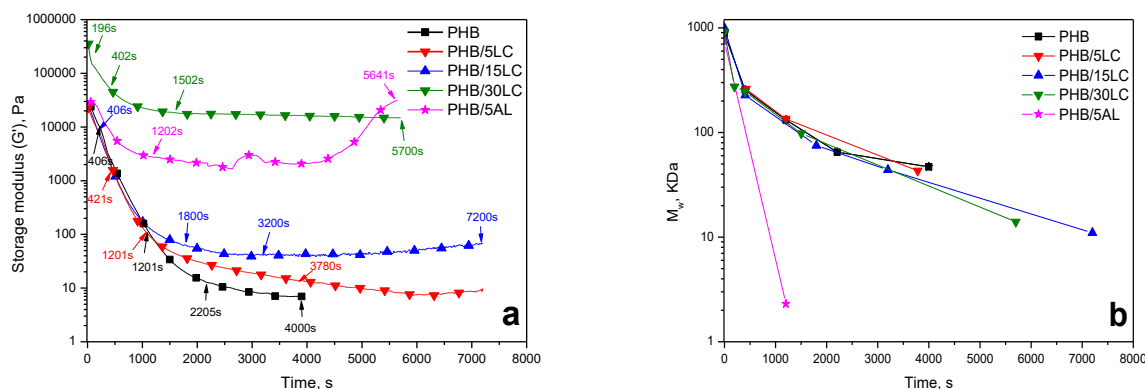


Figure 2.1: a) Time evolution of G' and b) M_w during *Dynamic Time Sweep* test for PHB and PHB-based blends; $T = 190\text{ }^\circ\text{C}$.

For PHB, G' started from a value of about 20000 Pa, then rapidly decreased due to thermal degradation, eventually reaching a plateau after about 4000 seconds [Persico et al., 2012].

GPC measurements confirmed that chain scission started as soon as the polymer melted, and after 400 s M_w dropped to 30% of the initial value. An early decay of G' was also noticed for all samples containing LC, with a similar trend as that observed for PHB. However, after approximately 2000 s G' reached a pseudo-plateau, whose value was related to the filler content. In particular, when the filler concentration was further increased to 30 wt.%, the rheological response changed significantly, modulus values higher by 1 order of magnitude were achieved and after a small decrease, constant G' values of about 20000 Pa were recorded. This outcome might be ascribed to the predominant stiffness of LC with respect to PHB and to the formation of a physical network, in which LC particles act as crosslinking points, resulting in a tight structure whose rheological behavior is mainly dictated by the filler. GPC measurement suggested that LC was not able to increase the thermal stability of the polymer, as the decreasing trend of molecular weight was comparable to that of the plain PHB sample.

Figure 2.1a also evidenced for PHB/5AL a slow decay of G' until 700 s, then the modulus reached a pseudo-steady state, and after about 4000 s a rise occurred which brought back G' to early values around 30000 Pa. According to the GPC data, this outcome was attributed to the noticeable PHB pro-degrading effect of AL, which was evidenced by the dramatic decay of M_w after only 1200 s. Recently, it was demonstrated that thermal degradation of PHB is greatly enhanced by carboxylate

groups *via* an elimination mechanism operating at temperatures as low as 120 °C [Kawalec et al., 2007; Kawalec et al., 2008].

Since AL yielded alkaline water solutions (pH = 10.5), alkali lignin could accelerate PHB thermal degradation by triggering carboxylate-catalyzed elimination reactions. Rapid polymer degradation was responsible for fast volatilization of PHB oligomers, accompanied by massive evolution of fumes occurring during the test. Eventually, after the rheological measurement, almost no PHB-based material remained in the rheometer plates, as shown by optical images (Figure 2.2a). FTIR-ATR spectroscopy confirmed that the residue only contained AL filler, as no signals due to PHB were detected in the FTIR spectrum (Figure 2.2b).

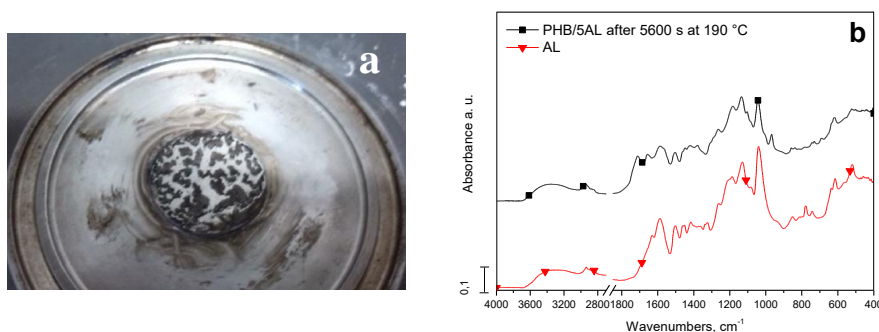


Figure 2.2: a) Optical image and b) FTIR-ATR spectrum of PHB/5AL after 5600 s during *Dynamic Time Sweep* test at 190 °C.

Therefore, the steep increase of G' at longer times during the *Dynamic Time Sweep* measurement can be attributed to the rheological response of the almost neat AL filler.

The result of the *Dynamic Frequency Sweep* test performed on pure PHB and PHB/30LC is reported in Figure 2.3.

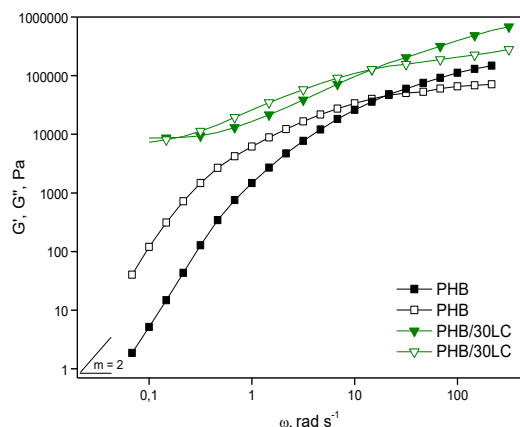


Figure 2.3: *Dynamic Frequency Sweep* curves of PHB and PHB/30LC; $T = 190\text{ }^{\circ}\text{C}$, G' (full symbols), G'' (empty symbols).

The logarithmic plot of the loss and storage moduli versus angular frequency showed a crossover around 20 rad s^{-1} between G' and G'' in the case of pure PHB.

Thus, two distinct regions of viscoelastic behavior were observed. In the low-frequencies terminal region the polymer melt behavior was mainly viscous ($G' < G''$). Then the elastic character of the polymer melt became dominant ($G' > G''$) in the transition zone. Finally G' and G'' approached an invariant value in the rubbery plateau region [Commereuc, 1999].

PHB/30LC exhibited a more irregular rheological curve, due to the heterogeneity of the filler. Predominantly elastic behavior was displayed for frequencies above 20 rad s^{-1} . The rigidity of the blend was slightly reduced with decreasing frequency, and a distinct plateau in G' indicative of the transition from liquid-like to solid-like viscoelastic behavior was observed. This non terminal behavior can be attributed to the formation of an interconnected particle network in the melt (so-called percolation threshold), and it has been typically observed in many particle-filled polymer composites [Prashantha et al., 2008]. PHB/30LC moduli were significantly higher than those of PHB; as an example, at 1 rad s^{-1} G' of the blend was more than 1 order of magnitude higher than that of pure polymer. This solid-like response was due to the physical contacts between lignin particles, which enhanced the rigidity and hindered viscous motions of the material. A similar viscoelastic response was noticed by Mousavioun et al., [2013 (c)] for PHB blends with 60 and 90 wt.% of a soda lignin. However, the moduli values measured for PHB/30LC were significantly higher than those reported in the cited work. From Figure 2.3, it can be also noticed that in the low-frequency region the gap between the PHB/30LC and PHB moduli values increased up to 4

orders of magnitude. This was mainly ascribed to the abrupt decrease in G' and G'' occurring in the terminal region of PHB. Typically for linear homopolymer melts the low-frequency terminal region shows a frequency dependence of $G'' \sim \omega$ and $G' \sim \omega^2$. However, in the case of PHB the decay slope of both G' and G'' on a logarithmic scale was even larger than 2. This finding was related to the occurrence of polymer thermal degradation during the rheological test. In fact, depending on the filler amount, 220 to 270 s were needed to achieve sample melting prior to measurement start. This time should be added to that necessary to collect datapoints at low frequency during the *Dynamic Frequency Sweep* test. As an example, about 200 s elapsed before reaching a measurement frequency of 0.3 rad s^{-1} . Therefore, evaluation of the viscoelastic properties at low frequencies required the polymer to stay for about 500 s at $190 \text{ }^\circ\text{C}$. A comparison with Figure 2.1a, clearly shows that such a long residence time resulted in a significant drop of moduli for all samples due to ongoing thermally-induced chain scission.

Determination of the weight loss through isothermal thermogravimetry at $190 \text{ }^\circ\text{C}$ (Figure 2.4) confirmed this hypothesis.

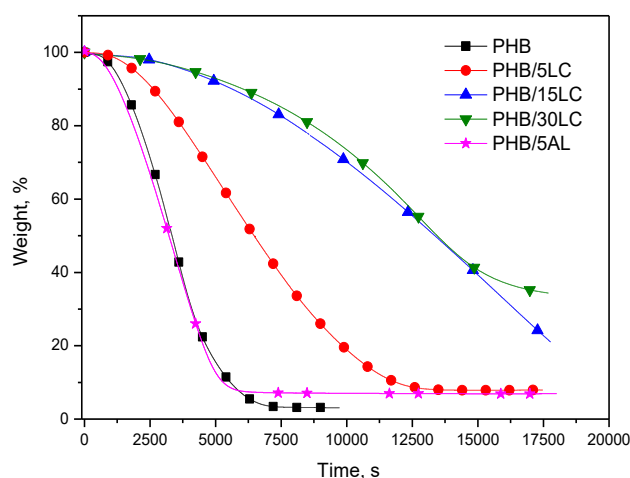


Figure 2.4: Isothermal TGA at $190 \text{ }^\circ\text{C}$ for PHB and PHB-based blends.

Blending PHB with increasing amounts of LC caused a progressive slowdown of weight loss rate up to a filler weight content of 15%.

Since GPC measurements demonstrated that LC had no effect on the thermal stability of PHB, it is likely that the observed decrease of weight loss rate is due to filler agglomeration in the polymer

sample. Such clusters are generated from the evaporation of PHB degradation products. These aggregated structures retarded the volatilization of the oligomers generated at high temperature, analogously to the shielding effect described for nanosized fillers in polymer composites [Sheshmani et al., 2013]. On the other hand, Figure 2.4 showed that addition of 5 wt.% AL increased the rate of blend weight loss, confirming that alkali lignin catalyzed the formation of low-molecular weight degradation products.

Figure 2.5a and 2.5b report the DSC curves of the cooling step after first heating run and the second heating scan of the unprocessed PHB and PHB-based blends, respectively. In Table 2.1 the melt crystallization temperatures and enthalpies ($T_{c \text{ melt}}$, $\Delta H_{c \text{ melt}}^*$), the cold crystallization temperatures and enthalpies ($T_{c \text{ cold}}$, $\Delta H_{c \text{ cold}}^*$), the melting temperatures and enthalpies of the second heating step (T_m , ΔH_m^*), as well as the glass transition temperatures (T_g) of all samples are detailed.

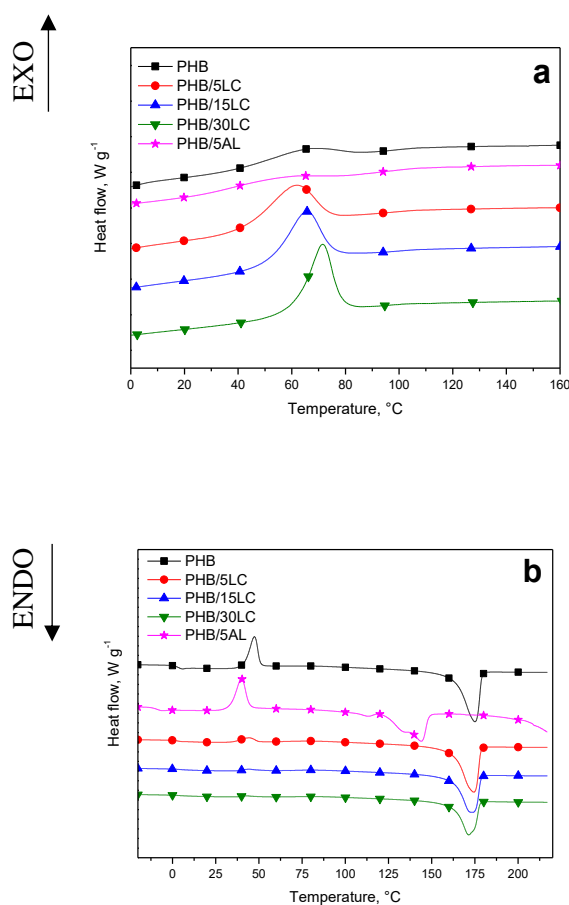


Figure 2.5: a) DSC cooling and b) second heating scans of PHB and PHB-based blends.

Table 2.1: Thermal parameters of PHB and PHB-based blends measured through DSC.

Sample	$T_{c\ melt}$ (°C)	$\Delta H_{c\ melt}^*$ (J g ⁻¹)	T_g (°C)	$T_{c\ cold}$ (°C)	$\Delta H_{c\ cold}^*$ (J g ⁻¹)	T_m (°C)	ΔH_m^* (J g ⁻¹)
PHB	66.9	12.0	3.9	47.4	68.7	175.0	87.4
PHB/5AL	55.7	8.2	-8.3	40.0	61.7	143.9	73.2
PHB/5LC	61.4	34.6	2.6	44.7	35.9	174.4	87.6
PHB/15LC	65.5	42.0	4.8	44.4	26.1	173.3	84.3
PHB/30LC	71.7	49.4	3.8	42.9	25.1	171.4	87.8

$\Delta H_{c,m}^*$ is the enthalpy value calculated considering the weight fraction of PHB in the formulation.

From Figure 2.5a it is worth to highlight that neat PHB displayed a small, broad peak of melt crystallization, since the rapid cooling inhibited chain mobility, and hindered the crystallization process of the polymer. El-Hadi et al., [2002] showed that the broadened signal of melt crystallization during a fast dynamic cooling scan, could be ascribed to the formation of spherulites of large size and low density, representative of bacterially synthesized PHB [El-Hadi et al., 2002]. In the second heating step (Figure 2.5b), the PHB glass transition was clearly evident at low temperature, thus confirming that most of the amorphous phase did not crystallize upon cooling.

Nevertheless, the slow heating of the second scan induced the formation of crystallites, as shown by the presence of a sharp cold crystallization peak, followed by a melting endothermic signal. From the analysis of Figure 2.5a, it was interesting to emphasize that the introduction of LC strongly influenced the crystallization behavior of PHB. In particular, it was evidenced that during cooling, the melt-crystallization of PHB was markedly enhanced by the presence of increasing amounts of the filler. The melt crystallization enthalpy $\Delta H_{c\ melt}$ values of the PHB/LC based samples, indeed, resulted to be much higher than that of plain PHB. Literature data suggest that the melt and cold crystallization temperatures are indirect measurements of the crystallization rate. Generally, a decrease of $T_{c\ cold}$ indicates faster crystallization, whereas lower $T_{c\ melt}$ indicates slower crystallization [Weihua et al., 2004].

As concerning the investigated system, Table 2.1 evidenced that the melt crystallization temperatures of plain PHB was 66.9 °C; the inclusion of increasing amounts of LC shifted $T_{c\ melt}$ towards higher values, up to 71.7 °C in the case of PHB/30LC, promoting the formation of sharp

crystallization peaks. The same samples showed a decreasing trend of cold crystallization temperatures, from 47.4 °C in the case of neat PHB to 42.9 °C of PHB/30LC. Therefore, the addition of LC significantly increased the crystallization rate of PHB, both on cooling and heating. Nevertheless, the drop of $\Delta H_{c\text{ cold}}$ values in PHB/LC based blends confirmed that the crystallization process mainly occurred during the cooling scan (Figure 2.5a). These results indicate that LC was a heterogeneous nucleating agent, potentially able to control the physical aging of the polymer [Weihua et al., 2004]. Finally, it should be observed that both ΔH_m and T_m values of PHB and PHB/LC based samples were not significantly different, suggesting that the introduction of lignocellulosic biomass, able to act as a nucleating agent, did not influence the overall crystallinity of PHB.

Differently from LC, AL did not promote melt crystallization of PHB (Figure 2.5a); indeed, in the second heating scan (Figure 2.5b), the glass transition was easily detectable, however its value was negative. This outcome was ascribed to the pro-degrading effect of AL on PHB. AL brought about PHB depolymerization, reducing considerably the molecular entanglements and improving chain to chain slipping already at low temperature. From Figure 2.5b and Table 2.1, it can be noticed that PHB/5AL showed a multiple melting signal at about 144 °C, whereas a single, sharp melting peak of plain PHB was observed at about 175 °C. These experimental data well-matched with thermal data on AL degradation effects. The drastic reduction of molecular weight promoted the mobility of shorter chain segments, allowing them to rearrange in small crystalline domains. This phenomenon was, indeed, responsible for the observed broad and multiple melting peak and the lower melting temperature (143.9 °C) than PHB (175 °C).

2.2.2 Morphological, Chemical and Mechanical Characterization of PHB and PHB-based Bio-Composites

The bio-composites were characterized in order to get insight on LC filler dispersion as well as on morphology and mechanical performance of the samples. Figure 2.6 reports the SEM micrographs of the cryogenic fracture surfaces of PHB/5LC and PHB/30LC composite films.

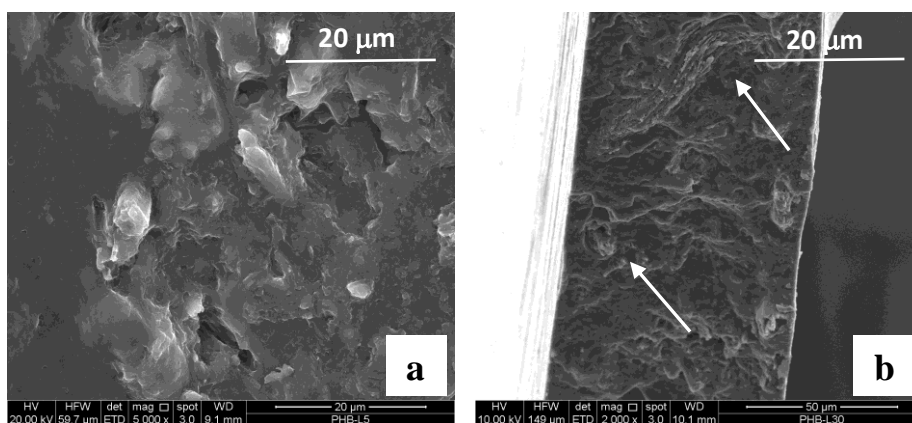


Figure 2.6: a) Fracture surfaces of PHB/5LC and b) PHB/30LC. Arrows indicate agglomerated particles.

The observation of the bio-composite filled with 5 wt.% LC (Figure 2.6a) revealed that the smaller-sized lignin particles and the cellulose fibers were embedded into the matrix, demonstrating that PHB was able to wet this filler fraction. However, the presence of cavities due to particle pull out suggests that interfacial bonding between the larger filler particles and the polymer matrix is relatively weak. Moreover, voids were also present, which were due to the inhibited diffusion of the polymer melt within the aggregated particle lumps. This phenomenon was particularly evident for PHB/30LC (Figure 2.6b), as high contents of LC favored particle agglomeration. The presence of these agglomerates resulted in the generation of flaws, and debonding zones between filler and the polymer matrix were apparent.

Infrared spectroscopy can provide information on the development of weak bonds and interactions such as hydrogen bonding between matrix and filler. Mousavioun et al., [2010 (a)] observed a shift in the carbonyl absorption for melt extruded blends of PHB and soda lignin, which was ascribed to hydrogen bonding interactions of the reactive functional groups of lignin with the carbonyl oxygen in PHB.

FTIR-ATR experiments were carried out on cross-sections cut from plate samples in order to investigate the interactions between PHB and LC. The spectra of PHB, PHB/15LC and PHB/30LC are displayed in Fig. 2.7a.

Upon filler addition, the IR absorptions are slightly modified with the appearance of a broad absorption band around 3300 cm^{-1} , associated to hydroxyl and phenolic groups of LC and a weak band at 1520 cm^{-1} attributed to the aromatic vibrations of the lignin component. Moreover, in the

lower frequency range of the spectrum, the relative intensity of some peaks changed. This was due to the presence in the filler and in the polyester matrix of some common functionalities such as the C-O bonds of alcohols and esters. As far as the 1720 cm^{-1} carbonyl peak is concerned, the presence of LC did not cause a significant shift of its maximum with respect to pure PHB. However, it is known that the infrared carbonyl absorption of PHB results from the combination of the C=O stretching band at 1721 cm^{-1} , attributed to C-H \cdots O=C hydrogen bonding between CH₃ and C=O groups of PHB, and the amorphous, free C=O stretching peaked at 1739 cm^{-1} [Sato et al., 2004]. It has been shown that the area ratio between these two peaks accounts for the relative content of crystalline and amorphous phase in PHB [Li et al., 2003]. Therefore, curve-fitting was employed to quantitatively deconvolute the carbonyl peak, in order to calculate the integrated intensity of the two separated bands. The result of the fitting procedure is shown in Figure 2.7b for PHB, and the quantitative analysis demonstrated that the carbonyl fraction involved in C-H \cdots O=C hydrogen bonding was 91.4% and 80.5% for PHB and PHB/30LC, respectively. The decrease of hydrogen-bonded carbonyl fraction suggested that weak interactions can be established between PHB and LC, although the formation of intermolecular hydrogen-bonding in the bio-composites was not observed.

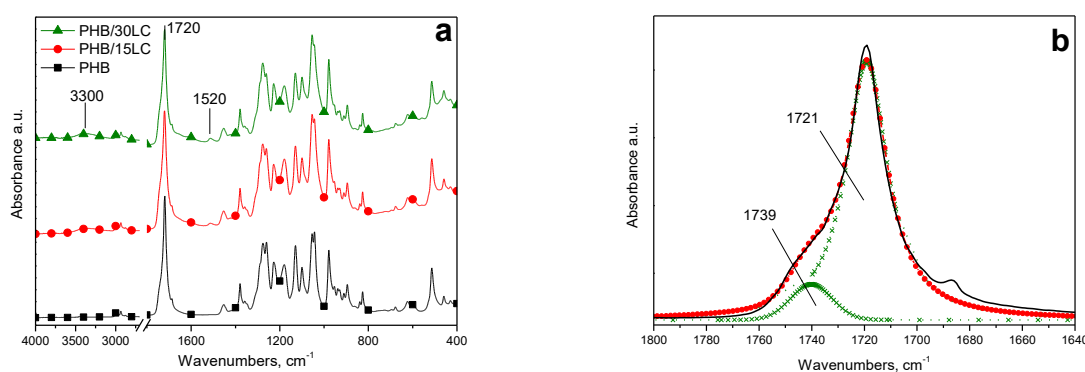


Figure 2.7: a) FTIR-ATR spectrum of PHB, PHB/15LC and PHB/30LC and
b) curve-fitting of the C=O peak of PHB.

Table 2.2 lists the mechanical parameters measured through tensile, flexural and impact tests.

Table 2.2: Average values of the PHB/LC bio-composites mechanical properties measured from tensile, flexural and impact tests.

Sample	Tensile properties			Flexural properties			Impact properties
	E_t (MPa)	σ_t (MPa)	ε_t (%)	E_f (MPa)	σ_f (MPa)	ε_f (%)	Resilience (kJ m ⁻²)
PHB	3144±323	29.6±3.1	1.54±0.30	2600±96	51.4±1.4	3.99±0.51	2.31±0.27
PHB/15LC	2847±130	21.6±1.5	0.92±0.06	2863±117	35.9±1.8	1.63±0.07	0.96±0.01
PHB/30LC	2554±473	11.6±2.5	0.55±0.10	3480±308	30.1±1.6	1.03±0.08	1.04±0.18

From the analysis of the tensile properties of PHB-based bio-composite films, it can be noticed that the presence of LC was responsible for an overall decrease of mechanical properties.

In particular, the sample filled with 30 wt.% LC showed a marked decrease in tensile strength (σ_t) and strain (ε_t). PHB is a rather stiff and brittle polymer, therefore its ductility is very poor unless it is plasticized by the use of a large amount of additives. In this frame, the use of lignocellulosic materials is not expected to increase tensile properties, as poor compatibility in terms of polarity between the phases introduces defects potentially acting as crack initiation sites during tensile tests. As indicated by SEM observations (Figure 2.6a; Figure 2.6b), the poor interfacial adhesion between filler and matrix caused the formation of voids, which acted as stress concentrators and starting points for fracture propagation under tensile stress, thus leading to the premature failure of the sample.

The flexural properties of the sample plates were also affected by the LC content. Similarly to the trend resulting from tensile tests, the composites exhibited lower strength and strain compared to the pure polymer. On the other hand, flexural modulus (E_f) increased with the addition of LC, and the modulus value of PHB/30LC was almost 40% higher than that of PHB. The flexural modulus in composites is mainly dependent on the modulus of each component and slightly sensitive to their mutual interfacial interactions [Sheshmani et al., 2013; Cerruti et al., 2014]. Therefore, the inclusion of a rigid filler such as LC particles is expected to induce a stiffness increase.

Impact strength is the capability of the material to withstand the application of a high deformation rate load, and it is sensitive to the occurrence of cracking in the weakest point of the composite, which is the connecting point between lignocellulosic material and polymer matrix. The effect of LC on the impact strength of the prepared bio-composites was evaluated in terms of resilience values. As can be observed from Table 2.2, the bio-composites were slightly less resilient than pure PHB. Lower impact strength values can be explained in terms of filler heterogeneity and poor interfacial adhesion with the polymer, which limited the stress transfer from the matrix to the filler. Moreover, the weak interface acted as a preferential path for the fracture propagation.

2.2.3 Soil Degradation of PHB and PHB-based Bio-Composites

The biodegradation behavior of the bio-composites was qualitatively assessed through SEM observation of garden soil buried specimens, in order to evaluate the effect of the content of lignocellulosic filler on the biodegradation rate of PHB. In a bioactive environment, polymer degradation occurs by heat, moisture and enzymatic activity of microorganisms which cause polymer chain to cleave, yielding material fragmentation and subsequent mineralization [Mohee et al., 2008]. Breakdown of polyhydroxyalkanoates proceeds by random hydrolytic chain scission of ester linkages [Sarasa et al., 2009]. In order to evaluate the effect of LC on the environmental degradation behavior of PHB, film specimens were buried in soil, taken out at time intervals and their surface was observed through SEM. The physical-chemical properties of the soil used for the degradation tests are illustrated in Table 2.3.

Table 2.3: Properties of the soil.

Moisture, wt.%	14.7
pH	7.4
Organic C, g/kg	19.3±0.07
Conductivity, mS/cm	0.08±0.03

The soil resulted to be sub-alkaline, characterized by a good content of organic carbon and a low conductivity value according to D.M. n. 79 11/05/1992 and D.M. n. 185 13/09/1999 routine analysis.

Figure 2.8 displays SEM pictures of PHB and PHB/30LC at different burial times (0-10-20-80 days). From the micrographs, significant degradation was evidenced by the partial removal of surface material, which acquired a rough appearance.

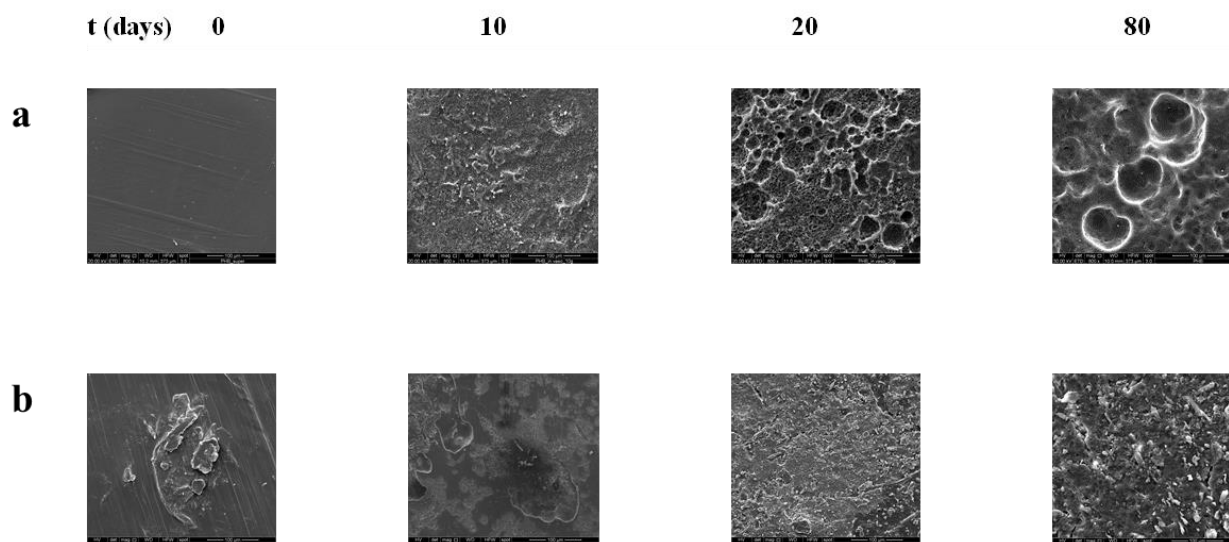


Figure 2.8: SEM micrographs of a) PHB and b) PHB/30LC after 0, 10, 20 and 80 days of soil burial.

Many small cavities were formed in the early burial period, which merged together over the course of the degradation process, eventually giving rise to large holes. SEM observation showed that degradation first took place in the amorphous regions of the polymer. This was demonstrated by the observation of large, intact spherulites appearing beneath the degraded fraction of the polymer. This result was in accordance with data on degradation of PHB and poly(hydroxybutyrate-*co*-hydroxyvalerate), which reported faster degradation of the less crystalline copolymer specimens [Boyandin et al., 2012].

The soil burial tests also showed that, the presence of the lignocellulosic filler LC, affected the surface degradation rate of PHB. After 10 days, the surface of the sample at the highest LC concentration was still rather smooth and compact, showing that a thin layer of polymer was removed. Degradation was more evident with increasing burial times, and bare lignin particles distinctly emerged on the sample surface as the polymer outer layer was progressively excised. After 80 days, cracks were formed, however no large holes were visible. The observed retarding effect of LC can be explained taking into account different aspects. Lignin is intrinsically less

sensitive to enzymatic degradation, possibly having a slight antimicrobial activity [Dong et al., 2011]. As a matter of fact, after 80 days PHB surface was cracked, while lignin and cellulose fibers were apparently less damaged. It is likely that during the degradation process, the developing filler surface layer acted as a barrier and delayed water diffusion and microbial digestion of polymer film. These data were in agreement with those reported in the study conducted by Mousavioun et al., [2012 (b)] based on the burial of PHB/lignin films in a garden soil for up to 12 months. Their work revealed that lignin in the blends inhibited the colonization of the microorganisms and caused the blends to be more resistant to microbial and fungal attack. This was attributed to lignin functional groups containing oxygen (hydroxyl and carboxylic acid) in LC, which play a stunning antimicrobial role. In this case-study, further analysis aimed at investigating the presence of biofilms on PHB samples were not performed. Therefore, it was not possible to ascertain the LC inhibitory effect on the PHB degradation promoted by the microbial population in the soil. However, on the basis of the previous discussion, we can state that the nucleating effect of LC towards PHB produces an increase of the polymer crystallization degree [Koyama and Doi, 1997; Weihua et al., 2004]. The latter phenomenon is responsible for the delay of hydrolytic sample degradation.

2.3 Conclusions

A lignocellulosic filler (LC) by-product from second generation bioethanol production, and a commercial alkali lignin (AL) used as a reference, were blended to PHB to prepare totally bio-based blends and compression molded bio-composites. The effect on the polymer rheology differed according to the kind and pretreatment the biomass was subject to. AL promoted massive thermal degradation of PHB even at temperatures nominally below melting, whereas LC did not affect polymer thermal stability significantly. A relevant observation of these effects concerns the polymer processability. In fact, the addition of a suitable amount of LC yielded a polymer melt whose rheological parameters remained substantially constant over time. This means that, at a given temperature, the addition of LC widens the time window available for polymer processing. LC acted as a heterogeneous nucleating agent, with a positive effect on the physical aging of PHB. Infrared spectroscopic analysis of the bio-composites showed that the chemical environment of the PHB carbonyl was slightly influenced by the presence of the filler, suggesting the existence of

a weak interaction between PHB and LC. This poor compatibility was responsible for a deterioration of the composite mechanical properties.

The biodegradation behavior of the composites was evaluated by soil burial of film samples. The SEM observation of the buried samples surfaces confirmed the high sensitivity of PHB to the combined effect of hydrolytic and biotic degradation. On the other hand, with increasing concentration of LC, the bio-composites were more resistant to the degradation, likely due to the antimicrobial activity of the lignin component, suggesting the possibility to modulate the rate of degradation of products made with these materials for packaging or agricultural purposes.

Driven by the necessity to identify which LC component was responsible for the aforementioned results, the biomass was subjected to chemical fractionation in order to isolate its lignin and polysaccharide components. Moreover, solvent extractions were also performed on the feedstock in order to purify it from apolar and polar substances, thus recovering extractive free solid-residues. Next chapter will deal with these methods of LC pretreatment along with the characterization of the obtained derivatives.

References

- A. Boyandin, S. Prudnikova, *Appl. Biochem. Microbiol.* 48 (2012) 28-36.
- P. Cerruti, F. Fedi, R. Avolio, G. Gentile, C. Carfagna, P. Persico, M. E. Errico, et al., *Polym. Comp.* 35 (2014) 1621-1628.
- S. Commereuc, *J. Chem. Educ.* 76 (1999) 1528-1532.
- X. Dong, M. Dong, Y. Lu, A. Turley, T. Jin, C. Wu, *Ind. Crop. Prod.* 34 (2011) 1629–1634.
- A. El-hadi, R. Schnabel, E. Straube, G. Muller, S. Henning, *Polymer Testing* 21 (2002) 665–674.
- M. Kawalec, G. Adamus, P. Kurcok, M. Kowalczyk, I. Foltran, M.L. Focarete, et al., *Biomacromol.* 8 (2007) 1053–1058.
- M. Kawalec, H. Janeczek, G. Adamus, P. Kurcok, M. Kowalczyk, M. Scandola, *Macromol. Symp.* 272 (2008) 63–69.
- N. Koyama and Y. Doi, *Macromol.* 30 (1997) 826-832.
- J. Li, B. Zhu, Y. He, Y. Inoue, *Polym. J.* 35 (2003) 384-392.
- R. Mohee, G.D. Unmar, a Mudhoo, P. Khadoo, *Waste Manag.* 28 (2008) 1624–1629.
- P. Mousavioun (a), W. O. S. Doherty, G. George, *Ind. Crops Prod.* 32 (2010) 656–661.
- P. Mousavioun (b), G. George, W. O. S. Doherty, *Polym. Degrad. Stab.* 97 (2012) 1114–1122.
- P. Mousavioun (c), P.J. Halley, W. O. S. Doherty, *Ind. Crops Prod.* 50 (2013) 270–275.
- P. Persico, V. Ambrogi, A. Baroni, G. Santagata, C. Carfagna, M. Malinconico, et al., *Int. J. Biol. Macromol.* 51 (2012) 1151–1158.
- K. Prashantha, J. Soulestin, M. F. Lacrampe, M. Claes, G. Dupin, P. Krawczak, *eXPRESS Polym. Lett.* 2 (2008) 735–745.
- F. L. Pua, Z. Fang, S. Zakaria, C. H. Chia, F. Guo, *Biotechnol. Biofuels* 4 (2011) 56-64.
- J. Sarasa, J. M. Gracia, C. Javierre, *Bioresour. Technol.* 100 (2009) 3764–3768.

H. Sato, R. Murakami, A. Padermshoke, F. Hirose, K. Senda, I. Noda, et al., *Macromolecul.* 37 (2004) 7203–7213.

B. A. Schumacher, Ph.D thesis “Methods for the determination of total organic carbon (TOC) in soils and sediments” (2002) United States Environmental Protection Agency.

S. Sheshmani, A. Ashori, M. A. Fashapoyeh, *Int. J. Biol. Macromol.* 58 (2013) 1–6.

K. Weihua, Y. He, N. Asakawa, Y. Inoue, *J. Appl. Polym. Sci.* 94 (2004) 2466–2474.

M. Yamaguchi, K. Arakawa, *Eur. Polym. J.* 42 (2006) 1479–1486.

Chapter 3

Extraction and Fractionation of Lignocellulosic Biomass

Prologue

In this chapter, a focus is given on extraction/fractionation methods performed on the lignocellulosic biomass from biorefinery, by-product from second generation bioethanol production. The lignocellulosic biomass was treated with a toluene/ethanol mixture and with water in order to extract organic and water soluble extractives. Moreover, the parent lignocellulosic biomass was fractionated in order to isolate its main components: acid-insoluble lignin and holocellulose (hemicelluloses and cellulose). The extractive-free solid residues and the isolated fractions were morphologically, chemically and thermally studied and the characterization outcomes are herein reported.

3.1 Experimental Section

3.1.1 Materials

A lignocellulosic biomass (LC), biowaste from a second generation bioethanol production process was provided by the Biomass Research Centre (CRB) of the University of Perugia, Italy. LC features are discussed in Chapter 1.

Concentrated sulfuric acid (95-98%), sodium chlorite (purity p.a. 80%), glacial acetic acid, HPLC grade toluene, absolute ethanol were purchased from Sigma-Aldrich.

3.1.2 Methods of Characterization

Preparation of extractive-free solid residues: Extractions were performed on LC to leach organic and water-soluble extractives. In particular, an extraction procedure with a toluene/ethanol mixture was carried out on LC in order to remove the organic-soluble extractives. In this procedure, 2.42 g of LC were treated with a mixture of toluene/ethanol (2:1 v/v) in a Soxhlet extractor for 6 h. The extractive-free solid-residue was air-dried for 24 h and dried to constant weight in an oven at 60 °C under vacuum. Subsequently, the solid-residue was further extracted with absolute ethanol in Soxhlet extractor for 4 h and dried to constant weight.

An extraction procedure with water was also performed on LC in order to remove water-soluble extractives. To this aim, 2.04 g of LC were treated with 100 mL of Millipore water at room temperature under intense magnetic stirring for 5 h. The sludge was filtrated on paper and washed with water. The extractive-free solid residue was dried to constant weight in an oven at 60 °C under vacuum. The solid residues from toluene/ethanol and water extractions procedures are here referred to as TE and W, respectively. The amount of extractives from toluene/ethanol solution and water, was calculated with respect to the dried starting biomass.

Preparation of acid-insoluble lignin and holocellulose: LC was processed through acid hydrolysis in order to isolate acid-insoluble lignin and by sodium chlorite with the aim to recover a complex of polysaccharides, defined as holocellulose.

Acid-insoluble lignin (IL) isolation was performed according to the following procedure. 5 g of LC were treated with 150 mL of 72 wt.% H₂SO₄ under magnetic stirring overnight. Then, the H₂SO₄ concentration was reduced to 3 wt.% by adding distilled water, and the suspension was kept under mechanical stirring for 4 h at 100 °C. IL was allowed to settle until the supernatant solution was clear. The supernatant solution was discarded and the lignin precipitate was filtrated on a Buchner funnel and washed with distilled water several times until neutral pH. Acid-insoluble lignin was dried to constant weight in an oven at 80 °C under vacuum.

Holocellulose (HC) was prepared by adapting an oxidation procedure reported by Rabemanolontsoa and Saka, [2011]. This isolation method is based on the delignification of biomass and the acidic hydrolysis of polysaccharides. Briefly, 10 g LC were dispersed in distilled water and treated with 5 g NaClO₂ along with 20 mL CH₃COOH at 90°C. This procedure was repeated every 30 min for 6 more times and a total time of 3h. HC was allowed to settle and then

the supernatant was discarded. The product was recovered through centrifugation and water washing cycles. The whitish pulp was dried in oven at 105 °C under vacuum for 2 h and then at 60 °C overnight.

Once isolated, IL and HC were sorted through a 140 mesh sieve and further dried.

IL and HC isolations were carried out in triplicate and their relative amount was calculated on the basis of the dry weight of the parent LC biomass.

Morphological analysis: Scanning Electron Microscopy (SEM) and Energy Dispersive X-Ray Spectroscopy (EDS) analyses were performed by means of a FEI Quanta 200 FEG device.

The morphological characterization of TE, W, IL and HC was performed by means of SEM. The samples were mounted onto stubs by means of carbon adhesive tape and coated with a 20 nm thick gold/palladium layer by means of a modular high vacuum coating system Emitech K575X. The elemental composition of the water-soluble extractive was determined by EDS.

Chemical analysis: FTIR- ATR spectroscopy was carried out on TE, W, IL and HC by means of a Perkin Elmer Spectrum 100 spectrometer, equipped with a Universal ATR diamond crystal sampling accessory. Infrared spectra were recorded by accumulating up to 32 scans with a resolution of 4 cm⁻¹, in the range of 4000-400 cm⁻¹.

Solid-state ¹³C CP MAS-NMR characterization was performed on TE, W, IL and HC. Measurements were carried out using a Bruker Avance II 400 spectrometer operating at 100.47 MHz. Samples were spun at 10 kHz in 4 mm zirconium oxide rotors. Spectra were collected using a single pulse excitation sequence with a ¹³C 90° pulse width of 3.2 s, a recycle delay of 2 s, a contact time of 2 ms, by averaging 16,384 scans.

Thermal analysis: Thermogravimetric investigations (TGA) were carried out by means of a Perkin Elmer Pyris Diamond TG/SDTA thermobalance with alumina pans using about 5 ± 0.5 mg of each sample (TE, W, IL and HC). Measurements were carried out in nitrogen atmosphere under a flow rate of 30 mL min⁻¹. Each sample was analysed according to the following thermal program: heating from 30 to 90 °C at 20 °C min⁻¹; isotherm at 90 °C for 30 min and heating from 90 to 800 °C at 10 °C min⁻¹. The measurements were carried out in duplicate.

All the characterizations were compared to LC, used as reference.

3.2 Results and Discussions

3.2.1 Morphological, Chemical and Thermal Characterization of Lignocellulosic Biomass Derivatives

SEM micrographs of the parent lignocellulosic feedstock (LC) and its derivatives (TE, W, IL and HC) are presented in Figure 3.1.

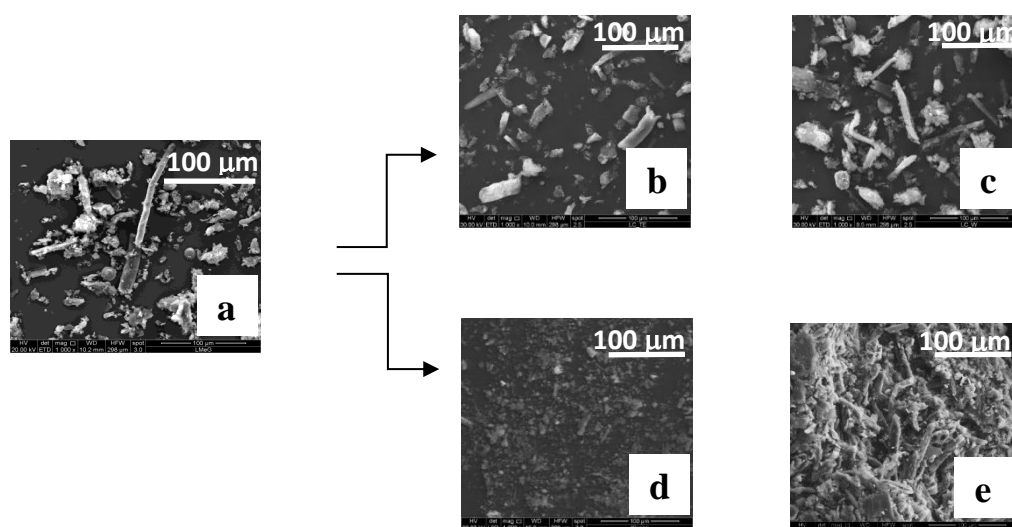


Figure 3.1: SEM micrographs of a) LC, b) TE, c) W, d) IL and e) HC.

The yield of the extractives in toluene/ethanol and water amounted to 12.4%, and 2.9%, respectively.

The removal of the water-soluble extractives from LC did not lead to remarkable morphological changes as revealed by the SEM micrograph shown in Figure 3.1c. Similarly, the extraction with the toluene/ethanol mixture caused only slight deterioration of the biomass along with the reduction of lignin particle size (Figure 3.1b).

As regard IL and HC, the amount of the two isolated fractions, calculated on the dry weight of the parent LC biomass was $53 \pm 1\%$ and $46 \pm 2\%$, respectively. Several studies investigated the relative content of acid-insoluble lignin and holocellulose in numerous types of plants: fern [Carrier et al., 2011], hazelnut shells [Haykiri-Acma et al., 2010], Loblolly pine [Sannigrahi et al., 2008], banana pseudostems [Cordeiro et al., 2004], pulp and paper mill sludge from softwood and hardwood [Jackson and Line, 1997]. It has been pointed out that botanical origin and treatments

performed on the feedstock affect the lignin and polysaccharide composition and morphology. Recently, it has been reported that the relative content of acid-insoluble lignin and holocellulose from *Arundo donax* native stems and foliage was about 14 and 58 wt.% [You et al., 2013]. LC used in the present study derives from humid and fine-cut *Arundo donax* that was processed through the typical treatments aimed at the production of second-generation bioethanol. Nevertheless, these treatments were not efficient as to completely open up the lignocellulosic network and to make the polysaccharides accessible to hydrolysis and fermentation stages. This was evidenced by the presence in LC of a significant amount of HC. This finding was probably due to the presence of hydrolysis-recalcitrant crystalline regions of polysaccharides or to the presence of covalent linkages between lignin and polysaccharides [Soo et al., 2015]. SEM investigation performed on IL and HC (Figure 3.1d, 3.1e) revealed the structural and morphological changes that occurs after the treatments performed to isolate IL and HC from LC. IL micrograph (Figure 3.1d) shows the presence of irregularly shaped particles, while HC (Figure 3.1e) is characterized by compact bundles of polysaccharide microfibers along with a small number of residual lignin particles. LC (Figure 3.1a) shows the typical structures of lignocellulosic materials, that are composed of heterogeneous granular lignin particles and polysaccharide fibrous moieties. Therefore, the morphological aspect of IL and HC suggested that both were isolated successfully from the feedstock. Spherical droplets were observed on the surface of HC polysaccharide fibres (Figure 3.1e). Similar structures were observed by Donohoe et al., [2008] on corn stover rinds that were dilute-acid or hot water pre-treated, and by Sannigrahi et al., [2011 (a)] on neat and acid treated holocellulose. In the latter study, the presence of these sphere-like microparticles was attributed to lignin. The formation of lignin spherical-like particles was previously studied by Micic et al., [2001] who discovered lignin globules hold together in a supramolecular structure. Lignin is generally seen as a barrier to enzymatic hydrolysis of biomass to sugars [Bon-Wook et al., 2012]. Therefore, it was supposed that the presence of such lignin structures on cellulose fibres could have inhibited enzyme activity during the bioethanol production pre-treatment and reduced the yield of fermented cellulose.

To investigate the chemical composition of all the products recovered after extractions and fractionations, spectroscopy measurements in the mid-infrared were performed.

FTIR-ATR spectra of LC-derivatives are illustrated in Figure 3.2a. In the same Figure, for comparison, the spectrum relative to LC is also shown.

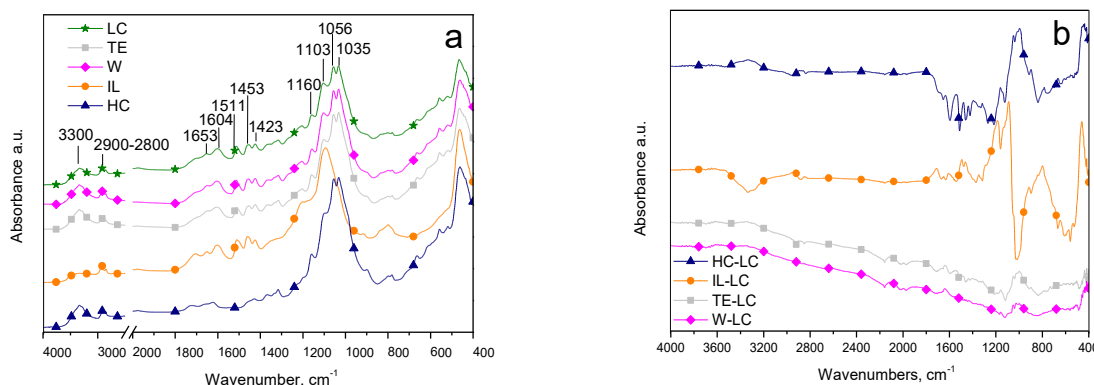


Figure 3.2: a) FTIR-ATR spectra of LC-derivatives and b) difference spectra between the derivatives and the feedstock. The curves were vertically translated.

In the high frequency region of the spectra, all samples showed similar spectral profiles, with a broad band located at 3300 cm^{-1} and a pattern of signals in the $2900\text{--}2800\text{ cm}^{-1}$ range. These features originated from hydroxyl groups and hydrocarbon moieties, respectively, and resulted scarcely affected by the kind of treatment performed.

The region in the $1655\text{--}1000\text{ cm}^{-1}$ frequency range, conversely, exhibited a series of absorptions that provide very useful information on the effectiveness of the fractionation process performed on the native feedstock. From a comparison between the LC and the IL spectra, a number of absorptions relative to lignin can be identified. In particular, in the carbonyl region, a peak at 1653 cm^{-1} was indicative of the presence of carbonyls conjugated with aromatic rings. At lower frequencies, the absorptions at 1604 , 1511 and 1423 cm^{-1} were assigned to the aromatic skeleton vibrations, while the signal at 1453 cm^{-1} to the C–H deformation of methoxy groups [Jahan et al., 2007]. In the low wavenumber range, the peak at 1103 cm^{-1} originated from alkyl aromatic ethers (Ar–O) of lignin [Donohoe et al., 2008, Angelini et al., 2014].

No signal relative to holocellulose can be identified in the IL spectrum. Such finding suggests that the acid treatment, addressed to hydrolyse the polysaccharide materials, was accomplished successfully. The spectrum relative to the LC feedstock, in addition to the signals originating from the lignin fraction, also shows some traits in common with the HC derivative. This is evidenced by three peaks at 1160 , 1056 and 1035 cm^{-1} , which are present in both spectra, and are associated to alcohol C–O stretching from C3–OH and β -(1-4) linkages between cellulose monomers [Jackson and Line, 1997]. The spectrum relative to the HC derivative is therefore typical of

holocellulose. However, the presence of the signals at 1453 and 1423 cm^{-1} , even if weak, suggested the contamination of HC from lignin traces.

The remarkable changes in the absorption bands in the spectra relative to the IL and HC fractions can be better evidenced if spectral subtraction is applied to the as-acquired FTIR-ATR spectra.

In Figure 3.2b, IL-LC and HC-LC difference spectra are shown. In the IL-LC plot, the band at around 3300 cm^{-1} , due to O-H stretching, was found to decrease, since the sulfuric acid treatment removed most of the polysaccharide fractions present in the parent LC. Small peaks in the frequency range around 2900-2800 cm^{-1} , attributed to C-H bonds of lignin and carbohydrate moieties, were also recorded. The spectral profile of this region evidenced that the acid treatment did not cause major changes in the shape or position of the bands. At lower frequencies, an absorption increase in the carbonyl region was observed with a maximum at 1720 cm^{-1} . This band was attributed to the presence of carboxylic acids, with the minor contribution of ketones, aldehydes and ester groups. In the same frequency range, a small peak at 1653 cm^{-1} was also detected and attributed to conjugated carbonyls. The presence of these carbonyl functionalities can be ascribed to the harsh acid treatment adopted to isolate the acid-insoluble lignin fraction, which resulted in oxidation of carbon atoms and hydrolysis of ester bonds. An increase in the absorptions generated from the skeleton vibrations of aromatic moieties in LC and IL was detected at about 1600 and 1500 cm^{-1} , whereas two peaks at 1453 and 1423 cm^{-1} accounted for the methoxy groups of guaiacyl and syringyl units. Finally, a marked increase at 1185 and 1100 cm^{-1} , attributed to C-O-C and C-O stretching vibrations between aromatic rings, secondary alcohols and aliphatic ethers, was also detected.

These absorptions resulted to be the major changes observed in the IL-LC spectrum. Their occurrence confirmed that the IL was mainly constituted by a condensed aromatic structure with side chains typical of lignin. It is also worth noting that the IL-LC spectrum displays a marked decrease in the 1050-1010 cm^{-1} absorption region, as a confirmation of the effective removal of the polysaccharide fraction.

On the other hand, the HC-LC spectrum (Figure 3.2b) evidenced a remarkable increase of two absorption peaks at 1050 and 1000 cm^{-1} , related to C-O deformation in secondary alcohols and aliphatic ethers, and C-O valence vibration from C3-OH and β -(1-4) linkages between cellulose monomers. Moreover, the content of O-H groups (3300 cm^{-1}) increased with respect to the parent biomass. Furthermore, a dramatic decrease in the 1750-1100 cm^{-1} region confirmed that most of

lignin was removed. Nevertheless, a close examination of the HC spectrum (Fig. 3.2a), revealed the presence of weak bands at 1453 (shoulder) and 1423 cm^{-1} . These absorptions were attributed to lignin traces remaining after the sodium chlorite treatment, as already evidenced by SEM analysis (Figure 3.1e). In literature, several authors reported the contamination of holocellulose samples by lignin, as Sannigrahi et al., [2011 (a)] who observed pseudolignin droplets on the surface of neat acid-treated holocellulose through SEM.

A comparison between the spectra of LC and the extractive-free solid residues recovered after organic and water extractions (TE and W) evidenced very small differences. The TE-LC spectrum (Figure 3.2b) showed a slight decrease in the aliphatic and aromatic C-H vibration regions at around 2900 cm^{-1} and 1600-1500 cm^{-1} due to the extraction of non-polar constituents, such as lipids, waxes and soluble lignin derivatives. The removal of this fraction was responsible for a relative increase of the polysaccharide fraction, as evidenced by the increase of the absorption band in the 1050-1000 cm^{-1} spectral region. As for the extractive-free solid residue recovered after water extraction, no significant differences were observed between the LC and W spectra.

^{13}C CP MAS-NMR was performed on all the samples in order to assess the efficiency of treatments carried out on LC. The relative spectra are illustrated in Figure 3.3, and signal assignments are reported in Table 3.1.

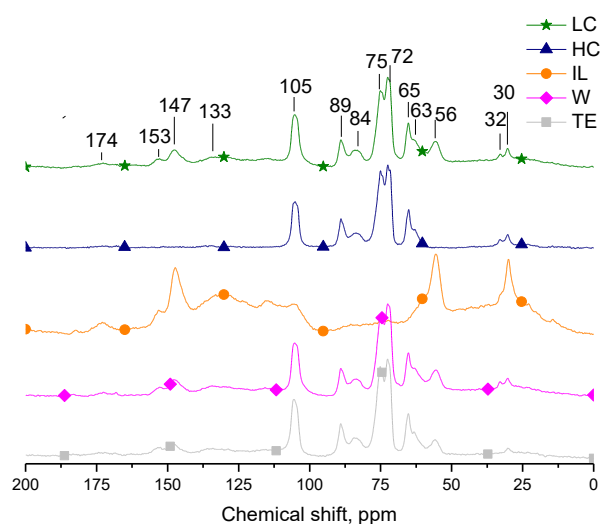
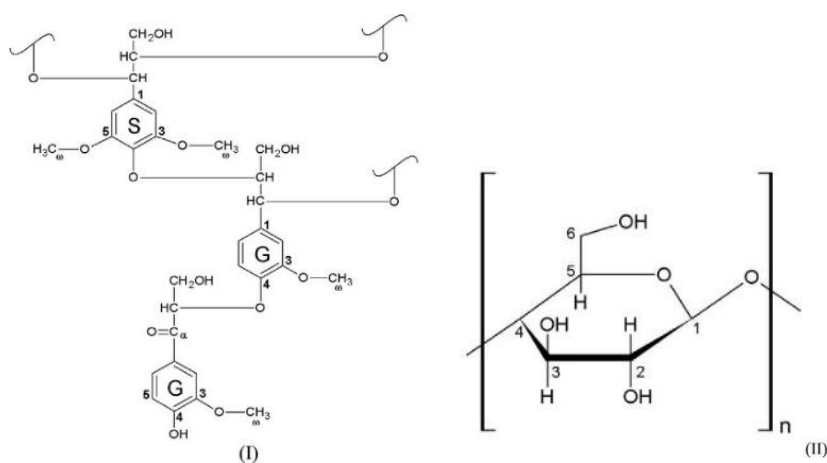


Figure 3.3: ^{13}C CP MAS-NMR spectra of LC and its derivatives. The curves were vertically translated.

Table 3.1: Signal assignment in ^{13}C CP MAS-NMR spectra of LC, IL, HC, W and TE.

Assigned carbon	δ (ppm)	Material	Unit
C_α	174	LC, IL	Carbonyl groups (I)
C_3 and C_5	153	LC, IL, W, TE	Etherified S units (I)
C_4	147	LC, IL, W, TE	Etherified G units (I)
C_3 and C_4	147	LC, IL, W, TE	Not etherified G units (I)
C_1	133	LC, IL, W, TE	Etherified S and G units (I)
C_5	115	LC, IL	G units (I)
C_1	105	LC, HC, W, TE	Glucosidic ring (II)
C_4	89; 84	LC, HC, W, TE	Glucosidic ring (II)
$\text{C}_2, \text{C}_3, \text{C}_5$	72; 75	LC, HC, W, TE	Glucosidic ring (II)
C_6	63; 65	LC, HC, W, TE	Glucosidic ring (II)
C_o	56	LC, IL, W, TE	Methoxy groups (I)
–	32	LC, IL, HC, W, TE	Waxes
–	30	LC, IL, HC, W	Aliphatic groups (I)

S = Syringyl; *G* = Guaiacyl



On the basis of what was discussed in Chapter 1, LC shows signals ascribable to both the main lignocellulosic macromolecular components, namely lignin and polysaccharides.

In the case of the isolated fractions, the ^{13}C CP MAS-NMR spectra show characteristic signals of lignin for IL, and of polysaccharides for HC. Such finding indicates the efficiency of the isolation procedures. More specifically, in the IL spectrum, aromatic carbons appeared between 110 and 170 ppm. In this range, the weak resonance centred at 153 ppm indicates etherified C_3 and C_5 of syringyl units. The sharp peak at 147 ppm refers to etherified C_4 and to both etherified and not

etherified C3 and C5 of guaiacyl units [Brosse et al., 2010; Lin and Dence, 1993]. Only a very weak resonance of carbonyl groups (C α) of lignin was detected at 174 ppm. Kolodziejcki et al., [1982] attributed the last resonance peak either to carbonyl lignin groups or to acetate hemicelluloses groups. Since we did not record any peak at around 22 ppm, which are generally attributed to methyl groups in hemicelluloses, we can definitely think that this component is not present in LC. At lower resonances the signal at 133 ppm refers to C1 in syringyl and guaiacyl units, the peak at 115 ppm is attributed to C5 of guaiacyl units [Wikberg and Maunu, 2004], and the signal at 56 ppm is due to methoxy groups (C ω). The HC spectrum displays signals characteristic of polysaccharidic components. Most of the resonances arise from glucosidic ring carbons of cellulose and range from 60 to 105 ppm. The sharp signal at 105 ppm corresponds to the anomeric carbon (C1) of the glucosidic ring. The resonances at 89 and 84 ppm are due to C4 of cellulose, the first one comes from crystalline domains, while the second one is from amorphous moieties of cellulose fibres [Maciel et al., 1982]. At lower frequencies, the C2,3,5 of cellulose generate a couple of resonances at 72 and 75 ppm. Finally, two peaks at about 63 and 65 ppm, ascribed to the C6 of amorphous and crystalline cellulose, were detected [Brosse et al., 2010]. In the vicinity of 30–32 ppm range, the resonances ascribed to alkyl carbon in long chain polymethylene type structures (e.g. lignin alkyl chains, fatty acids, waxes and resins) [Baldock et al., 1992; Donohoe et al., 2008] were detected. In the same region, the IL spectrum shows a sharp peak at 30 ppm with a weak shoulder at 32 ppm. The sharp signal at 30 ppm has been already described for lignin extracted through Klason method, and it was historically attributed to the alkyl groups of the side chains of lignin [Zeck et al., 1987]. On the other hand, the signal at 32 ppm is due primarily to extractable matter, such as fats and waxes that are part of the plant cell wall [Lichtfouse et al., 1998; Love et al., 1998]. This attribution was confirmed by the disappearance of this signal in the ^{13}C CP MAS-NMR spectrum of the solid residue, TE, obtained by the toluene/ethanol extraction of LC. As can be observed, water extraction did not affect the peak at 32 ppm since W was not deprived of its non-polar extractives.

TGA and DTG curves relative to LC and its derivatives are presented in Figures 3.4a and 3.4b, while the average thermal data are listed in Table 3.2.

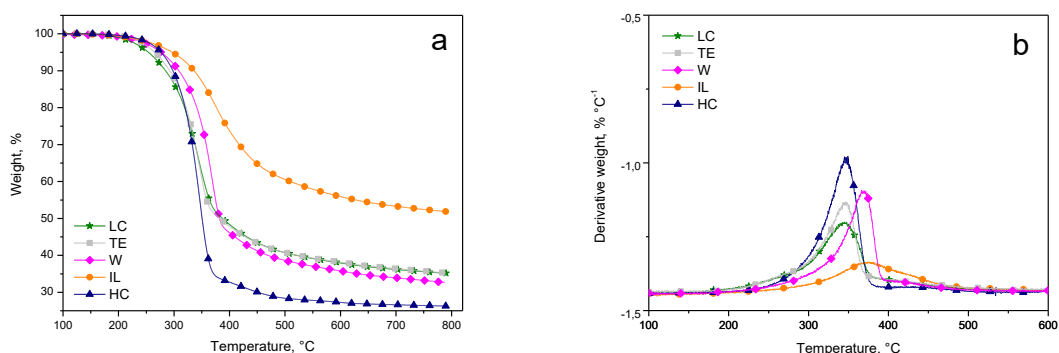


Figure 3.4: a) TGA and b) DTG curves under inert atmosphere of LC and its derivatives.

Table 3.2: Average thermal data of LC and its derivatives measured through TGA.

Sample	$T_{5\%}$ (°C)	T_{max} (°C)	$Char_{800}$ °C (%)
LC	253 ± 0.9	344 ± 1.1	35 ± 0.7
TE	263 ± 2.8	346 ± 0.7	33 ± 2.1
W	276 ± 2.1	369 ± 1.4	33 ± 0.1
IL	297 ± 1.8	374 ± 2.1	52 ± 0.5
HC	275 ± 0.8	346 ± 2.2	28 ± 3.5

The parent feedstock showed a rapid mass decrease which started at about 220 °C. More specifically, the onset temperature ($T_{5\%}$) and the temperature of the maximum decomposition rate (T_{max}) of LC were 253 °C and 344 °C, respectively. Toluene/ethanol extraction scarcely affected the thermal behaviour of LC and only modest variations of the thermal parameters were detected. Water extraction, on the contrary, caused a noticeable enhancement of the thermal performances of the extractive-free solid residue, W, which showed a considerable increase of $T_{5\%}$ and T_{max} compared to LC. The char yields, conversely, showed no relevant differences between LC and its extractive-free solid residues. These outcomes indicate that the water extraction treatment caused the removal, from the biomass, of a small quantity of a thermally unstable material, which also acted as a pro-degrading agent towards the lignocellulosic feedstock [Farid et al., 2015]. In order to get an insight into the nature of this pro-degrading component, the supernatant recovered after

the water extraction of LC was analysed by means of EDS spectroscopy. It was found that the extraction liquor contained approximately 3 mol% potassium ions, which were deliberately added to the *Arundo donax* biomass to adjust pH in the first stage of the bioethanol production process. Therefore, it is likely that the presence of potassium was responsible for the accelerated degradation.

The IL fraction that was obtained through the chemical removal of the whole polysaccharide component by acid treatment showed major variations with respect to LC. This sample exhibited a $T_{5\%}$ value of 297 °C and a T_{max} of 374 °C. These values were much higher than those recorded both for LC and the extractive-free solid residues. Moreover, the decomposition process appeared to be slower and spread over a broader temperature range. In addition, the char yield at 800 °C reached a much higher value equal to 52%.

These findings could be related to the chemical structure of the acid-insoluble lignin that was mainly made up of thermally stable, condensed aromatic moieties, since the more thermolabile polysaccharide fraction was removed. The HC sample, which was obtained through an oxidative delignification treatment, showed a $T_{5\%}$ similar to W. The T_{max} parameter, conversely, was close to that of the parent LC, while the char yield was the lowest among the examined samples. This can be attributed to the oxidative treatment and water washing the sample underwent. Such treatments selectively removed the lignin component, leaving a polysaccharidic cycloaliphatic material. In fact, HC showed a thermal behaviour comparable to LC, but it was more stable at the start of the thermodegradation process, due to the removal of pro-degrading agents by water washing [Gani and Naruse, 2007]. Finally, the occurrence of a low char yield was explained considering that the chlorite oxidative treatment, even if in mild acidic conditions, promotes a mechanism of acid hydrolysis that makes HC molecular weight decrease. Such reduced molecular weight molecules are more sensitive to degradation and decompose in a narrow thermal range [Hubbell and Ragauskas, 2010].

3.3 Conclusions

Lignocellulosic biowaste (LC) was chemically fractionated in order to isolate its main components, polysaccharides (HC) and lignin (IL). LC was also extracted with a toluene/ethanol mixture and water in order to remove organic and water-soluble extractives, and to recover two solid residues, TE and W. SEM and FTIR-ATR analyses performed on LC and its derivatives

showed that the removal of organic and water-soluble extractives from the biomass slightly affected the morphology and chemical structure. On the contrary, the chemical fractionations affected in a remarkable way IL and HC morphology, that differed significantly from LC. The chemical structure analysis, along with the morphological evidences, confirmed that the fractionation processes were carried out successfully. Two derivatives of lignin and polysaccharidic nature, indeed, were correctly isolated as also TGA analysis evidenced. IL showed the typical thermal attitude of lignin materials, which is rather different from HC, because of its more stable aromatic condensed structure. As regards the solid residues recovered after solvent extraction, TGA analysis evidenced that W was also characterized by a noticeable enhancement of thermal stability because water extraction allowed to remove a thermally unstable component. The extraction and fractionation treatments performed on LC allowed to isolate potential fillers to be used individually in poly(3-hydroxybutyrate) (PHB). The preparation and characterization of PHB-based lignocellulosic derivatives blends and bio-composites will be discussed in the next chapter in depth. According to this approach, it was possible to investigate which component of the lignocellulosic biomass affects polymer properties.

References

- S. Angelini, P. Cerruti, B. Immirzi, G. Santagata, G. Scarinzi, et al., *Int. J. Biol. Macromol.* 71 (2014)163-173.
- J. A. Baldock, J. M. Oades, A. G. Waters, X. Peng, A. M. Vassallo, M. A. Wilson, *Biogeochem.* 16 (1992) 1-42.
- K. Bon-Wook, M. Byeong-Cheol, G. Ki-Seob, L. Soo-Min, C. Joon-Weon, Y. Hwanmyeong, C. In-Gyu, *Biomass and Bioenergy* 42 (2012) 24-32.
- N. Brosse, R. El Hage, M. Chaouch, M. Pétrissans, S. Dumarçay et al., *Polym. Degrad. Stab.* 95 (2010) 1721-1726.
- M. Carrier, A. Lappinet-Serani, D. Denux, J. M. Lasnier, F. Ham-Pichavant, F. Cansell, C. Aymonier, *Biomass and Bioenergy* 35 (2011) 298-307.
- N. Cordeiro, M. N. Belgacem, I. C. Torres, J. C. V. P. Moura, *Ind. Crops Prod.* 19 (2004) 147-154.
- B. S. Donohoe, S. R. Decker, M. P. Tucker, M. E. Himmel, T. B. Vinzant, *Biotechnol. Bioeng.* 101 (2008) 913-925.
- A. Gani and I. Naruse, *Renew. Energy* 32 (2007) 649-661.
- H. Haykiri-Acma, S. Yaman, S. Kucukbayrak, *Fuel Process. Technol.* 91 (2010) 759-764.
- C. A. Hubbell and A. J. Ragauskas, *Bioresour. Technol.* 101 (2010) 7410-7415.
- M. J. Jackson and M. A. Line, *J. Agric. Food Chem.* 45 (1997) 2354-2358.
- M. S. Jahan, D. A. Nasima Chowdhury, M. Khalidul Islam, S. M. Iqbal Moeiz., *Biores. Technol.* 98 (2007) 465-469.
- W. Kolodziejcki, J. S. Frye, G. E. Maclell, *Analytical Chem.* 54 (1982) 1419-1424.
- S. Y. Lin and C. Dence, *Methods in lignin chemistry* (T. E. Timell, ed.) Springer-Verlag Editors, New York, (1993).

- E. Lichtfouse, C. Chenu, F. Baudin, C. Leblond, M. De Silva, et al., *Organic Geochem.* 28 (1998) 411-415.
- G. D. Love, C. E. Snape, M. C. Jarvis, *Phytochem.* 49 (1998) 1191-1194.
- G. E. Maciel, W. Kolodziejcki, M. Bertran, B. Dale, *Macromolecules* 15 (1982) 686-687.
- H. Rabemanolontsoa and S. Saka, *Holocellulose Determination in Biomass* (T. Yao, ed.), *Zero-Carbon Energy Kyoto*, Springer (2011) pp. 135-140.
- P. Sannigrahi (a), D. H. Kim, S. Jung, A. Ragauskas, *Energy Environ. Sci.* 4 (2011) 1306-1310.
- P. Sannigrahi (b), A. J. Ragauskas, S. J. Miller, *Bioenergy Resource* 1 (2008) 205-214.
- J. L. Soo, J. K. Hyun, J. C. Eun, S. Younho, B. Hyeun-Jong, *Int. J. Biol. Macromolecules* 72 (2015) 1056-1062.
- H. Wikberg and S. I. Maunu, *Carbohydrate Polym.* 58 (2004) 461-466.
- T. T. You, J. Z. Mao, T. Q. Yuan, J. L. Wen, F. Xu, *J. Agr. Food Sci.* 61 (2013) 5361-5370.
- W. Zeck, M. B. Johansson, L. Haumaier, R. L. Malcolm, *J. Plant Nutrition Soil Sci.* 150 (1987) 262-265.

Chapter 4

Poly(3-hydroxybutyrate)/Lignocellulosic Derivatives Blends and Bio-Composites

Prologue

This chapter deals with the use of LC derivatives as fillers in a thermoplastic biodegradable polyester (PHB). LC derivatives (TE, W, IL and HC) were obtained through solvent extractions or chemical fractionations performed on the biomass. All the derivatives were used at a 30 wt.% concentration, so as to make a comparison with the results recorded using the parent LC as filler in the same polymer matrix, as discussed in Chapter 2. This study provides an insight on the effect of lignocellulosic-based derivatives on the rheological, thermal, mechanical properties of PHB. A detailed focus is also given on the effect of the polysaccharidic fraction (HC) isolated from LC (used at 2, 5 and 10 wt.% concentration), after a sonication treatment on isothermal and non-isothermal polymer crystallization.

4.1 Experimental Section

4.1.1 Materials

A non-commercial, additive-free poly(3-hydroxybutyrate) (PHB) (lot T19, $M_w = 223$ kDa, $T_m = 175 \pm 0.3$ °C, $M_w/M_n = 1.23$), was supplied by Biomer (Germany).

Methanol, HPLC grade tetrahydrofuran and chloroform were purchased from Romil.

A lignocellulosic biomass (LC), biowaste from second generation bioethanol production process was provided by the Biomass Research Centre (CRB) of the University of Perugia, Italy.

Acid-insoluble lignin (IL), holocellulose (HC), extractive-free solid residues (TE, W) were isolated from LC according to the extraction and fractionation procedures described in the paragraph 3.2 of Chapter 3.

LC and its derivatives features are discussed in Chapter 1 and Chapter 3, respectively.

4.1.2 Methods of Preparation and Characterization

PHB/Lignocellulosic-derivatives blends preparation: TE, W, IL and HC were introduced as fillers at 30 wt.% in PHB matrix. The blends were obtained by a solvent-assisted method according to the conditions reported in paragraph 3.2 of Chapter 3. A LC-loaded blend was also prepared as reference. The obtained blends are referred to as PHB/TE, PHB/W, PHB/IL, PHB/HC and PHB/LC. Prior to measurements, all the samples were stored at 60 °C for 48h under vacuum.

PHB/sonicated holocellulose blends preparation: 1.25 g HC were dispersed in 30 mL of methanol and sonicated using an ultrasonic processor (Sonics Vibracell, 500 W, 20 kHz, Sonics & Materials, Newtown, CT, USA) at room temperature for 15 min alternating ON/OFF cycles lasting 40 and 30 s, respectively, with an amplitude of 30%. 11.25 g of PHB were added to the dispersion under mechanical stirring. The resulting dispersion was kept under continuous stirring at 190 rpm for 1 h. The blend was air-dried and then desiccated in an oven under vacuum at 60 °C until constant weight. The blend is referred to as PHB/HC10. Then blends with 5 and 2 wt.% HC were obtained by dilution of the PHB/HC10 parent formulation. The obtained blends are referred to as PHB/HC5 and PHB/HC2.

PHB bio-composites preparation: Compression moulded films were obtained by pressing 1.0 g of each blend at 190 °C and 4 ton for 5 min by means of a Carver Laboratory Press Model C.

Gel Permeation Chromatography essay: GPC was performed to evaluate average molecular weights and polydispersity (M_w/M_n) of freshly prepared and thermally treated PHB and PHB-based blends. A GPC Max Viscotek system was used, equipped with a TDA 305 triple detector at 30 °C, using Phenomenex Columns: precolumn, 10^6 and 10^3 Da.

Thermally treated samples were prepared as follows: 10 ± 1 mg of samples were put in aluminum pans and heat-treated at 190 °C for 900, 1800 and 2700 s by means of a Mettler DSC 822 calorimeter, under nitrogen (30 mL min^{-1}). Each sample was removed from the pan and suspended in chloroform (5 mg mL^{-1}), then the suspensions were kept at 50 °C under magnetic stirring for 48 h. In order to facilitate dissolution of the non-treated samples, the suspensions were cyclically sonicated by a Bransonic B 2200-E1 ultrasound processor. All the suspensions were filtrated

through PTFE pore size 0.20 μm filters, and 0.1 mL of each filtrate was injected. Tetrahydrofuran (THF) was used as eluent (0.8 mL min^{-1}) at $30 \text{ }^\circ\text{C}$. Universal calibration was made by using 10 polystyrene standard, ranging between 3×10^3 and 3×10^6 Da.

Rheological analysis: Rheological measurements were carried out in the dynamic flow field on neat PHB and its blends by means of a Thermo Fisher RS6000 stress controlled rotational rheometer, equipped with a 20 mm parallel plate geometry. *Dynamic Amplitude Sweep* (DAS) tests were performed in order to establish the linear viscoelastic range of the blends. A strain value of 0.09% was selected and used in the *Dynamic Time Sweep* and *Dynamic Frequency Sweep* tests. *Dynamic Time Sweep* (DTS) tests were performed at $190 \text{ }^\circ\text{C}$ for 4000 s, at 10 rad s^{-1} , with a gap size between plates of 1 mm.

Dynamic Frequency Sweep (DFS) tests were performed at $190 \text{ }^\circ\text{C}$, from high to low frequency over a $500\text{-}0.1 \text{ rad s}^{-1}$ range, with a gap size of 0.8 mm. In all experiments, the samples, in the form of cold-sintered discs, were loaded into the rheometer at the desired test temperature, under a nitrogen flow. The plates were rapidly approached to a gap size of 2 mm, then the gap was stepwisely reduced in about 100 s up to the measurement value.

Thermal analysis: Thermogravimetric investigations (TGA) were carried out by means of a Perkin Elmer Pyris Diamond TG/SDTA thermobalance with alumina pans using about 5 ± 0.5 mg of PHB and PHB-based blends. Measurements were carried out in nitrogen atmosphere under a flow rate of 30 mL min^{-1} . Each sample was analysed according to the following thermal program: heating from 30 to $90 \text{ }^\circ\text{C}$ at $20 \text{ }^\circ\text{C min}^{-1}$; isotherm at $90 \text{ }^\circ\text{C}$ for 30 min and heating from 90 to $800 \text{ }^\circ\text{C}$ at $10 \text{ }^\circ\text{C min}^{-1}$. The measurements were carried out in duplicate.

Differential Scanning Calorimetric (DSC) measurements were performed by means of a TA DSC-Q2000 instrument on 6 ± 0.7 mg of neat PHB and PHB-based blends, in nitrogen atmosphere. The samples were first heated from -50 to $200 \text{ }^\circ\text{C}$ at $10 \text{ }^\circ\text{C min}^{-1}$, kept in isothermal conditions for 1 min, then rapidly cooled to $-50 \text{ }^\circ\text{C}$ at $-50 \text{ }^\circ\text{C min}^{-1}$, kept in isothermal conditions for 4 min and reheated up to $220 \text{ }^\circ\text{C}$ at $10 \text{ }^\circ\text{C min}^{-1}$. DSC cooling rate for the blends was selected considering the typical cooling rates used during the polymer processing by means of a water chilled platen press. The glass transition and melting temperatures (T_g and T_m) were determined from the second heating scan. The crystallization temperatures, $T_{c \text{ melt}}$ and $T_{c \text{ cold}}$ were obtained from the cooling and the second heating scan, respectively. Melting enthalpy (ΔH_m), and melt and cold

crystallization enthalpy values ($\Delta H_{c\ meli}$; $\Delta H_{c\ cold}$) were determined by integrating the respective melting and crystallization peaks from melt and cold. The enthalpy values of the blends were obtained dividing the experimental value by the actual weight fraction of PHB (70 wt.%).

Bulk crystallization analysis: DSC measurements in dynamic and isothermal conditions were performed by means of a DSC 822 Mettler-Toledo instrument on neat PHB, PHB/HC2, PHB/HC5 and PHB/HC10 bio-composite films, in nitrogen atmosphere (20 mL/min).

The measurements in dynamic conditions were performed on 4.6 ± 0.2 mg of neat PHB, PHB/HC2, PHB/HC5 and PHB/HC10 blends in form of films, in nitrogen atmosphere (20 mL/min). The samples were first heated from -30 to 192 °C at 20 °C min⁻¹, kept in isothermal conditions for 5 min, then rapidly cooled to -30 °C at -30 °C min⁻¹, kept in isothermal conditions for 2 min and finally re-heated up to 200 °C at 10 °C/min.

The measurements in isothermal conditions were carried out on 6 ± 1 mg of each sample according to the following thermal program: heating from 30 to 192 °C at 20 °C min⁻¹, isotherm for 5 min, cooling up to selected crystallization temperatures, here in brackets, (118; 120; 122; 125; 127; 129 °C) at -30 °C min⁻¹. The films were kept in isothermal conditions for a time ranging from 60 to 180 min on the basis of the chosen crystallization temperatures. Finally, they were re-heated in a second heating scan up to 200 °C at 10 °C min⁻¹.

Optical polarized microscopy: Measurement of the spherulite radial growth rate (G_{MO}) of PHB, PHB/HC2, PHB/HC5 and PHB/HC10 crystals under isothermal conditions was performed using an optical polarized light microscope (Zeiss polarizing microscope, lens 10X) equipped with a hot stage (Linkam THMS-600). A small piece of each sample was squeezed between two microscope slides, then inserted in the hot stage in the microscopy. The samples were heated from 30 to 192 °C at a rate of 30 °C/min, melted at 192 °C for 5 min, rapidly cooled at a rate of 20 °C/min to the selected crystallization temperatures (T_c) and allowed to isothermally crystallize. Then, the films were re-heated at 10 °C/min up to 192 °C. The radius of the growing crystals was monitored by taking micrographs at appropriate intervals of time (15 s), using a JVC TK-1085E Video Camera coupled with the software Image-Pro Plus 7.0. Dried nitrogen was used as purge gas in the hot stage during all measurements and thermal treatments. For each sample around 30 photomicrographs of almost two different spherulites were taken. The spherulite radius (μm) was measured and plotted versus time. From the slope of the curves it was possible to record the spherulite growth rate, G_{MO} , at different crystallization temperatures (T_c).

Mechanical tests: PHB, PHB/LC, PHB/HC, PHB/IL, PHB/TE and PHB/W bio-composites films were cut in order to obtain dumbbell-shaped specimens (average thickness = 0.090 mm, width = 4 mm, length = 50 mm).

The specimens were conditioned in an environmental chamber at 25 °C and 50% relative humidity for 72 h prior to testing. Tensile tests were performed by means of a Instron model 4505 dynamometer, equipped with a 1 kN load cell. The tests were performed with a 2 mm min⁻¹ clamp separation rate. The reported mechanical parameters were the average values of 8 repetitions.

Morphological analysis: Fracture surfaces of neat PHB and the lignocellulosic derivatives-based bio-composites films, obtained from tensile tests, were observed by means of a FEI Quanta 200 FEG scanning electron microscopy (SEM). Before the observation, the surfaces were coated with Au-Pd alloy by means of a sputtering device (MED 020, Bal-Tec AG). The coating provided the entire sample surfaces with a homogeneous layer of metal of 18 ± 0.2 nm.

PHB and sonicated HC-based blends were cut in slides of 3 cm length and 1 cm width, then they were covered by an aluminum fold and placed in a hot stage where they were heated from 40 to 192 °C at 20 °C/min. Then, they were left in isothermal conditions for 5 min and cooled from 192 to 120 °C at 20 °C/min. In order to ensure the crystallization, all the samples were left at 120 °C for 30 min and cooled up to room temperature.

The samples were stored in a desiccator for 24 h; then they were fractured in liquid nitrogen. The obtained fracture surfaces were metallized with an Au-Pd alloy coating and examined through SEM.

4.2 Results and Discussions

4.2.1 Processability and Thermal Stability of PHB and PHB-Lignocellulosic Derivatives Blends

PHB-based blends were thermally treated at 190 °C, a temperature above the polymer melting point. The thermally treated samples were dissolved in chloroform, then the soluble portion was filtered and analysed by GPC in order to assess the effect of fillers on thermally-induced structural decay of PHB. The weight average molecular weight ($M_{w(t)}$), measured at different treatment times, was normalized dividing it by the molecular weight of the plain, non-treated PHB ($M_{w(0)}$). The

normalized parameter ($M_{w(t)}/M_{w(0)}$) as a function of time relative to PHB and its blends is reported in Figure 4.1a. Fresh neat PHB shows an M_w value of about 200,000 Da. Upon thermal treatment, after 2700 s at 190 °C PHB undergoes massive thermal degradation. Its M_w value, indeed, drops to 20% of the initial value (Table 4.1).

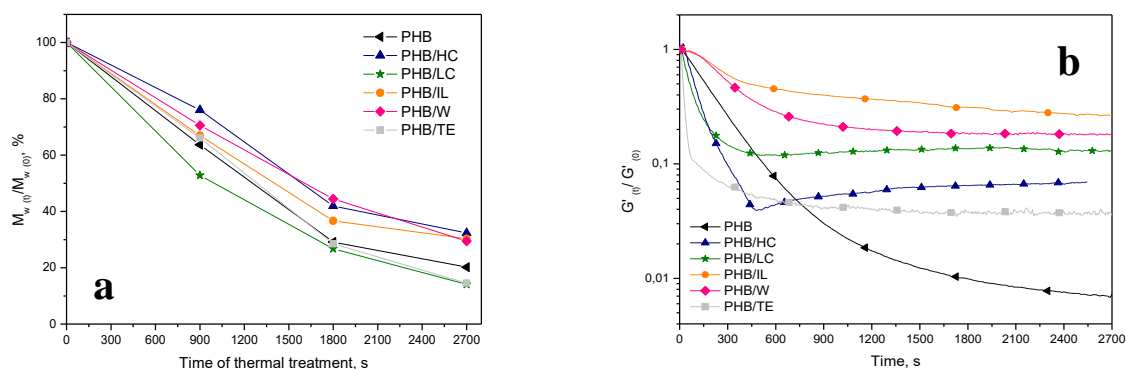


Figure 4.1: a) Normalized M_w vs time for heat-treated PHB and PHB-based blends; T=190 °C. b) Normalized G' vs time from *Dynamic Time Sweep* measurements.

GPC measurements showed that the decreasing trend of M_w for the soluble fractions of PHB/LC and PHB/TE was faster than that of the neat PHB. On the contrary, the drop in M_w for PHB/IL, PHB/HC and PHB/W was slightly slower than that of PHB. In particular, after 1800 s of thermal treatment, PHB/W loses 56% of M_w , compared with 72% lost by PHB/LC and PHB/TE. The improvement of molecular weight trend for PHB/W was correlated to the removal of a water-soluble fraction that is able to trigger PHB depolymerisation [Angelini et al., 2015 (a)]. The supernatant recovered after the water extraction of LC was characterized through EDS spectroscopy and an approximately 3 mol% potassium ions content emerged from the analysis. It was demonstrated that the presence of cations at carboxylate chain-ends accelerates PHB β -elimination-induced chain scission [Jiang et al., 2015; Farid et al., 2015]. Therefore, it is likely that the presence of potassium ions was responsible for the accelerated degradation and detrimental effect on the thermal stability of PHB. In addition, a direct effect of the filler on the chain scission mechanism of the macromolecule can also be envisaged. As known, the PHB thermal degradation involves the formation of a pseudo-six-membered transition structure, in which the carbonyl oxygen abstracts a labile acidic hydrogen ion from the γ -methylene. Eventually, crotonic acid and

oligomers with crotonate end groups form, and degradation is autocatalysed by the conjugation of crotonate end groups [Nguyen et al., 2002]. Therefore, the slight improvement of the molecular weight trend observed for some blends can be attributed to a retardation of the autocatalytic degradation due to the reaction between filler phenolic units and crotonic end groups.

The presence of the filler also influenced the effect of the degradation process on the molecular weight distribution of the polyester matrix (Table 4.1). An increase of plain PHB polydispersity index (M_w/M_n) from 1.23 to 1.85 by prolonging the time of thermal treatment was recorded and attributed to polymer degradation along with a larger distribution of molecular fragments with different weight-average molecular weights. This increase of polydispersity index was more significant for PHB/LC, where the filler acted as a pro-degrading agent toward the polymer. On the contrary, the presence of W and IL as fillers in PHB slowed down polymer degradation, as revealed by a lower polydispersity index.

The viscoelastic response of the polymer and its blends was investigated in order to evaluate the effect of the fillers on PHB melt stability and processing [Arza et al., 2014]. Shear storage modulus (G') was measured as a function of time at 190 °C for PHB and PHB-based blends. The storage modulus recorded at different times ($G'(t)$) was normalized dividing by the initial modulus value ($G'(0)$). The rheological trend of the normalized modulus ($G'(t)/G'(0)$) of PHB and its blends is displayed in Figure 4.1b as a function of time.

The initial PHB storage modulus, $G'(0)$, was about 28,000 Pa, then it rapidly dropped and reached a plateau stage. This trend is a rheological confirmation of the polymer thermal degradation indicated by the GPC measurements, which detected a drastic M_w drop for plain PHB. (Figure 4.1a, Table 4.1). As a matter of fact, after 2700 s in the rheometer chamber a dark-yellow molten material was recovered from the plates, as a clear evidence of thermal degradation.

Table 4.1: Storage modulus, weight-average molecular weight and polydispersity index of PHB and PHB-based blends after 2700 s at 190 °C.

Sample	G' (Pa)	M_w (kDa)	M_w/M_n
Neat PHB	207	45	1.85
PHB/LC	11000	20	2.54
PHB/HC	7700	55	1.60
PHB/IL	67000	67	1.18
PHB/TE	1608	27	1.60
PHB/W	9749	53	1.35

All blends showed higher $G'_{(0)}$ values compared to PHB. In particular the initial value of $G'_{(0)}$ was about 44,000 Pa for PHB/TE, 54,000 for PHB/W, 90,000 Pa for PHB/LC, 140,000 Pa for PHB/HC, and 250,000 Pa for PHB/IL. Similar to PHB, the rheological trend of the blends was decreasing over time. As for PHB/LC, in the first 400 s the decay of modulus was faster than that of PHB, confirming the pro-degrading effect of this filler evidenced by GPC and explained with EDS data. PHB/W, which was free of the water extractives, showed a more elastic behaviour than PHB/LC, since the polymer thermal degradation was retarded. On the other hand, PHB/TE exhibited a more pronounced decrease of $G'_{(t)}/G'_{(0)}$, reaching plateau values lower than PHB/LC.

This remarkable drop was related to a rapid reduction in molecular weight, suggesting that, in these experimental conditions, rheometry was more sensitive than GPC analysis in revealing polymer degradation. As for PHB/HC, the initial value of storage modulus ($G'_{(0)}$) was higher than that of PHB/LC. However, during the measurement it decreased steeply and eventually reached a pseudo steady state, whose values were lower than those recorded for PHB/LC. Conversely, PHB/IL showed the highest storage modulus values, that practically remained unchanged throughout the experiment. Therefore, rheological measurements indicated that the addition of IL to PHB improves melt stability over time. This outcome was attributed to the predominant stiffness of IL whose condensed and tight structure make it a more effective rheological modifier.

It can be hypothesized that degradation of PHB over the rheological test allows the creation of a co-continuous IL network percolated within the polymer matrix. The composite melt behaves as an elastic solid, responsible for the observed rheological properties.

To better investigate the effect of IL and HC on PHB and support the previously discussed hypothesis, *Dynamic Frequency Sweep* (DFS) tests were also performed and compared to the reference LC.

Figure 4.2a displays the logarithmic dependence of G' and G'' on the angular frequency, ω .

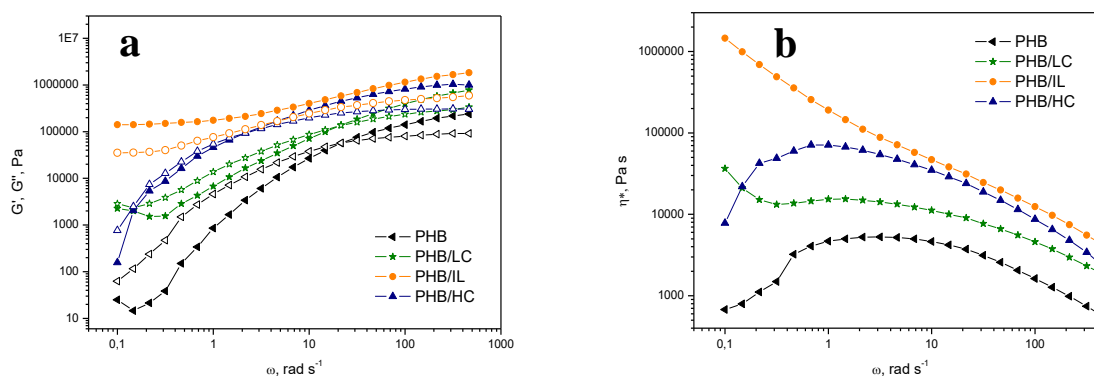


Figure 4.2: DFS plots of the viscoelastic properties vs the angular frequency for PHB and PHB-based blends: G' , G'' (a), η^* (b). Full and empty symbols refer to G' and G'' , respectively.

For plain PHB, in the low-frequency region the polymer melt behaviour was mainly viscous ($G' < G''$), while above 20 rad s⁻¹ the elastic character of the melt became dominant ($G' > G''$), and the moduli approached constant values in the rubbery plateau region [Commereuc, 1999]. On the other hand, a decrease in G' and G'' , with a slope even larger than 2, occurred in the low frequency terminal region of PHB. This finding was related to the occurrence of polymer thermal degradation during the DFS test. Indeed, the evaluation of the viscoelastic properties at low frequencies required a residence time of about 500 s at 190 °C, which brought about chain scission, as also demonstrated by the GPC and DTS measurements previously shown (Figure 4.1a, Figure 4.1b). This finding was also confirmed by the complex viscosity curve of pure PHB (Figure 4.2b). The latter, in addition to shear thinning behaviour for frequency values higher than 10 rad s⁻¹, and a Newtonian plateau at low frequencies, showed a distinct decay of viscosity in the lower-frequencies terminal region, due to the thermal degradation of the polyester matrix. PHB/LC exhibited a more marked viscoelastic behaviour, as G' and G'' values exceeded those of pure PHB all over the frequency range investigated. This result can be explained considering that the rigid LC particles, homogeneously dispersed in the composite, established an interparticle interaction with each other, limiting the mobility of the polymer chains in the melt [Lin et al., 2014, Reza

Barzegari et al., 2012]. It is worth noting that a distinct plateau in G' and G'' was observed at low frequency, relative to the transition from liquid-like to solid-like viscoelastic behaviour. This non-terminal behaviour can be attributed to the formation of an interconnected particle network in the melt, which has been reported for many particle-filled polymer composites [Jahani, 2010].

An evident confirmation of the network structure is provided by the complex viscosity curve, which at low-frequency turned up from a Newtonian plateau (Figure 4.2b). For lower frequencies, the material put up considerable resistance to flow (plastic response) and the corresponding viscosities were large (>1000 Pa s). At a frequency of about 0.3 rad s^{-1} the material exhibited a viscosity plateau. For even higher frequencies, the viscosity continued to drop down, with a typical shear thinning behaviour. This doubly shear-thinning behaviour results from two distinct and widely spaced shear-thinning mechanisms. The high frequency departure from Newtonian behaviour of PHB is over imposed with the lower frequency ($<0.3 \text{ rad s}^{-1}$) non Newtonian flow of the flocculated suspension of LC filler in the polymer melt, resulting in a complex curve which is reminiscent of the existence of a yield stress [Barnes, 1999]. The presence of 30 wt.% HC had an even larger impact on the viscoelastic properties of PHB, as a significant increase was observed for G' , G'' and η^* . The holocellulose filler was able to further restrict the molecular mobility of PHB, due to the hydrodynamic effect of the particles, resulting in a blend with a more elastic behaviour. This effect was confirmed by the shift of the crossover point between G' and G'' to lower frequency (about 3 rad s^{-1}), compared to pure PHB and PHB/LC. An interesting insight on the influence of HC on the microstructure of the blend is provided by the observation of the viscoelastic response at low frequencies. In this region, the rheological curves of PHB/HC resembled very much to that of pure PHB, showing a conventional terminal behaviour for G' and G'' ; moreover, no pseudo-yielding was observed from the complex viscosity curve. These observations suggest that, in spite of the strong thickening effect, HC particles are not able to form a stable interconnected network; it is likely that the interparticle interaction can be disrupted under shearing due to the orientation of the high aspect ratio fibrous filler. Further evidence of the importance of the filler size and shape on the microstructure of the blend melt is provided by the rheological results regarding PHB/IL. This blend displayed even higher values of moduli and complex viscosity. Moreover, a limited dependence of moduli on the frequency was found, confirming the formation of a strongly tightened particle network within the matrix.

The solid-like response due to the physical contacts between lignin particles hindered viscous motions of the material, and resulted in a more evident shear thinning behaviour. The complex viscosity curve was devoid of any Newtonian plateau, as the rheological performance of the blend was mainly dictated by the formation of a three-dimensional lignin particulate network. The strong particle interaction increased the non-Newtonian range and caused it to occur at a lower, experimentally inaccessible, shear rate with respect to that of the unfilled polymer melt.

It was thus found from rheology that the addition of all fillers significantly enhanced the viscoelastic response of PHB. However, holocellulose mainly restricts molecular mobility due to hydrodynamic effect of the particles, whereas the lignin and lignocellulosic-filled composite behaved as a physical gel due to the formation of a three-dimensional particulate network.

In Figure 4.3 and in Table 4.2, TGA thermograms and average thermal data of all the PHB-based blends are shown.

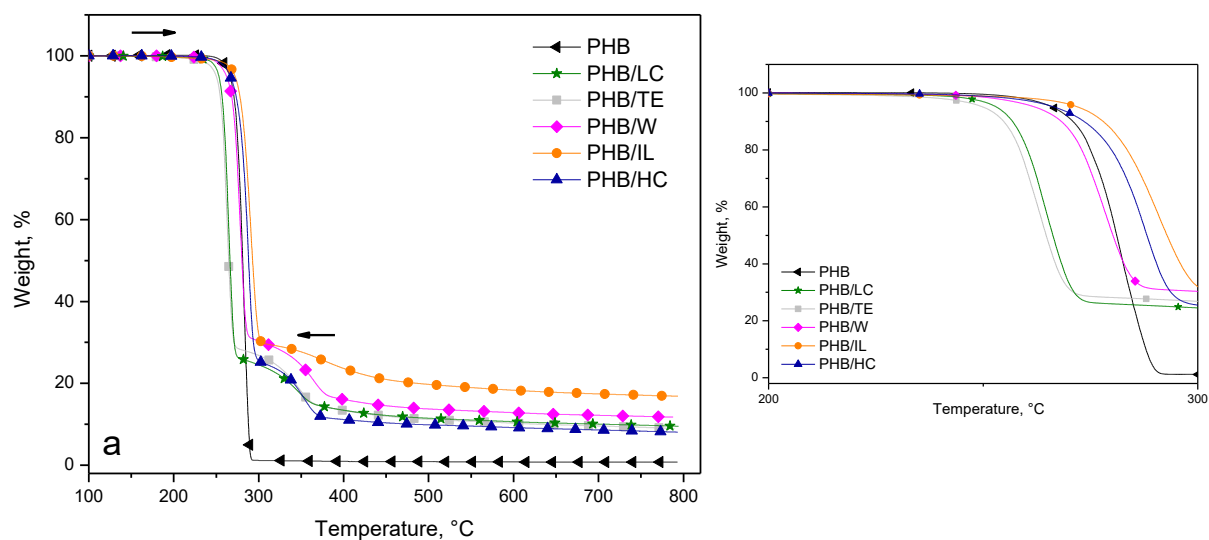


Figure 4.3: TGA curves under inert atmosphere of neat PHB and PHB-based blends.

Table 4.2: Average thermal data of neat PHB and PHB-based blends measured through TGA.

Sample	$T_{5\%}$ (°C)	T_{max1} (°C)	T_{max2} (°C)	$Char_{800\text{ °C}}$ (%)
PHB	266±0.3	282±0.2	-	0.6±0.2
PHB/LC	253±0.1	265±1.2	347±0.5	8.7±0.4
PHB/TE	253±4.0	265±2.3	348±1.4	9.9±1.2
PHB/W	265±3.0	279±2.7	365±0.9	11.8±0.2
PHB/IL	272±0.1	291±0.1	378±0.5	16.0±1.2
PHB/HC	267±2.1	289±2.7	354±0.3	9.7±2.4

Neat PHB degraded through a single weight loss step that started at about 250 °C. The polymer decomposition process was very fast, as complete volatilization was achieved within 300 °C. All the blends showed a second weight loss step, ascribed to the thermal degradation of the respective fillers. It is worth noting that the thermal stability of PHB was significantly affected by the kind of treatment the fillers were subjected to. In particular, LC and TE acted as pro-degrading agents, since the PHB weight loss step was anticipated by more than 10 °C, as evidenced in the inset of Figure 4.3 and by thermal parameters reported in Table 4.2.

Conversely, the W filler had no effect on PHB, as confirmed by the $T_{5\%}$ value. It was also noticed that none of the fillers caused significant changes in the thermogram slope, suggesting that the degradation mechanism was not affected, although the curves were shifted in temperature.

The different behaviour between PHB/LC and PHB/W confirmed that LC contained a water-soluble fraction able to trigger the depolymerisation of PHB. The enhancement of the thermal parameters relative to the PHB/W blend pointed out that its removal restored the thermal degradation behaviour of the polymer.

Finally, it is noteworthy to observe that both HC and IL slightly improved the thermal stability of PHB. In particular, IL was able to increase the $T_{5\%}$ value by about 6 °C. Persico et al., [2012] reported an enhancement of the thermal stability of PHB by adding grape pomace extract, hypothesizing that the formation of hydrogen bonds between the hydroxyl groups of the phenolic additive and polymer carbonyls could interfere with the formation of the transition structure involved in the random chain scission. Similarly, in the present case, lignin phenols in IL might interact with the PHB polar moieties, thus retarding polymer degradation.

4.2.2 Crystallization of PHB and PHB-Lignocellulosic Derivatives Blends

PHB and the PHB-based blends were characterized through DSC analysis to get insight on the effect of the fillers on polymer crystallization. All samples were submitted to a thermal treatment including a first heating scan from room temperature up to complete melting, a successive rapid cooling step to below the glass transition temperature and a second heating run. The first heating scan and the following rapid cooling were carried out to erase the thermal history of the polymer and to simulate the thermal treatment typical of compression moulding processing. The second heating run was carried out to evaluate the effect of fillers on the calorimetric properties of the specimens. Figure 4.4 reports the DSC thermograms relative to the cooling scan (a) and the second heating run (b) of PHB and PHB-based blends. Table 4.3 lists the main DSC thermal parameters.

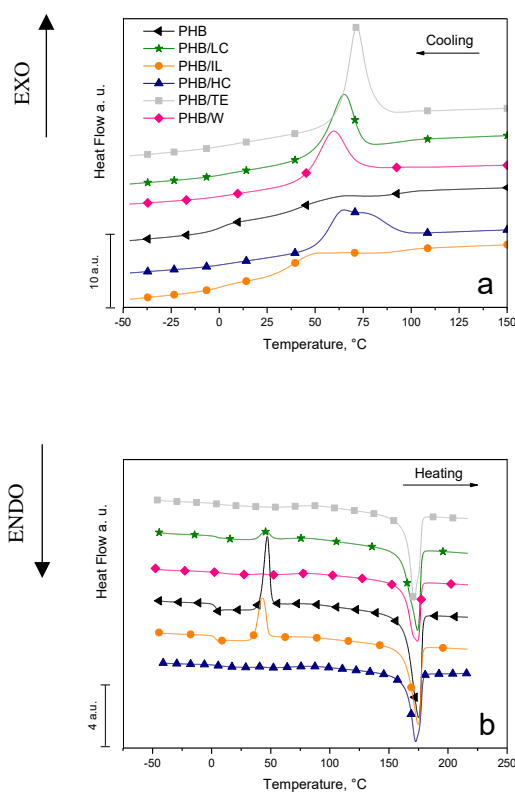


Figure 4.4: DSC a) cooling and b) second heating scans of PHB and PHB-based blends. All the curves were vertically translated.

Table 4.3: Main thermal parameters of PHB and PHB-based blends measured through DSC.

Sample	$T_{c\ melt}$ (°C)	$\Delta H_{c\ melt}$ (J g ⁻¹)	T_g (°C)	$T_{c\ cold}$ (°C)	$\Delta H_{c\ cold}$ (J g ⁻¹)	T_m (°C)	ΔH_m (J g ⁻¹)
PHB	63.2±0.9	15.3±0.7	3.8±0.2	46.6±0.7	72.8±7.3	175.0±0.3	83.3±1.5
PHB/LC	62.9±3.1	45.0±3.9	4.6±0.2	46.7±0.4	30.0±2.9	173.6±0.7	83.1±0.2
PHB/IL	47.3±4.0	27.9±4.0	3.8±0.1	41.6±2.1	50.0±2.2	174.8±0.1	83.7±1.9
PHB/HC	62.2±1.9 (75±1.3)	49.7±4.5	4.7±0.8	41.2±0.7	15.7±0.5	172.4±0.2	82.3±2.6
PHB/TE	73.2±2.2	60.2±3.5	5.4±1.1	-	-	172.0±1.3	84.2±2.9
PHB/W	60.0±1.1	45.9±2.3	5.9±0.9	-	-	174.5±0.5	80.5±0.3

During the fast cooling step (Figure 4.4a), plain PHB displayed only a broad signal of melt crystallization. This effect was due to the growth of sporadic PHB spherulites and to the rapid cooling rate that limited the capability of polymer chains to arrange regularly [El-Hadi, 2012]. This phenomenon is typical for PHB and gives rise to irregular DSC exotherms because of the growth and impingement of a limited number of crystals.

In the second heating scan (Figure 4.4b) the PHB glass transition signal at about 4.0 °C (Table 4.3) was detected, followed by a cold crystallization exothermal peak at 46.6 °C and a melting endotherm signal at 175 °C. The cold crystallization phenomenon, detected during the second heating scan, represents an indirect measurement of the crystallinity of the sample after the previous fast cooling stage. The presence of this signal indicates that PHB was unable to crystallize properly during the rapid cooling scan. During the successive heating run, above glass transition the macromolecules acquire enough mobility to aggregate and crystallize.

From DSC measurements carried out on PHB/TE and PHB/W blends, it was evidenced that both the blends showed melt crystallization (Figure 4.4a). Moreover, it can be emphasized that the TE based sample exhibited a melt crystallization temperature remarkably higher with respect to the W blend (at 73 and 60 °C, respectively). The effect can be ascribed to the action of water extractives that were still present in TE specimen. It has been previously shown that these water extractable compounds are able to promote PHB degradation [Angelini et al., 2015 (a)]. As pointed

out above, these pro-degrading products, still present in TE, caused a PHB molecular weight drop. The low molecular weight chains produced were more prone to crystallize with respect to the parent polymer. As a result, the melt crystallization phenomenon occurs at a higher temperature compared to PHB/LC. As regarding PHB/W, the absence of pro-degrading water extractives caused the melt crystallization peak to be shifted to lower temperatures than PHB/LC.

In both samples, the occurrence of complete crystallization during the cooling scan resulted in a negligible cold crystallization peak during the following re-heating run (Figure 4.4b).

Lastly, the only filler that was not able to promote melt crystallization was IL. The presence of IL, indeed, caused the remarkable decrease of $T_{c\ melt}$ and $\Delta H_{c\ melt}$ values (Table 4.3).

Generally, it has been reported that lignin can favour or inhibit PHB crystallization, depending on the plant source and isolation procedures [Weihua et al., 2004; Bertini et al., 2012]. An acid-insoluble lignin with a strongly condensed structure was obtained and it was able to form a co-continuous percolated network within the PHB melt. The presence of a stiff IL network reduced chain mobility, thus hampering PHB crystallization. In the subsequent heating run, an exothermal signal due to cold crystallization was detected.

None of the used fillers affected PHB melting and glass transition temperature. However, a strong influence on the crystallization behaviour was found. In particular, during the quenching step, the presence of HC and LC promoted PHB melt crystallization in spite of the rapid cooling. More specifically, the inclusion of HC resulted in the formation of a double crystallization peak, located at about 75 and 62 °C. This outcome was in agreement with literature data, which reported that cellulose and some of its variants were able to promote crystallization of some bio-based polymers as PHB and poly(L-lactide) (PLLA) [El-Hadi et al., 2012; Pei et al., 2010]. The introduction of LC also promoted PHB crystallization, as confirmed by a sharp melt crystallization peak at about 63 °C. This result can be related to the presence in the biomass of a considerable portion of holocellulose that, as evidenced above, promotes PHB crystallization. From an examination of the heating runs, relative to both the HC and LC-based blends (Figure 4.4b), it can be noticed that the exothermal peak associated with the cold crystallization process undergoes a remarkable reduction, since most of the polymer melt properly crystallized during the cooling scan.

4.2.3 Crystallization of PHB/Sonicated Holocellulose Bio-Composites

PHB crystallinity is strongly dependent on the physicochemical conditions occurring during the crystallization process. The presence of fillers, as described in the previous section, can affect the crystallization behaviour of the polyester in a noticeable way. The action depends on their nature, size and shape, which can play a relevant role on crystallization parameters. This effect has been shown for many kinds of fillers such as silica [Hong and Huang, 2015], nanotubes [Xu and Qiu, 2009] as well as lignocellulose and its derivatives [Weihua et al., 2004; Borysiak, 2012] introduced in polymeric matrices.

Cellulose is a well-known component of lignocellulosic biomass, which is largely used as filler in PHB and other bio-based polymers with the aim to obtain bio-composites. It has been shown that the introduction of this component accelerates the crystallization process to such an extent that depends on the degree of aggregation, dimensions and distribution of the filler in the matrix [Pei et al., 2010; Kamal and Khoshkava, 2015].

In the previous section, the morphological and chemical analyses demonstrated that HC is mainly made up of cellulose microfibrils aggregated in compact bundles. On the other hand, the calorimetric investigation proved that HC was able to promote PHB crystallization process when it was added as filler. In the studied system, however, the HC tendency to aggregate hampers a more detailed analysis of its effect on PHB crystallization.

Therefore, driven by the aim to overcome these shortcomings, the holocellulose fraction isolated from LC biomass was submitted to sonication on the basis of Saito et al., [2013] work. Then, it was introduced as filler in PHB and its effect on isothermal and dynamic polymer crystallization was investigated.

It was shown that the ultrasound treatment affected aggregation, shape and dimension of HC in a remarkable way. The HC bundles resulted completely disaggregated; the length of the fibres was dramatically reduced to an average of 50 μm , and most of them appeared fragmented in rigid rod-like particles with irregular rough surfaces (Figure 4.5).



Figure 4.5: SEM micrographs of HC before and after sonication treatment.

Figure 4.6 reports the DSC thermograms, recorded in dynamic conditions, relative to the cooling scan (a) and the second heating run (b) of plain PHB and sonicated HC bio-composites.

Table 4.4 lists the main DSC thermal parameters.

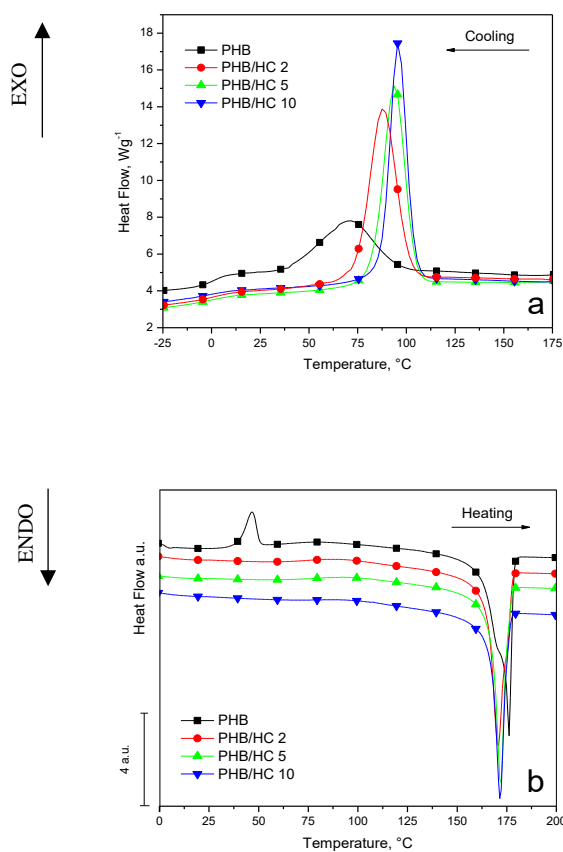


Figure 4.6: DSC a) cooling and b) second heating DSC scans of PHB and PHB/sonicated HC bio-composites. All the second heating curves were vertically translated.

Table 4.4: Main thermal parameters of PHB and PHB/sonicated HC bio-composites measured through DSC.

Sample	$T_{c\ melt}$ (°C)	$\Delta H_{c\ melt}$ (J g ⁻¹)	T_g (°C)	$T_{c\ cold}$ (°C)	$\Delta H_{c\ cold}$ (J g ⁻¹)	T_m (°C)	ΔH_m (J g ⁻¹)
PHB	71.2	37.9	2.8	46.7	42.1	170.2 175.7	82.8
PHB/HC2	88.5	65.4	3.6	-	-	170.2	87.8
PHB/HC5	94.5	70.7	7.8	-	-	171.4	91.4
PHB/HC10	96.6	71.9	-	-	-	171.2	92.1

Figure 4.6a illustrates the heat-flow DSC profiles of PHB/sonicated HC bio-composites, measured during cooling after the melting stage.

Before being cooled, the samples were heated up to 192 °C in order to erase previous polymer thermal history. In this way, complete melting of PHB crystals is allowed, avoiding the self-nucleation process of non-completely melted crystallites according to Di Lorenzo et al., [2009 (a)]. From a comparison of Figure 4.4a and Figure 4.6a it is evident that PHB melt crystallization is strongly dependent on the rate during cooling. In the plain PHB heat-flow profiles, in fact, a poorly defined crystallization signal is visible when the polymer is cooled at -50 °C/min (Figure 4.4a). By decreasing the cooling rate from -50 up to -30 °C/min, an irregular bell-shaped exothermal signal starting from 100°C occurs (Figure 4.6a). The signal is broad and asymmetric, due to the simultaneous spherulites growth, which provokes impingement phenomena. PHB nucleation occurs homogeneously because microbially-produced PHB is an almost pure material, which lacks impurities or defects that could act as nucleating points [Di Lorenzo et al., 2007 (b)]. In addition, the irregular melt crystallization shape was attributed to the formation of different groups of crystals, having different degrees of perfection due to the occurring impingement phenomenon (Figure 4.6a).

During the second heating run after cooling, cold crystallization was detected in the plain PHB curves (Figure 4.4b and Figure 4.6b). In particular, regular bell-shaped signals followed by a broadening of the baseline were observed. The relative areas and half-height widths of cold crystallization peaks depended on the rate adopted during the cooling stage [Wellen et al., 2015].

Decreasing the cooling rate from -50 to -30 °C/min, indeed, resulted in a $\Delta H_{c\ cold}$ value of 42.1 J g⁻¹ (Table 4.4). This value was significantly lower than that recorded when PHB was cooled at -50 °C/min (72.8 J g⁻¹, Table 4.3). The presence of this signal represents an indirect measurement of the crystallinity of the sample and indicates that PHB was unable to crystallize properly during the previous rapid cooling stage.

Multiple melting peaks were observed during the second heating scan: a major peak at 175.7 °C was preceded by a shoulder at 170.2 °C (Figure 4.6b). This outcome is a rather common feature for the most of semi-crystalline polymers and was attributed to the melting of the different types of formed crystals, with different sizes and thermal stabilities [Wellen et al., 2015]. Specifically, smaller and less perfect crystals melt at a lower temperature than larger and more perfect ones do.

As regards the bio-composites (Figure 4.6a and Table 4.4), in the cooling stage an increase of the maximum melt crystallization temperatures ($T_{c\ melt}$) was noticed, along with relative higher enthalpy values ($\Delta H_{c\ melt}$) with respect to plain PHB. These changes were proportional to the content of sonicated HC, suggesting a nucleating effect of HC fibres on PHB. Several researchers pointed out the nucleating activity of cellulose or lignocellulose fibres in their works on crystallization of PHB blends [Krishnaprasad et al., 2009; El-Hadi, 2012; Chen et al., 2015].

However, in the present case, further investigations with the aim to confirm this interpretation are necessary and still in progress.

During the second heating run, no cold crystallization phenomena were detected, suggesting that all the bio-composites were able to crystallize completely on cooling. Moreover, from Figure 4.6b it was observed that melting of bio-composites occurs with a sharp and simple endothermal signal, at lower temperatures (T_m) compared to PHB. This outcome could be due to formation of more defective PHB spherulites promoted by the presence of sonicated HC [Chen et al., 2015]. Furthermore, these data could be also explained by the sonication-induced size reduction of HC fibres that could have improved interfacial adhesion between filler and matrix, giving rise to more miscible systems [Wang et al., 2003].

In order to better investigate the effect of sonicated HC on PHB crystallization, isothermal DSC and polarized optical microscope analyses were also performed. Figure 4.7 (top row) shows the optical micrographs under polarized light relative to plain PHB and sonicated HC bio-composites, taken at a selected crystallization temperature (127 °C).

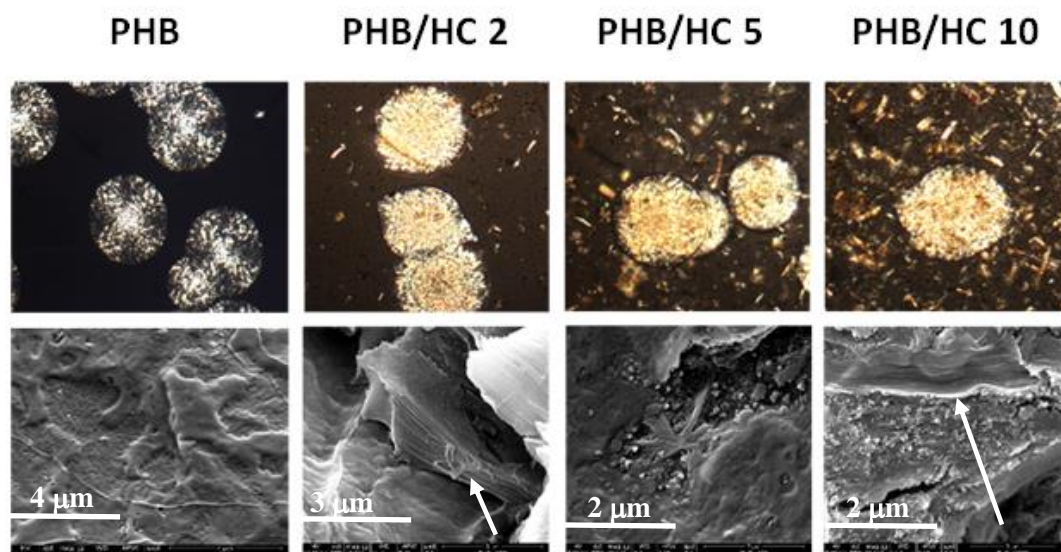


Figure 4.7: (top row) Optical photomicrographs of PHB spherulites grown at 127 °C; (bottom row) SEM images of fracture surfaces of crystallized samples.

The optical microscopy analysis evidenced that sonicated HC microfibers were clearly visible as birefringent spots characterized by a wide range of shapes and dimensions. During the isothermal crystallization the HC randomly oriented fibres only contributed a weak diffuse birefringence. On the other hand, plain and filled PHB produced big size spherulites with irregular and zigzag textures that grew until they impinged on each other.

These data were in agreement with those reported by Chen et al., [2015], who observed this kind of spherulite morphology when PHB crystallized at temperatures higher than 110 °C. In this thesis, the bio-composites mostly presented similar spherulite morphological evolution. However, the presence of HC fibres slightly disturbed crystal growth, whereas no trans crystallinity phenomena were observed. Unfortunately, it was not possible to provide quantitative data on the number of spherulites due to the very low nucleation density and the large size of crystals, which was a typical feature of the studied polymer. Therefore, the area visualized under the optical microscopy may be not representative of the whole sample.

SEM images of the fracture surface of crystallized samples are shown in the bottom row of Figure 4.7. Plain PHB shows an almost smooth surface. The bio-composites, on the contrary, exhibit rough fracture surfaces, and it is possible to observe the cross-section of PHB spherulites,

characterized by a thick lamellar structure (indicated by arrows). Polarized optical microscopy was successfully used to monitor spherulite radial growth rate (G_{MO}) as a function of the crystallization temperature, as illustrated in Figure 4.8a.

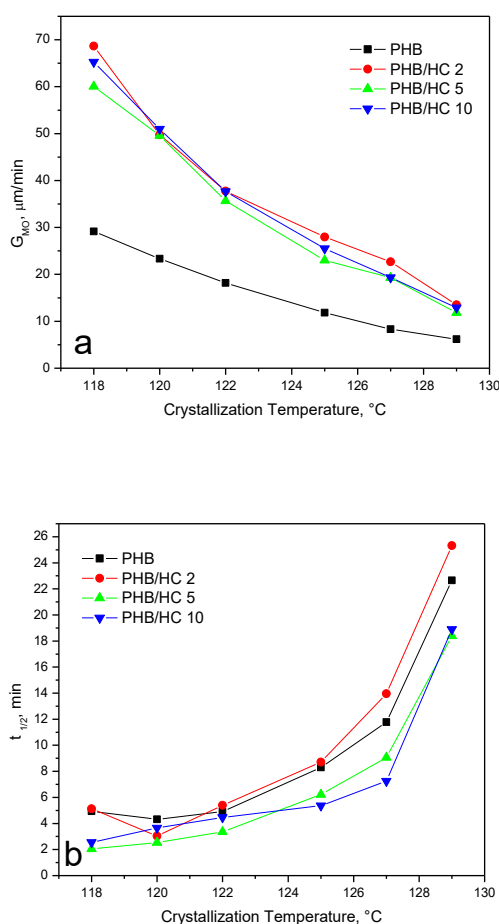


Figure 4.8: a) Spherulite radial growth rate (G_{MO}) and b) Half-time of crystallization ($\tau_{1/2}$) as a function of crystallization temperature.

As expected, in the analysed crystallization temperature range, PHB and bio-composites G_{MO} values decreased with increasing crystallization temperature. This result was well explained by the Hoffman–Lauritzen theory, that describes the crystallization of a polymer in terms of kinetics and thermodynamics factors [El-Taweel and Stoll, 2012]. Typically at very high as well as very low temperatures the polymer chain mobility is not as appropriate to allow the formation of crystal lamella.

As regards the bio-composites, a significant effect of sonicated HC on growth rate of PHB crystals was noticed. All the analysed bio-composites, indeed, showed a higher spherulite growth rate with respect to plain PHB. This outcome was tentatively attributed to a higher mobility of PHB molecules due to the addition of a filler containing low molecular mass fragments. The sonication treatment was probably responsible for the holocellulose fragmentation and deconstruction, that was accompanied by a reduction of molecular weight. This finding was observed in literature when PHB was filled with low molecular weight additives as lauric acid, dodecanol, tributyrin [Yoshie et al., 2000].

The overall crystallization rate of PHB and its sonicated HC bio-composites was also analysed by means of DSC analysis in isothermal conditions. Analyses were carried out on rather thick samples, where PHB spherulites can freely grow in three dimensions.

The investigation provided information on bulk crystallization kinetics, including nucleation. The experimental data of isothermal bulk crystallization rate were analysed according to the theory of phase transformation proposed by Avrami, which relates the overall change of crystallinity to the crystallization time [Avrami, 1939]:

$$1 - X_c(t) = \exp[-(Kt)^n]$$

where $X_c(t)$ is the relative crystallinity at crystallization time t , while K and n are constants related to the crystalline morphology and the mechanism of nucleation: K is the temperature-dependent crystallization rate constant, and n is the Avrami index. The values of Avrami index, reported in Table 4.5, are around 2-2.6 for plain PHB and for all the bio-composites, independently of temperature. This finding proves that sonicated HC did not affect the crystallization mechanism of PHB.

A value of Avrami index $n=2$ suggests heterogeneous nucleation coupled with bidimensional growth of the crystals.

Table 4.5: Avrami index, n determined at the indicated crystallization temperatures.

Sample	118 °C	120 °C	122 °C	125 °C	127 °C	129 °C
PHB	2.5	2.6	2.0	2.6	2.1	2.3
PHB/HC2	2.3	2.3	2.3	2.5	2.5	2.6
PHB/HC5	2.1	2.5	2.2	2.3	2.2	2.2
PHB/HC10	2.3	2.5	2.5	2.3	2.3	2.5

DSC data were in agreement with optical microscopy results, despite in the latter technique very thin samples, melt squeezed between two microscope slides were examined [Avella et al., 2006]. Figure 4.8b illustrates the dependence of the half-time of crystallization ($\tau_{1/2}$) versus crystallization temperature. $\tau_{1/2}$ represents the time required for one half of total crystalline phase to crystallize. It was calculated from the DSC melt exothermal crystallization signal, and mathematically from the measured kinetic parameters reported in the equation below:

$$\tau_{1/2} = \left(\frac{\ln 2}{Kt}\right)^{1/n}$$

It was shown that the addition of sonicated HC produced a reduction of the half-time of crystallization value, in the case of PHB/HC5 and PHB/HC10. Conversely, no remarkable effect on $\tau_{1/2}$ of the PHB/HC2 sample was observed. Overall, a promotion of PHB crystallization was observed when sonicated HC filler was added.

4.2.4 Mechanical and Morphological Characterization of PHB and PHB-Lignocellulosic Derivatives Bio-Composites

The PHB-based bio-composites, in the form of dumbbell-shaped films, were characterized through tensile tests in order to get an insight into their mechanical performance. Table 4.6 lists the mechanical parameters measured from the stress-strain curves.

Table 4.6: Average mechanical data of neat PHB and PHB-based bio-composites measured through tensile tests.

Sample	Tensile properties		
	E (MPa)	σ_b (MPa)	ε_b (%)
PHB	3028±165	18.8±3.7	2.2±1.1
PHB/LC	2554±437	11.6±2.5	0.5±0.1
PHB/TE	4187±141	14.6±1.7	0.6±0.1
PHB/W	3599±123	14.0±1.3	0.6±0.1
PHB/IL	3326±193	14.0±1.2	0.6±0.1
PHB/HC	3606±391	12.0±3.5	0.5±0.1

Plain PHB exhibited a stress-strain behaviour typical of a brittle polymer, characterized by failure occurring at low strain values [Abbate et al., 1991]. Compared to PHB, all the bio-composites displayed an overall worsening of mechanical properties, whatever the filler used.

In particular, an abrupt drop in tensile elastic modulus (E) and strength at break (σ_b) was evident for PHB/LC. On the other hand, the decrease in mechanical performance was less pronounced for the other lignocellulosic-derivatives based bio-composites. Their decay, with respect to the plain PHB, can be due to poor interfacial adhesion between filler and matrix, which causes the formation of voids acting as stress concentrators and starting points for fracture propagation under tensile stress [Angelini et al., 2014 (b)]. It is worth noting, however, that no detrimental effect was observed on modulus values. The elastic modulus (E) of PHB-based derivatives films was even higher than that of PHB. In particular, the E value of PHB/TE was almost 40% higher than that of PHB. It is likely that the toluene and ethanol mixture removed a non-negligible amount of low molecular weight products, which were able to plasticize the thermoplastic matrix. The resulting TE, indeed, behaved as a stiffer reinforcing agent than the parent LC. Moreover, the evident difference between PHB/LC and the other bio-composites also suggested that the pro-degrading effect ascribed to LC could lead to polymer degradation during film compression moulding.

Overall, these results demonstrate that the final properties of the bio-composites depend both on the type of filling biomass [Avèrous and Le Digabel, 2006] and the kind of pre-treatment carried out.

The morphological structure of plain PHB and its bio-composites with LC, IL and HC was analysed by SEM (Figure 4.9). The investigation was performed on fracture surfaces of film specimens obtained from the tensile tests reported previously [Angelini et al., 2015 (a)].

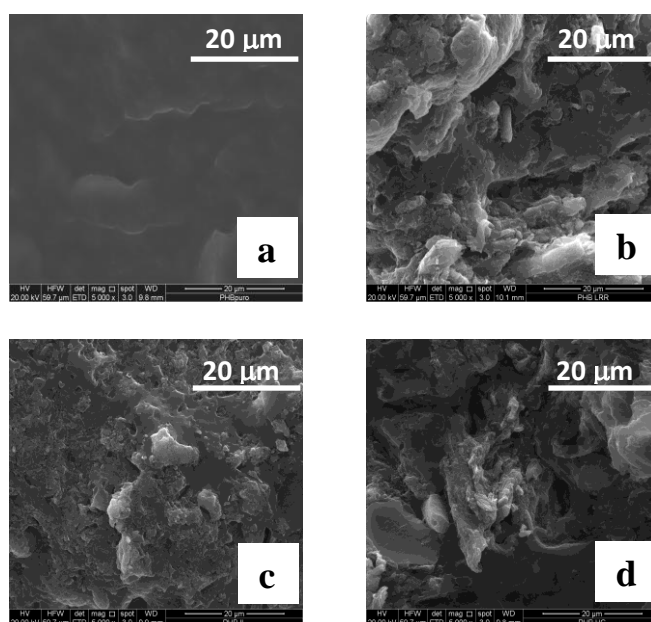


Figure 4.9: SEM micrographs of fracture surfaces of a) PHB; b) PHB/LC; c) PHB/IL and d) PHB/HC.

PHB exhibited a smooth and homogeneous appearance, typical of brittle materials (Figure 4.9a). The addition of LC and HC produced a more rough and irregular fracture surface, with clear evidences of phase separation between matrix and filler (Figure 4.9b and Figure 4.9d). Moreover, the presence of voids, probably caused by the filler pull out, was also detected. This latter feature can be attributed to the presence of particle lumps that were not embedded in the polymer melt during compression moulding of the films. In this regard, a poor matrix-filler adhesion can be pointed out. The presence of filler agglomerates, and their scarce interfacial adhesion with the matrix, produces an increase of internal tensions which result in a decrease of the stress at break during the tensile tests [Angelini et al., 2015 (a)]. On the contrary, there was no evidence of such flaws in the PHB/IL fracture surface (Figure 4.9c). In addition, in comparison with the LC and HC

based blends, the surface was smoother with a more homogeneous dispersion of the filler. Besides, no filler-matrix detachment was detected.

4.3 Conclusions

In summary, this chapter provides an insight on the effects of lignocellulosic derivatives on PHB. LC and its derivatives (TE, W, IL and HC) at 30 wt.%, and sonicated HC at 2, 5 and 10 wt.% were used as fillers in poly(3-hydroxybutyrate) (PHB). The rheological investigation, performed on PHB and lignocellulosic derivatives-based blends, evidenced a remarkable improvement of polymer viscoelastic properties. The effect was remarkable for the IL-based blend that showed, with respect to plain PHB, much higher moduli and complex viscosity values, with a limited dependence on time and frequency. The rheological response of this sample was due to the existence of a percolated co-continuous filler network inside the matrix. This finding was supported by SEM observation of the PHB/IL fracture surface, that was characterized by a smoother and more homogeneous aspect with respect to the other blends. The high melt viscosity of PHB/IL hampered polymer chain mobility and consequently crystallization phenomenon. On the other hand, HC promoted PHB crystallization. In particular, the sonication treatment performed on HC reduced the fibres into low molecular weight structures that acted as nucleating agents towards PHB. Compared to the plain polymer, most of the bio-composites displayed an overall worsening of mechanical properties, in terms of ductility, due to poor interfacial adhesion between the fillers and the matrix. However, in the case of the PHB/TE film an increase in elastic modulus (E) up to 40% was measured. Overall, the mechanical properties of the bio-composites depended both on the type of biomass used as filler and the kind of pre-treatment. As regarding the thermal stability, LC accelerates PHB thermal degradation, due to the presence of pro-degrading agents. Their removal through water extraction restored PHB thermal stability properties. The reported results, especially those from rheological and calorimetric analysis, are interesting since demonstrate that the addition of lignocellulosic fillers can modify the properties of PHB. This finding allow to produce bio-composites able to comply with some requirements needed in several market applications, such as better processability and limited physical aging.

References

- M. Abbate, M. Martuscelli, G. Ragosta, G. Scarinzi, *J. Mater. Sci.* 26 (1991) 1119-1125.
- S. Angelini (a), P. Cerruti, G. Scarinzi, M. Malinconico, *Cellulose Chem. Technol.* 50 (2015) 429-437.
- S. Angelini (b), P. Cerruti, B. Immirzi, G. Santagata, G. Scarinzi et al., *Int. J. Biol. Macromol.* 71 (2014)163-173.
- C. R. Arza, P. Jannasch, P. Johansson, P. Magnusson, A. Werker, F. H. J. Maurer, *J. Appl. Polym. Sci.* 132 (2014) 41836-41842.
- M. Avella, S. Cosco, M. L. Di Lorenzo, E. Di Pace, M. E. Errico, G. Gentile, *Europ. Polym. J.* 42 (2006) 1548-1557.
- L. Avérous, F. Le Digabel, *Carbohydr. Polym.* 66 (2006) 480-493.
- M. Avrami, *The Journal of Chemical Physics* 7 (1939) 1103.
- H. A. Barnes, *Applied Rheology* 9 (1999) 262-266.
- F. Bertini, M. Canetti, A. Cacciamani, G. Elegir, M. Orlandi, et al., *Polym. Degrad. Stab.* 97 (2012) 1979-1987.
- S. Borysiak, *J. Appl. Polym. Sci.* 127 (2012) 1309-1322.
- J. Chen, C. Xu, D. Wu, K. Pan, A. Qian, Y. Sha, L. Wang, W. Tong, *Carbohydrate Polym.* 134 (2015) 508-515.
- S. Commereuc, *J. Chem. Educ.* 76 (1999) 1528-1532.
- M. L. Di Lorenzo (a), P. Sajkiewicz, A. Gradys, P. La Pietra, *e-Polymers* 9 (2009) 313-324.
- M. L. Di Lorenzo (b), P. Sajkiewicz, P. La Pietra, A. Gradys, *Polym. Bulletin* 57 (2007) 713-721.
- A. M. El-Hadi, *Colloid Polym. Sci.* 291 (2012) 743-756.
- S. H. El Tawell and B. Stoll, *J. Macromol. Sci., Part B* 51 (2012) 567-579.

- N. F. S. M. Farid, H. Ariffin, M. R. Z. Mamat, M. A. K. M. Zahari and M. A. Hassan, RSC Adv. 5, (2015) 33546-33553.
- S.-G. Hong and S.-C. Huang, J. Therm. Anal. Calorim. 119 (2015) 1693-1702.
- Y. Jahani, J. Vinyl Additive Technol. 16 (2010) 70-77.
- Y. Jiang, G. Mikova, R. Kleerebezem, L. Van der Wielen, M.C. Cuellar, AMB Express 5 (2015) 1-13.
- M. R. Kamal and V. Khoshkava, Carbohydrate Polym. 123 (2015) 105-114.
- R. Krishnaprasad, N. R. Veena, H. J. Maria, R. Rajan, M. Skrifvars, K. Joseph, J. Polym. Environ. 17 (2009) 109-114.
- T. Liu, Q. Wang, Y. Xie, Q. Fu, Polym. Composites 37 (2014) 379-384.
- S. Nguyen, G. E. Yu, R. H. Marchessault, Biomacromolecules 3 (2002) 219-224.
- A. Pei, Q. Zhou, L. A. Berglund, Composites Sci. Technol. 70 (2010) 815-821.
- P. Persico, V. Ambrogi, A. Baroni, G. Santagata, C. Carfagna, et al., Int. J. Biol. Macromol. 51 (2012) 1151-1158.
- M. Reza Barzegari, A. Alemdar, Y. Zhang, D. Rodrigue, Polym. Composites 33 (2012) 353-361.
- T. Saito, R. Kuramae, J. Wohler, L. A. Berglund, A. Isogai, Biomacromolecules 14 (2013) 248-253.
- T. Wang, G. Cheng, S. Ma, Z. Cai, L. Zhang, J Appl. Polym. Sci. 89 (2003) 2116-2122.
- K. Weihua, Y. He, N. Asakawa, Y. Inoue, J. Appl. Polym. Sci. 94 (2004) 2466-2474.
- R. M. R. Wellen, M. S. Rabello, I. C. A. Junior, G. J. M. Fachine, E. L. Canedo, Polimeros 25 (2015) 296-304.
- C. Xu and Z. Qiu, Polym J. 41 (2009) 888-892.
- N. Yoshie, K. Nakasato, M. Fujiwara, K. Kasuya, H. Abe, Y. Doi, Y. Inoue, Polym. 41 (2000) 3227-3234.

Chapter 5

Lignosulfonates from Paper Mill

and

Their Use in Wood Flour-Based Particleboard

Prologue

In this chapter the outcomes acquired from the morphological, chemical and thermal characterization of calcium lignosulfonates, main biowastes of paper mill, are reported. Due to the significant polysaccharide content, the feedstock was purified by means of dialysis. The purification outcome was assessed investigating the chemical and thermal properties of the dialysed products. Plain and dialysed lignosulfonates were used as additives for the preparation of wood flour-based particleboards by using urea-formaldehyde resin as binder. The effect of the lignosulfonates on the particleboards fire performance was assessed by means of cone calorimeter tests and compared to that of a typical commercial fire retardant. Moreover, thermal stability and mechanical properties of the obtained particleboards were examined in detail.

5.1 Experimental Section

5.1.1 Materials

Calcium lignosulfonates (LS) were obtained from Burgo Group. Wood flour (WF) with particle size between 0-400 μm was provided by Beologic, Belgium. Urea-formaldehyde resin (UF Q110T) was obtained from KRONOSPAN Chemicals. Flame retardant Exolit AP 420 aqueous solution (45 wt.% solid content of a short-chain ammonium polyphosphate) was purchased from Clariant. In the following this product will be referred to as APP.

MilliQ water was used to perform the dialysis of LS solution. Concentrated sulfuric acid (95-98%) was purchased from Sigma-Aldrich.

5.1.2 Lignosulfonates Purification and Characterization

Dialysis: Dialysis was performed using SpectraPor 3 tubes of regenerated cellulose with a molecular mass cut-off of 3.5 kDa, 29 mm diameter and 45 mm flat width. LS aqueous solution at 10 wt.% concentration was filtered on paper (porosity 1-11 μm) and the brown, cloudy filtrate was dialysed against water for 12 h. After the dialysis, the solution was evaporated to dryness, under reduced pressure, at 80 °C. The obtained product, referred to as LD, was further dried in oven, under vacuum at 60 °C.

Morphological analysis: Morphological characterization of LS and WF was performed by means of Scanning Electron Microscopy (SEM) using a FEI Quanta 200 FEG device. The samples were mounted onto stubs by means of carbon adhesive tape and coated with a 20 nm thick gold/palladium layer by means of a modular high vacuum coating system Emitech K575X.

Chemical characterization: Solid-state ^{13}C CP MAS-NMR characterization was performed on LS and LD. Measurements were carried out using a Bruker Avance II 400 spectrometer operating at 100.47 MHz. Samples were spun at 10 kHz in 4 mm zirconium oxide rotors. Spectra were collected using a single pulse excitation sequence with a ^{13}C 90° pulse width of 3.2s, a recycle delay of 2s, a contact time of 2ms, by averaging 16,384 scans.

The dialysate before and after acid hydrolysis with H_2SO_4 was analysed by a Thermo Scientific Dionex Ultimate 3000 High Performance Liquid Chromatography (HPLC) equipped with an Aminex Biorad HPX87H column and a refractive index detector.

Thermal analysis: Thermogravimetric investigation (TGA) was carried out by means of a Perkin Elmer Pyris Diamond TG/SDTA thermobalance with alumina pans using about 5 ± 0.5 mg of LS or LD. Measurements were carried out in nitrogen atmosphere under a flow rate of 30 mL min^{-1} . Each sample was analysed according to the following thermal program: heating from 30 to 90 °C at 10 °C min^{-1} ; isotherm at 90 °C for 20 min and heating from 90 to 500 °C at 10 °C min^{-1} . The measurements were carried out in duplicate.

5.1.3 Particleboards Preparation and Characterization

Particleboard preparation: Particleboards were prepared using wood flour (WF) as filler, urea-formaldehyde resin (UF) as binder and LS, LD and APP as additives. UF was used at 15 wt.%

with respect to the total solid amount (150 g). First, WF was soaked in about 380g of water. Then, UF was added and the sludge was vigorously stirred in order to homogenize it. LS and LD were added to the system as a powder, while APP as an aqueous solution. The prepared formulations were poured in vessels and evaporated in oven at 60 °C overnight. Next, the samples were ground and sieved (using a sieve of 500 μm porosity) and vacuum-dried in oven, at 50 °C for 1 h. Finally, particleboards were obtained through hot pressing by means of Cortazar Especial platen press. The compounds were pre-heated for 1 min at 220 °C, then pressed for 3 min at 100 bar and cooled up to room temperature.

The obtained particleboards (density around 0.6 g/cm^3) were cut in order to obtain (10 x 10 x 0.5) cm^3 plates. All the plates were stored in a conditioning chamber at 23 °C and 48% relative humidity for a week before being tested. The particleboard codes and compositions are reported in Table 5.1.

Table 5.1: Particleboard codes and compositions (wt.%).

Sample	WF	LS	LD	APP
WF100	100	-	-	-
WF95-LS5	95	5	-	-
WF85-LS15	85	15	-	-
WF95-APP5	95	-	-	5
WF85-APP15	85	-	-	15
WF85-LS10-APP5	85	10	-	5
WF95-LD5	95	-	5	-
WF85-LD15	85	-	15	-
WF85-LD10-APP5	85	-	10	5

Cone Calorimeter test: Combustion experiments were performed on (10 x 10 x 0.5) cm^3 particleboards plates by means of a cone calorimeter (Fire testing Technology, FTT), at an incident heat flux of 35 kW/m^2 and a distance of 25 cm from the heater. The experiments were carried out in a 800 s time span. Time to ignition (t_{ig} , s), maximum heat release rate (HRR_{max} , kW/m^2), total heat release (THR, MJ/m^2), maximum average rate of heat emission (MARHE, kW/m^2), mass loss (%), total smoke production (TSP, m^3) and specific extinction area (SEA, m^2/kg) were measured. All tests were performed in triplicate and in accordance with the ISO 5660-1:2002.

Thermal analysis: TGA investigation was carried out on particleboards by means of a Mettler-Toledo TG-SDTA 851 thermobalance equipped with a differential thermal analyzer, using alumina pans under nitrogen flow (35 mL/min). After a rapid heating from 25 to 100 °C at 20 °C/min, the

samples were kept in isothermal conditions for 30 min and then heated up to 700 °C at 10 °C/min. The weight of each sample was kept within 7 ± 1 mg.

Mechanical tests: Flexural tests were performed on specimens (length = 70 mm, thickness 5 mm and width = 10 mm) cut from the particleboards panels by means of a Instron model 4505 dynamometer, at a deformation speed of 1 mm min^{-1} with a span of 48 mm. Four specimens were used for each formulation.

Morphological analysis: The morphological characterization of particleboards fracture surfaces after flexural tests was performed by means of Scanning Electron Microscopy (SEM) analysis, using a FEI Quanta 200 FEG device. The samples were mounted onto aluminium stubs by means of carbon adhesive tape and coated with a 20 nm thick gold/palladium layer by means of a Emitech K575X modular high vacuum coating system.

5.2 Results and Discussion

5.2.1 Characterization of Lignosulfonates

Lignosulfonates are co-products of the sulphite pulping process. The latter is one of the most used pulping methods in paper mills, and it is aimed to the production of pulp, which is composed by almost pure cellulose fibres. In this process, lignin is removed from wood chips by means of sulphite salts. The more common salts used in the sulphite pulping process are either sulphites or bisulphites of sodium, calcium and ammonium [Eugenio et al., 2008].

The sulphite treatment involves the cleavage of ether linkages between the phenylpropanoid moieties of lignin and introduction of sulfonic acid groups on the aliphatic chains. The presence of these polar functionalities promotes their water solubility. Lignosulfonates show a broad molar mass range (around $5,000\text{--}60,000 \text{ g mol}^{-1}$) and consist of branched phenylpropanoid monomers [Lemes et al., 2010]. It is thought that lignosulfonates are characterized by a negatively charged compact spherical structure due to the presence of sulfonic and carboxylic acids, which, due to their high polarity, are positioned mainly on the surface of the phenylpropanoid aromatic core. The degree of sulfonation varies from 0.4 to 0.7 sulfonate groups per phenylpropane residue [Lemes et al., 2010].

The lignosulfonates (LS) used in this thesis were characterized through SEM and their morphology along with their chemical structure is illustrated in Figure 5.1.

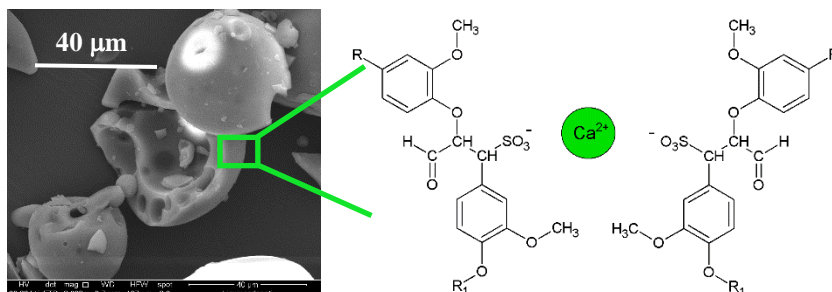


Figure 5.1: SEM micrographs and chemical structure of calcium lignosulfonates.

As shown in Figure 5.1, LS are characterized by spherical and hollow particles. The latter are characterized by a wide size distribution, with diameters from 17 to 90 μm .

In order to investigate in depth the chemical composition of LS, ^{13}C CP MAS-NMR analysis was performed. NMR spectra are reported in Figure 5.2 (black trace), while resonance assignments are listed in Table 5.2. LS spectrum shows signals ascribable to both main lignocellulosic macromolecular components, namely lignin and polysaccharides. The weak peak at 177 ppm can be attributed to carbonyl carbons located on the C_γ of lignin aliphatic chain [Feng-Bing et al., 2012]. This signal can also be due to the acetyl carbons of hemicelluloses. However, this assignment is not supported by the presence of any signal relative to methyl carbons in the up field region of the spectrum. The characteristic signals of lignin aromatic carbons are located between 110 and 160 ppm. In this spectral range, the resonance at 147 ppm can be attributed to etherified C4 of guaiacyl units (G) and to C3 and C5 of etherified syringyl (S) units. The peaks at 125 ppm and 115 ppm are also due to G units, in particular to unsubstituted C6 and C5 carbons. [Wikberg and Maunu, 2004; Savy and Piccolo, 2014]. In addition to these aromatic signals, lignin also exhibits a distinctive peak in the aliphatic portion of the spectrum, centred at 56 ppm, and attributed to carbons of methoxy functionalities [Sannigrahi et al., 2010]. The other resonances detected in the aliphatic range of the spectrum are mostly generated from the carbohydrate fraction of the material, in particular from hemicelluloses. The signal at 72 ppm could be attributed to C2, C3, C5 of hemicelluloses units contained in raw lignosulfonates [Duchesne et al., 2001]. For this resonance, a contribution from the C_α linked to sulfonic acid group of LS cannot be excluded

[Feng-Bing et al., 2012]. In this range, the NMR plot shows two further signals at 94 and 65 ppm, attributed to C4 and C5 of xylopyranosic ring in hemicelluloses [Duchesne et al., 2001]. These assignments are in agreement with the typical structure of hemicelluloses, which are characterized by a linear chain composed of β -D-xylopyranose units, that can be acetylated, and of arabinofuranose or xylofuranose branching [Wedig et al., 1987]

The ^{13}C CP MAS-NMR spectrum of the dialyzed sample (LD) (Figure 5.2, red trace) exhibits only the typical signals of lignin materials. Resonances relative to the sugar units of hemicellulose centred at 72 and 94 ppm, along with the peak at 177 ppm attributed to carbonyl groups, are almost absent.

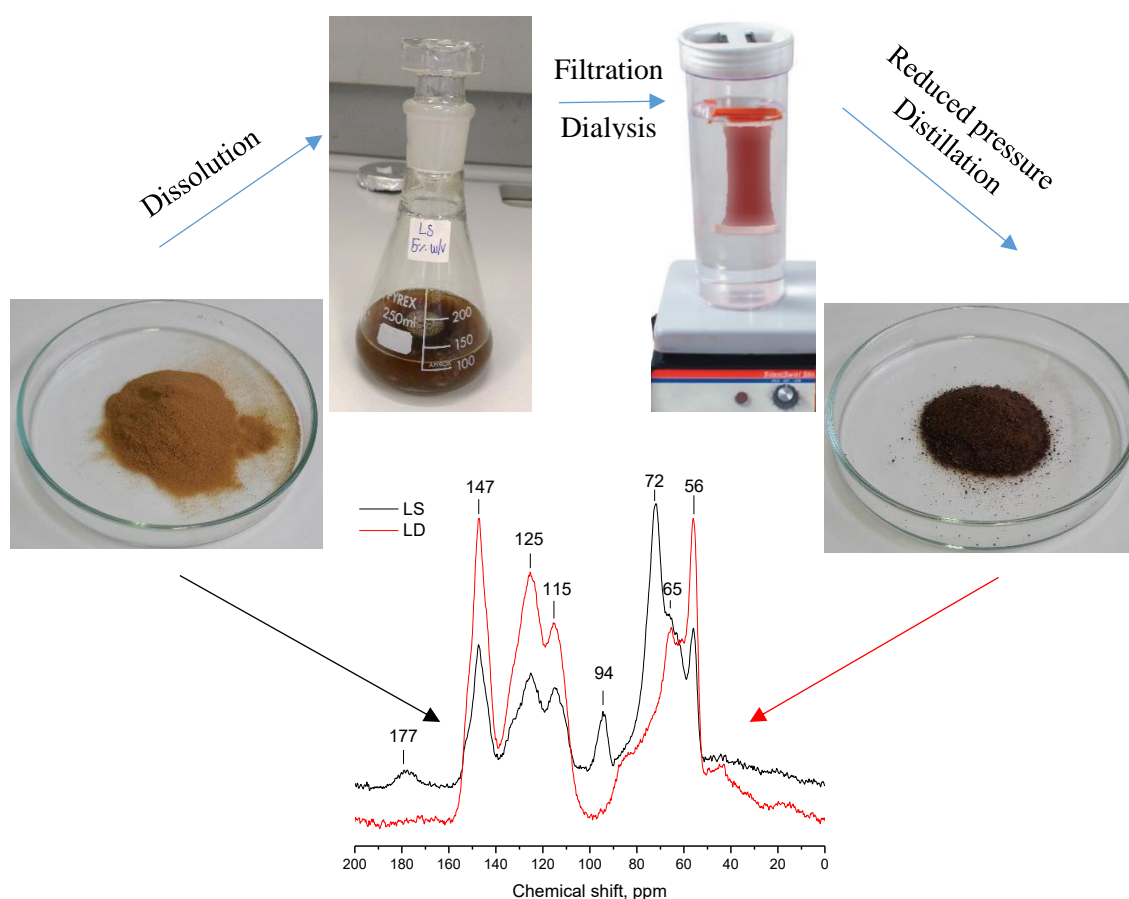
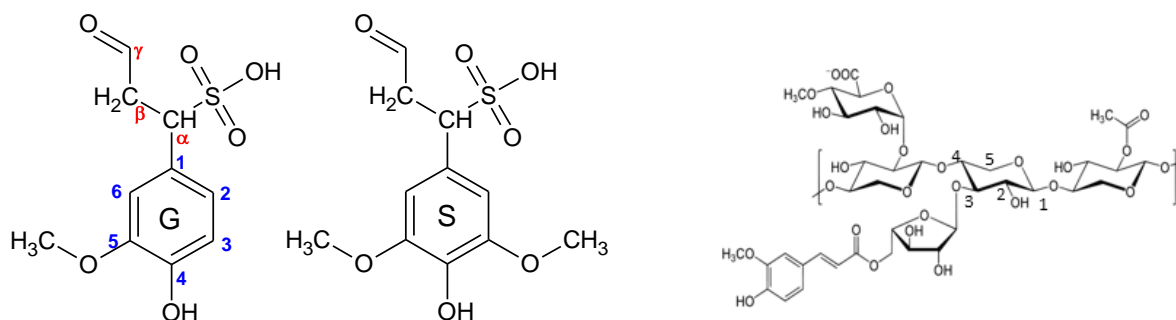


Figure 5.2: Dialysis treatment and ^{13}C CP MAS-NMR spectra of LS and LD.

Table 5.2: Signal assignment in ^{13}C CP MAS-NMR spectra of LS and LD.

δ (ppm)	Material	Assignment
177	LS	Carbonyl groups on lignin C γ or hemicelluloses
147	LS, LD	Etherified C4 G units; Not etherified C3, C5 G units
125	LS, LD	C6 G units
115	LS, LD	C5 G units
94	LS	C4 hemicelluloses
72	LS	C2, C3 hemicelluloses C α -SO $_3$ H
65	LS, LD	C5 hemicelluloses
56	LS, LD	Methoxy groups

S = Syringyl; *G* = Guaiacyl



Lignin Monomers

Hemicellulose-type Structure

The outcomes from ^{13}C MAS-NMR analysis are in agreement with the significant weight drop (around 50 wt.%) recorded after purification by dialysis, evidencing that this treatment removes most of the carbohydrate portion along with some lower molecular weight sulfonated lignin fragments.

As a matter of fact, the chemical composition of the dialysate was analysed through HPLC in order to assess the chemical composition of the carbohydrate fraction removed from LS by dialysis. Additionally, the same analysis was performed on the dialysate subjected to acid hydrolysis, to determine the relative amount of carbohydrates. The results of the chemical characterization of the dialysate before and after hydrolysis are reported in Table 5.3.

Table 5.3: Chemical composition of the dialysate. Concentrations are expressed in [mg/mL].

Sample	Arabinose	XMG	Glucose	Total
Dialysate before hydrolysis	0.0043	0.0977	0.0099	0.1119
Dialysate after hydrolysis	0.0057	0.0941	0.0107	0.1105

XMG= xylose/mannose/galactose

As it is shown in the table, most of the products present in the dialysate were cyclic monosaccharides, such as arabinose in the arabinofuranose or arabinopyranose forms, but especially a mixture of sugars indicated as XMG, that stands for xylose, mannose and galactose. As mentioned above, these sugars are typical of hemicelluloses. However, HPLC results suggested that the contaminating carbohydrates present in LS were predominantly in form of oligo/monosaccharides, and that the dialysis treatment allowed to efficiently remove them from the lignosulfonates, yielding an almost pure lignin.

The thermo-degradative behaviour of LS and LD was investigated through TGA. In Figure 5.3 the thermograms along with DTG graph are shown. The average thermal data are reported in Table 5.4.

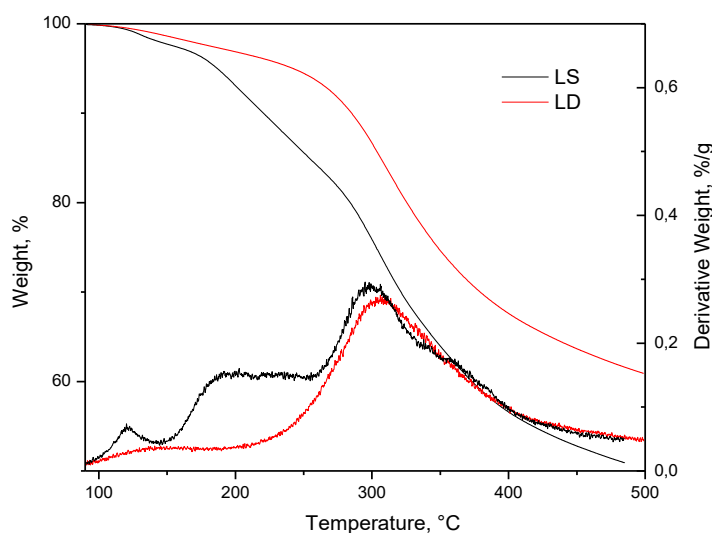


Figure 5.3: TGA and DTG curves of LS and LD under inert atmosphere.

Table 5.4: Average thermal data of LS and LD measured through TGA.

Sample	$T_{5\%}$ (°C)	T_{max1} (°C)	T_{max2} (°C)	T_{max3} (°C)	$Char_{500\text{ °C}}$ (%)
LS	186	133	200	300	51
LD	241	150		304	61

The thermogram relative to plain LS shows three weight loss steps. This feature can be appreciated in more detail in the first derivative curve reported in the same figure. From the analysis of the curve, three temperature ranges, corresponding to different thermo-degradative phenomena can be envisaged. In the DTG thermogram, these processes are characterized by broad peaks and can be separated into the following temperature zones: 1) 100–160 °C; 2) 160–250 °C and 3) 250–500 °C [Lemes et al., 2010]. The complexity of the plots is due to the heterogeneity of the material.

On the basis of literature evidences [Luo et al., 2012; Lemes et al., 2010], the first weight drop can be attributed to loss of adsorbed water, the second to the evolution of CO, CO₂, SO₂ and water due to dehydration reactions from hemicellulose and aliphatic lignin chains, and the third to CO and CO₂ losses from the decomposition of the aromatic skeleton of lignin.

At higher temperatures, crosslinking between degraded products occurs, giving rise to the formation of a carbonaceous char. TGA outcomes are in agreement with ¹³C MAS-NMR and HPLC analyses, that demonstrate that LS contain, in addition to the lignin fraction, also a relevant amount of hemicelluloses components. As observed in literature, generally, the main mass loss stage for hemicellulose occurs between 190 and 360 °C [Ramachandran and Feldman, 1971]. In this range the decomposition of hemicellulose 4-O-methylglucuronic acid and acetyl groups in side units along with the cracking of the main xylan chain occurs [Shen and Bridgwater et al., 2010].

The thermogram relative to LD appears characterized by a $T_{5\%}$, remarkably higher than LS and by two weight loss steps, with temperatures of maximum weight loss at 150 and 304 °C. The lack of the thermal decomposition stage between 160 and 250 °C can be explained by the effective reduction of oligo/monosaccharides amount in the sample after the dialysis process. Thus, this outcome was a further confirmation of the effectiveness of dialysis treatment that allowed to purify LS and isolate an almost pure lignin. TGA analysis shows that, through purification, the thermo-

degradative stability of the dialysed lignosulfonate is improved in a remarkable way. This finding is noteworthy for applications where good thermal performances are required.

5.2.2 Fire Reaction Evaluation of Wood Flour Particleboards Through Cone Calorimeter Tests

Cone calorimeter is the most significant bench-scale equipment in the characterization of material fire performance. Its name derives from the shape of the truncated conical heater that is used to irradiate the test specimen as it is shown in Figure 5.4.



Figure 5.4: Cone calorimeter equipment.

The technique is based on the empirical principle that heat released by burning materials is directly proportional to the oxygen consumed during the combustion process [Babrauskas, 1984 (a)]. The rate of heat release is determined by measuring combustion product gas flow and oxygen depletion, while the mass loss is recorded simultaneously. The main advantage of the cone calorimeter is the simulation of different fire scenarios by the variation of the thermal attack levels (flux 0-100 kW/m²) by means of a temperature-controlled radiant heater.

The selection of the thermal attack to be used in the test is a critical point in the research on fire retardancy [Babrauskas, 1995 (b)]. In this thesis the thermal attack was selected as a medium value of the typical that are used for these kind of studies, according to ISO/TS 5660-3:2012.

The most useful method used to increase flame resistance of products consists in the incorporation of flame retardants, i.e. additives able to interfere with combustion [Werther and Winter, 2015]. Most of flame retardants are inorganic, halogenated and phosphorous compounds, such as hexabromo cyclododecane or ammonium polyphosphate. Since the use of fire retardants leads to a cost increase of final products, the amount of fire retardant used should be as low as possible [Arao et al., 2014].

As regards the lignocellulosic biowastes, they have found an interesting and promising role in plastic industry due to their satisfactory processing characteristics, biodegradability, low-cost and flame retardancy properties [Arao et al., 2014; Xing et al., 2013].

In this section the results obtained from cone calorimeter tests on wood flour (WF) based particleboards are discussed.

WF is a finely pulverized, relatively inexpensive wood, whose consistency is similar to sand; it is readily available and it represents an environmentally friendly alternative to petroleum-based or inorganic fillers. SEM micrographs of WF are illustrated in Figure 5.5.

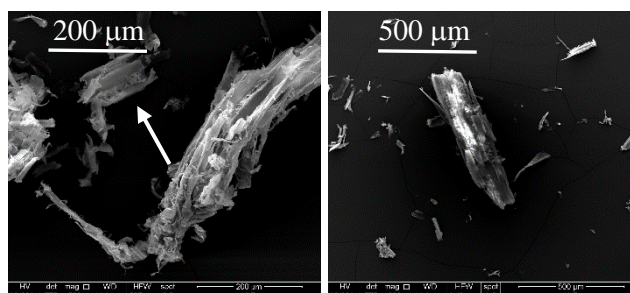


Figure 5.5: SEM micrographs of wood flour.

The appearance of WF is complex and heterogeneous. Elongated structures with irregular shapes and dimensions are visible. Moreover, it is evident the presence of pits, indicated by the arrow in Figure 5.5. Pits are small cavities representing the most conspicuous wood anatomical structures in plants, which play a role in the hydraulic conductivity of tracheary elements [Baas, 1986].

The effect of plain (LS) and dialysed liginosulfonates (LD) on fire performance of wood-flour particleboards was tested in detail. The liginosulfonates were used as additives into the compounds, and their potential synergistic effect with the commercial fire retardant ammonium polyphosphate (APP) was investigated.

The appearance of some of the particleboards prior to the cone calorimeter tests and after the combustion process is shown in Figure 5.6.

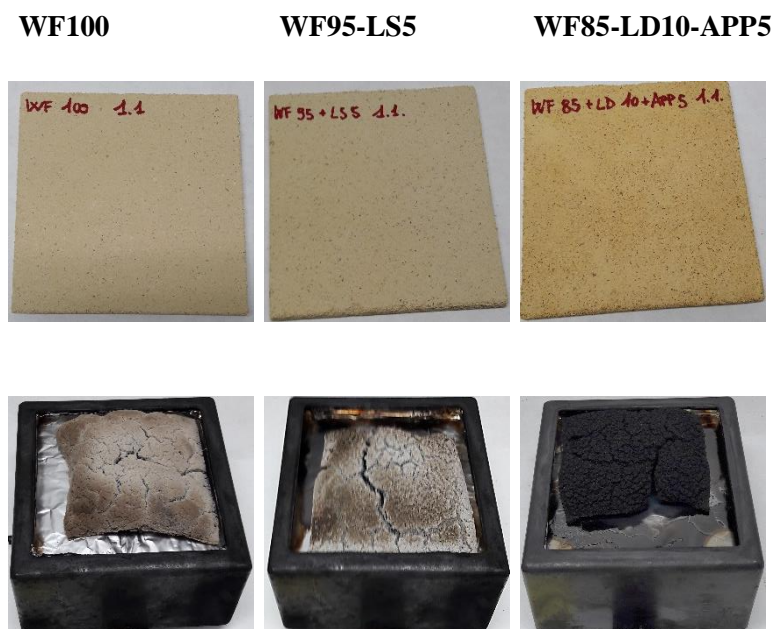


Figure 5.6: Appearance of some of the prepared particleboards prior to the cone calorimeter test (up row) and after combustion (bottom row).

Prior to be tested the samples appeared as compact and sufficiently homogeneous panels. The reference WF100 and the lignosulfonate-modified particleboards appear brittle and a bit dusty, while the samples containing APP were more compact and stiff with a more brilliant colour than the others. All the lignosulfonates-modified particleboards after the combustion tests showed a carbonized aspect with several cracks and no morphological differences with the reference emerged. Conversely, the fire-retarded samples filled with APP appeared black, solid and characterized by a thick and compact aspect.

The main average cone calorimeter test results are reported in Table 5.5.

Table 5.5: Average results obtained from cone calorimeter characterization of particleboards.

Sample	t_{ig} (s)	HRR_{max} (kW/m ²)	THR (MJ/m ²)	MARHE (kW/m ²)	Mass Loss (%)	TSP (m ²)	SEA (m ² /kg)
WF100	45.7±5.0	310.81±11.9	53.20±2.7	136.46±2.8	91.4±1.5	1.76±0.1	44.67±3.9
WF95LS5	45.7±6.6	259.12±20.4	49.52±0.9	125.83±3.5	94.0±0.7	1.46±0.1	35.44±11.2
WF85LS15	47.0±1.7	280.24±35.5	52.06±0.7	128.24±0.8	89.1±2.7	1.50±0.2	45.05±1.8
WF95APP5	42.7±5.7	228.02±7.1	41.54±2.9	98.24±2.0	88.7±2.1	0.53±0.0	14.93±5.5
WF85APP15	<i>n.d.</i>	53.60±14.6	21.79±2.2	28.23±3.0	77.8±0.9	4.00±0.4	158.15±14.5
WF85LS10APP5	44.0±19.5	202.96±22.9	43.00±1.9	96.64±2.6	86.7±0.3	0.53±0.0	7.80±4.6
WF95LD5	46.3±3.8	268.89±47.5	54.74±6.0	124.19±12.0	93.35±2.3	1.67±0.3	50.70±5.6
WF85LD15	49.0±6.1	230.49±20.4	50.85±2.6	115.57±1.8	87.35±2.1	1.30±0.1	34.36±10.9
WF85LD10APP5	41.3±3.8	187.58±11.0	39.96±1.1	92.70±1.0	83.64±2.2	0.46±0.1	4.63±4.8

n.d.: not detected

All the samples were characterized by a t_{ig} in the range 41-49 s, except for WF85-APP15 that did not present an ignition time due to the well-known effect of APP as fire suppressor [Shih-Hsuan and Wun-Ku, 1998]. As for the other samples, the effect of the additives on t_{ig} resulted negligible. Conversely, the other fire parameters related to heat release, particularly mass loss and smoke production, resulted to be influenced by the nature and content of the additive even in a remarkable way. In the following paragraphs all the parameters, obtained after cone calorimeter tests, related to heat and smoke release (HRR, THR, TSP, ARHE, SEA) and mass loss are analysed in depth.

In the subsequent graphs the cone data on lignosulfonates-modified particleboards are reported. In Figure 5.7a-c, heat rate release (HRR), average rate of heat release (ARHE) and total heat release (THR) vs combustion time are shown.

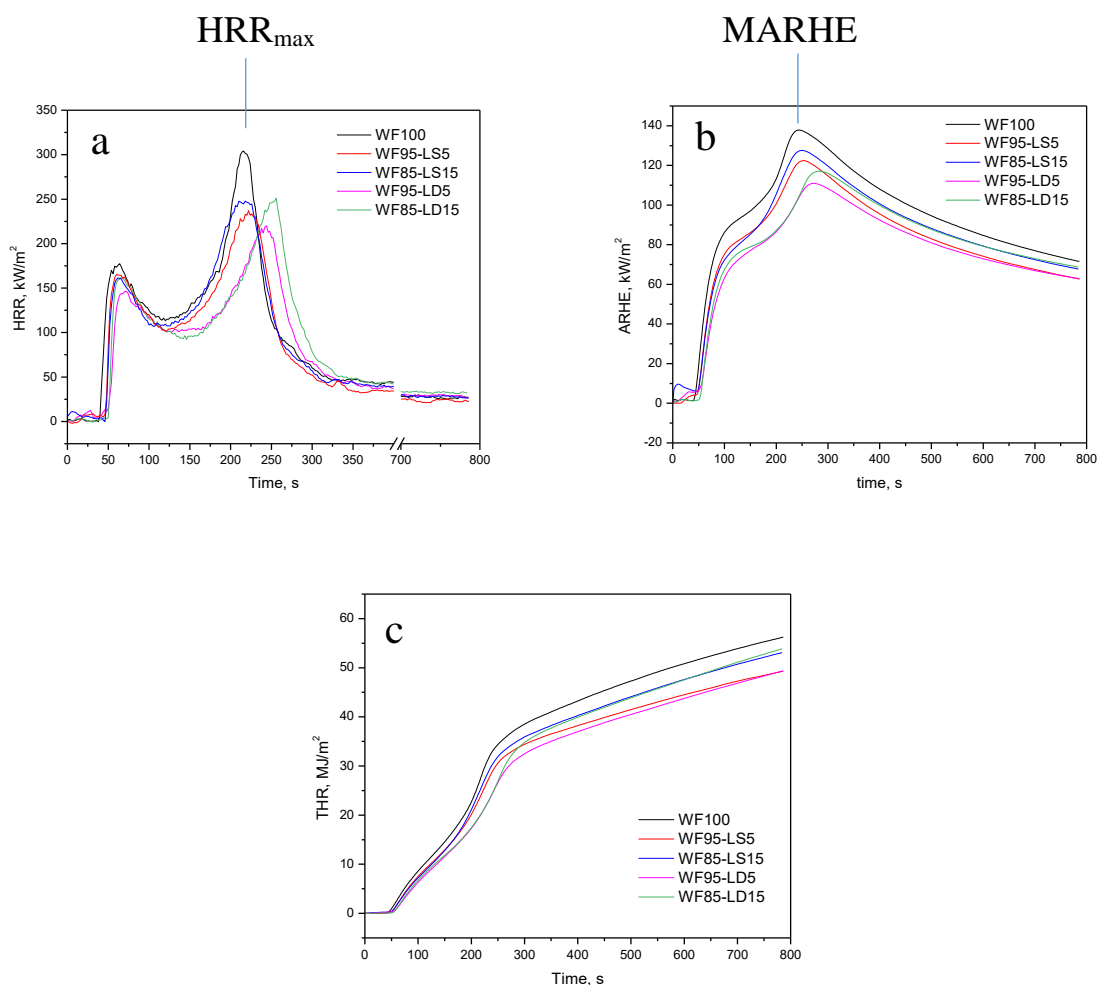


Figure 5.7: a) HRR, b) ARHE and c) THR curves vs combustion time of lignosulfonates-modified particleboards.

HRR is one of the most important parameters for characterizing material fire performance because it expresses the intensity of a fire [Arao et al., 2014]. Typically, wood burns according to the HRR curves shown in Figure 5.7a. After an initial heating induction period, a significant amount of pyrolysis volatile gases evolves as to allow ignition. Ignition is promoted by an external spark igniter. This is the start of combustion where the reaction between oxygen and volatile gases occurs. The heat generated by these exothermic reactions, along with the externally applied heat, keeps pyrolysis of wood going, thus releasing more volatiles for ongoing sustenance of the flaming combustion process. This corresponds to the first peak in the HRR curve. After the initial release of volatiles, an insulating char layer forms, which makes heat transfer more difficult, thus slowing the pyrolysis process. If the wood is sufficiently thick, the HRR reaches a more or less steady state.

The second peak in the HRR curve results from the char layer breaking down and contracting, thus producing small cracks on the surface. These cracks facilitate the escape of volatiles that combust and result in the observed increase of HRR. After the volatiles exhaust, flaming combustion ends, heat release ceases and a solid char residue is generated [Marney et al., 2008].

Compared with the reference WF100, the samples modified with lignosulfonates were characterized by a slight delay of t_{ig} and a decrease in HRR_{max} (Figure 5.7a).

This phenomenon was also observed in the ARHE graph (Figure 5.7b) where the curves maximum corresponds to the MARHE parameter [Shartel and Hull, 2007], reported in Table 5.4. The same behaviour is recorded in THR curves (Figure 5.6c), which represents the area below the HRR plot; it was observed that all the lignosulfonate-modified particleboards showed lower THR values with respect to the reference WF100.

In Figure 5.8 the mass trend in % vs combustion time is reported.

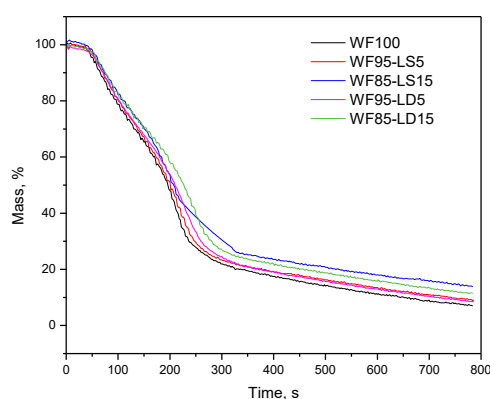


Figure 5.8: Mass (%) vs combustion time of lignosulfonate-modified particleboards.

As regards the char recovered after 800 s of combustion, all the lignosulfonate-modified particleboards were characterized by a higher char yield with respect to the reference WF100.

An increased production of char is a positive outcome, because in this way the material flame performance improves [Abu Bakar et al., 2010]. The most common flame retardants, in fact, are generally char producers. By creating a surface layer of char, fire retardants slow down escape of gases.

Smoke performance of flame retardant materials is a significant parameter in fire safety fields.

The total smoke production (TSP) vs combustion time is reported in Figure 5.9.

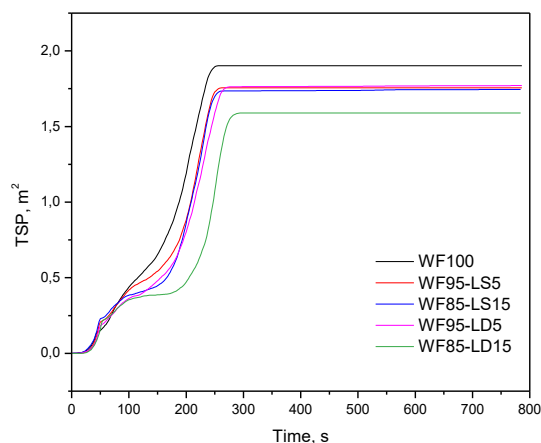


Figure 5.9: TSP vs combustion time of lignosulfonates-modified particleboards.

As it is evident from the graph, the particleboards containing the two types of lignosulfonates released less smoke during combustion than the reference. This outcome is positive in terms of fire retardancy. Most traditional fire retardants, indeed, help retarding fire evolution by decreasing smoke production.

As regards the measurement of smoke yield, the specific extinction area, referred as SEA, can be recorded from both large and small scale tests. SEA is the value determined multiplying the extinction coefficient by the ratio of volume flow rate to sample mass loss rate and is expressed in m^2/kg . The extinction coefficient of smokes is measured through the attenuation of a laser intensity by obscuring particles. The attenuation of light is proportional to the projected area (m^2) of particles blocking the beam and is normalized by the mass (kg) of burned sample. The higher the SEA, the more is the amount of smoke emitted per kg of sample [Ostman, 1995]. By comparing SEA of neat WF100 with that of lignosulfonates-modified particleboards, 5wt.% LS and 15wt.% LD caused a decrease in this parameter, but a definite trend can hardly be noticed [Table 5.5].

In order to assess the effective role of LS and LD in presence of a conventional flame retardant, the flame performances of particleboards containing ammonium polyphosphate (APP) and mixtures of lignosulfonates and APP were investigated through cone calorimeter. Therefore, a possible synergistic effect between LS or LD and APP was studied.

In the following graphs the cone calorimeter data on fire-retarded particleboards are shown.

In Figure 5.10a-c heat rate release (HRR), average rate of heat release (ARHE) and total heat release (THR) vs combustion time are reported.

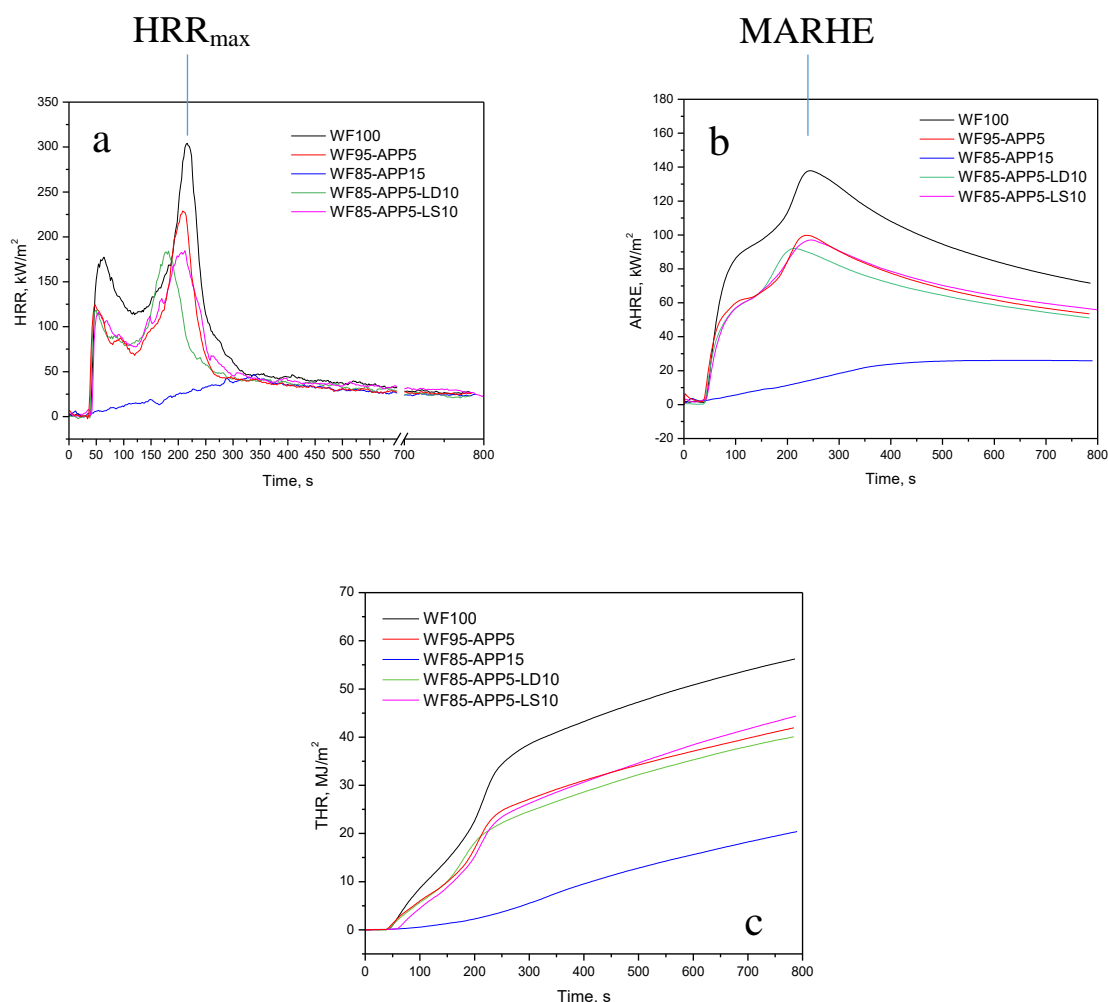


Figure 5.10: a) HRR, b) ARHE and c) THR curves vs time of fire-retarded particleboards.

From Figure 5.10a it was possible to observe that WF85-APP15 showed a remarkable reduction of HRR. As expected, this sample achieved the best results in terms of fire retardancy. Moreover, during the experiment, it was observed that the specimen expanded and did not present ignition. WF85-APP5-LS10 and WF85-APP5-LD10 samples also exhibited an improvement in fire performances. These samples, compared to WF100, but in particular to WF95-APP5 that contains the same amount of commercial fire-retardant, showed a slight decrease of HRR_{max}. This finding was a hint of a potential synergistic effect between liginosulfonate and ammonium polyphosphate.

The same results, even if less pronounced, were found in the ARHE and THR graphs (Figure 5.10b and 5.10c).

In Figure 5.11 the mass trend in % vs combustion time of fire-retarded particleboards is reported.

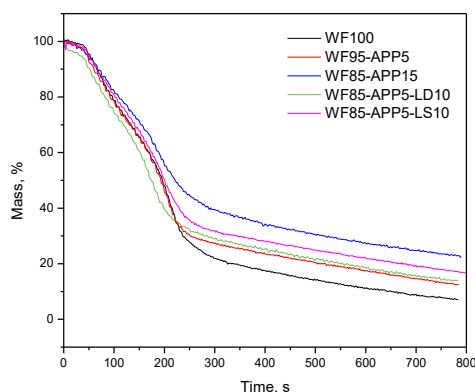


Figure 5.11: Mass (%) vs time of fire-retarded particleboards.

The char production for the samples filled with APP was higher with respect to the others. APP, indeed, when is exposed to a combustion, starts to decompose into poly(phosphoric acid) and ammonia. Poly(phosphoric acid) reacts with hydroxyl groups to form an unstable phosphate ester. When the phosphate ester starts to dehydrate, a carbon foam forms, thus creating the so-called charring effect. The carbon foam acts as an insulating layer thus preventing the development of the combustion and decomposition of the material [Pin et al., 2005]. This charring mechanism appears to be more effective when lignosulfonates are introduced in the formulation along with APP. Similarly to the HRR data reported before, WF85-APP5-LS10 and WF85-APP5-LD10 exhibited higher char yields with respect to WF95-APP5.

In Figure 5.12 total smoke production (TSP) vs combustion time of fire-retarded particleboards is reported.

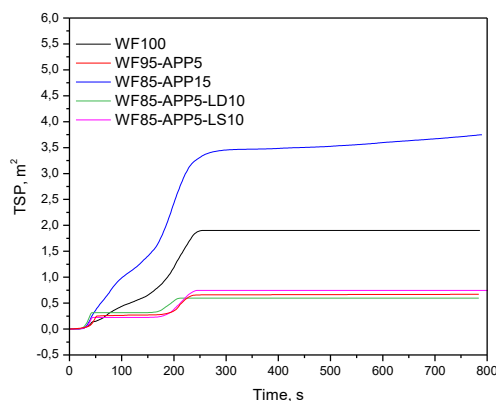


Figure 5.12: TSP vs time of fire-retarded particleboards.

WF85-APP15 was characterized by the largest smoke production. The higher smoke production than the other samples is attributed to dehydrogenation reactions that lead to the formation of soot and emission of aromatic volatiles during the fire.

On the other hand, TSP values significantly decreased with the addition of APP at 5wt.% as well as with both plain and dialysed lignosulfonates. For example, at the end of the experiments, the TSP values of WF100 and WF85-APP5-LD10 were 1.9 and 0.6 m², respectively. The reason for the total smoke decrease is related to the smoke suppression properties of the commercial fire retardant and lignin aromatic component. Some studies have shown that the smoke suppression effect can be due to the soot particles oxidation to CO and CO₂ or to the formation of a compact carbon layer, likely char, able to prevent combustible gases diffusion [Chen et al., 2014]. It can be supposed that the large amount of OH groups present in lignosulfonates caused the major release of hydration water and CO₂ favouring the smoke suppression effect [White and Dietenberger, 2001]. However, investigations on fire-retarded particleboards charged with both lignosulfonates and APP at a concentration below 5wt.% are in progress in order to assess the effective influence of the aromatic lignin component on flame retardancy properties of wood flour particleboards.

As regards the SEA value, the samples containing mixtures of LS/LD and APP showed a more pronounced decrease of the smoke yield than the reference WF100 and the lignosulfonates-modified particleboards. In particular, when LD was used, a 3-fold decrease in SEA was noticed compared to WF95-APP5 (Table 5.5), suggesting the occurrence of a cumulative effect in using both APP and lignosulfonates. Indeed, LD is the sample with the largest amount of lignin, that

along with APP is a good char former. APP is able to form char through the cleavage of lignin C–O bonds and catalytic crosslinking of polyphosphoric acid produced over its decomposition [Li et al., 2002]. The char inhibits the gases diffusion and this causes a smaller attenuation of the laser intensity.

In conclusion, plain and dialysed lignosulfonates were selected as functional additives because of their lignin content and low-cost. LS and LD showed a fire-retardant activity, by slightly reducing HRR, ARHE, THR and TSP parameters and increasing char formation. The lignin aromatic component act as a char former, which represents a well-known feature in fire retardants additives. Char, indeed, reduces the combustion rate of wood hindering oxygen diffusion to the burning zone [Abu Bakar et al., 2010].

This fire behaviour improvement was magnified if, along with lignosulfonates, a relatively small amount of APP is added to the particleboard. These results suggest a potential synergistic effect between lignosulfonates and APP. The interaction is probably based on the reaction of C-OH groups of lignin and polyphosphoric acid moieties produced from APP during combustion, with the production of phosphoric esters that improve the char-forming effect [Costes et al., 2016].

Even if the fire performance of the particleboards containing LS or LD and APP were lower with respect to the particleboards containing solely APP, the recorded results are encouraging. The use of cheap harmless lignosulfonates, indeed, could allow the reduction of commercial fire retardants to be used to prepare particleboards for building purposes. In addition, their use to replace partially commercial flame retardants is desirable because it might reduce the production costs of the final objects and emission of toxic gases in case of combustion [Abu Bakar et al., 2010].

5.2.3 Thermal Stability

The thermo-degradative behavior of the prepared particleboards was assessed through TGA measurements performed in nitrogen. The TGA curves, along with the DTG graphs, are reported in Figure 5.13a-b. Thermal parameters as 5 wt.% loss temperature ($T_{5\%}$), maximum decomposition rate temperatures (T_{max}), and char yield at 700 °C ($Char_{700\text{ °C}}$) are summarized in Table 5.6.

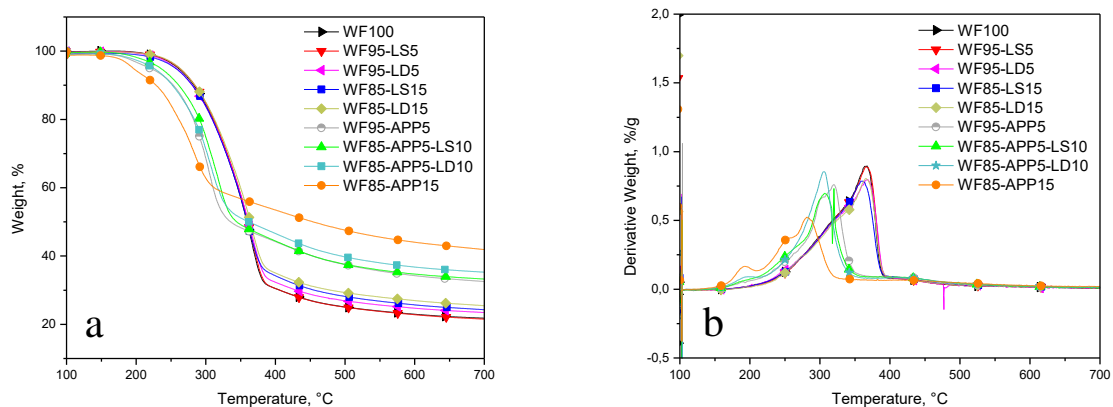


Figure 5.13: a) TGA and b) DTG curves of particleboards.

Table 5.6: Average thermal data of particleboards measured through TGA.

Sample	$T_{5\%}$ (°C)	T_{max1} (°C)	T_{max2} (°C)	T_{max3} (°C)	Char ₇₀₀ °C (%)
WF100	253	-	-	366	22
WF95-LS5	262	-	-	366	21
WF85-LS15	257	-	-	360	23
WF95-APP5	219	-	-	319	32
WF85-APP15	195	190	252	282	42
WF85-LS10-APP5	235	-	-	308	33
WF95-LD5	257	-	-	368	23
WF85-LD15	263	-	-	367	25
WF85-LD10-APP5	225	195	-	305	35

The thermogravimetric parameters reported in Table 5.6 show that the introduction of liginosulfonates into the particleboards did not affect the thermal stability of the material, as $T_{5\%}$ and T_{max} kept almost constant. The same observation can be made regarding the char yield. As regard the thermal stability, the presence of liginosulfonates slightly influenced the onset thermal degradation of the compounds, whereas the addition of APP resulted in a noticeable decrease of $T_{5\%}$ and T_{max} with respect to the WF100 sample. In addition, three different weight loss steps were

identified in the WF85-APP15 composite. This feature is better appreciated in the DTG graph and can be partially attributed to the APP thermal decomposition. Moreover, both the APP filled samples, differently from the lignosulfonates-modified compounds, showed high char yields.

The particleboards prepared using mixtures of lignosulfonates and APP, namely WF85-APP5-LS10 and WF85-APP5-LD10, showed lower $T_{5\%}$ values than the unmodified particleboard but higher than the APP-based specimens. T_{max} values were always lower with respect to the reference material (WF100), but higher than the WF85-APP15 sample.

Finally, the char yields of the specimens containing mixtures of lignosulfonates and APP showed lower values with respect to the compounds doped with only APP but, compared to the unmodified composite, their char forming capability resulted greatly increased. Overall, these results show that the addition of lignosulfonates as additives can improve thermal stability of particleboards filled with only APP. These findings, as reported in the previous section, are probably related to interaction of the lignosulfonates with polyphosphoric acid derived from APP decomposition that limits thermal degradation and improves char production.

5.2.4 Mechanical Properties and Morphological Analysis

Mechanical properties of the prepared particleboards were evaluated by flexural tests. Fig. 5.14 shows the testing apparatus and the appearance of the specimens before and after the measurement. Table 5.7 lists modulus (E_f) and strength (σ_f) values measured through flexural tests and Figure 5.15 the SEM micrographs of the fracture surfaces after failure during mechanical tests.



Figure 5.14: Flexural test.

Table 5.7: Main flexural properties of particleboards.

	E_f (MPa)	σ_f (MPa)
WF 100	146±35.4	0.50±0.21
WF95-LS5	133±31.3	0.63±0.10
WF85-LS15	242±10.6	0.89±0.30
WF95-LD5	115±38.7	0.36±0.07
WF85-LD15	36±8.7	0.13±0.02
WF85-APP5-LS10	130±25.7	0.31±0.07
WF85-APP5-LD10	121±28.5	0.49±0.09
WF95-APP5	233±72.2	0.88±0.16
WF85-APP15	413±101.1	1.59±0.47

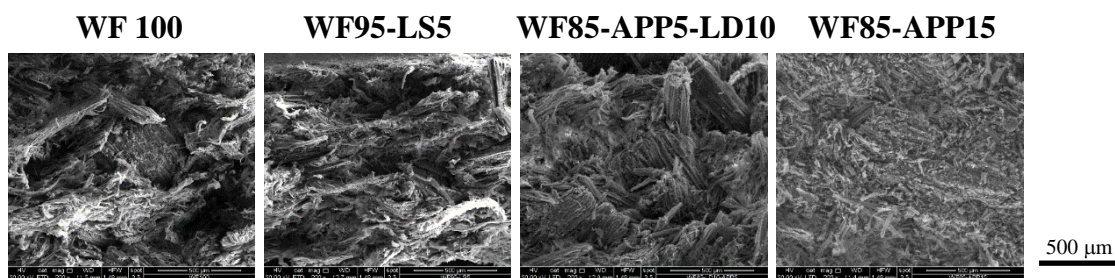


Figure 5.15: SEM micrographs of the fracture surface of specimens after failure in the flexural tests.

Compared to the plain particleboard, the samples containing LS show modulus values (E) almost equal or slightly higher. The LD-based specimen, conversely, exhibits a decrease of the flexural parameters. This outcome can be related to the poor compatibility between the purified lignosulfonates and the urea-formaldehyde resin used as binder in the particleboards. In the samples containing LS such detrimental effect is partly compensated by the presence of a polysaccharidic fraction that, probably affects, the compatibility between resin and additive, improving the modulus of the final particleboard.

The APP-filled samples, compared with the plain and lignosulfonates-modified particleboard, exhibit an improvement of the mechanical performances. This effect can be related to an improved binding capability of the urea-formaldehyde resin related to the APP addition. The good interaction between these two materials has already been reported in literature, as amino resins are often used for APP encapsulation in fire retardant formulations [Wang et al., 2014]. The improved binding effect is confirmed by the SEM analysis of the fracture surfaces obtained after the flexural tests

and reported in Figure 5.15. The LS and LD-modified samples show irregular surfaces where large particles and fibres aggregates are visible. Conversely, the micrograph relative to WF85-APP15 was the only characterized by a more regular, compact, relatively smooth aspect with well distributed wood flour particles.

The particleboards containing both lignosulfonates and APP show no variation, or only a slight decrease, of the flexural parameters. These results are probably related to the detrimental action of the lignin component that results to be partly compensated by the presence of the APP additive.

5.3 Conclusions

In this chapter a lignosulfonate (LS), obtained as a biowaste from a paper mill plant, was purified through dialysis, characterized through SEM, ¹³CP MAS-NMR and TGA. Its fire retardancy properties were tested in wood flour-based particleboards.

The spectroscopic characterization, performed on both LS and the purified sample (LD) showed that dialysis was an effective method for the removal of hemicellulosic oligo/monosaccharides. The TGA investigation, carried out on both samples, evidenced that the removal of such contaminants produced a noticeable improvement of the thermo-degradative properties of the material.

Both LD and LS were introduced as additives in wood flour-based particleboards using a urea formaldehyde resin as binder. Their fire performances were compared to those of particleboards containing a commercial flame retardant, ammonium polyphosphate. The presence of LS and LD involved the improvement of some fire retardancy features, but the most interesting results were recorded when, along with lignosulfonates, a moderate amount of ammonium polyphosphate was added. The charring forming capability of LS and LD and the occurrence of a synergistic effect between the lignosulfonate and APP, during combustion process, positively affected the main fire features.

From a thermal point of view, the use of ammonium polyphosphate was responsible for a noticeable decrease of onset weight loss temperature even if the char yield increased in a remarkable way. Samples prepared with both the lignosulfonates and the commercial additive showed a moderate decrease of thermal stability and a relatively high char yield.

The presence of dialysed lignosulfonates worsened particleboards mechanical properties, whereas the samples filled with the largest amount of ammonium polyphosphate resulted the most

performant due to the better compatibility between the phases, confirmed by SEM fracture surfaces observations.

References

- M. B. Abu Bakar, Z. A. Mohd Ishak, R. Mat Taib, H. D. Rozman, S. Mohamad Jani, *J. Appl. Polym. Sci.* 116 (2010) 2714-2722.
- Y. Arao, S. Nakamura, Y. Tomita, K. Takakuwa, et al., *Polym. Degrad. Stab.* 100 (2014) 79-85.
- P. Baas, *Int. Association Wood Anatom. Bulletin, New Series* 7 (1986) 82-86.
- V. Babrauskas (a), *Fire Mater.* 8 (1984) 81-95.
- V. Babrauskas (b), *Fire Mater.* 19 (1995) 243-252.
- X. Chen, Y. Jiang, C. Jiao, *J. Haz. Mat.* 266 (2014) 114-121.
- L. Costes, F. Laoutid, M. Aguedo, A. Richel, S. Brohez, C. Delvosalle, P. Dubois, *Europ. Polym. J.* 84 (2016) 652-667.
- I. Duchesne, E. Hult, U. Molin, G. Daniel, T. Iversen, H. Lennholm, *Cellulose* 8 (2001) 103-111.
- M. E. Eugenio, J. M. Carbajo, M. C. Terrón, A. E. González, J. C. Villar, *Bioresource Technol.* 99 (2008) 4929-4934.
- L. Feng-Bing, S. Yan-Lei, H. Chong-Pin, L. Ying-Xia, C. Biao-Hua, *Ind. Eng. Chem. Res.* 52 (2013) 1267-1274.
- A. P. Lemes, M. A. Soto-Oviedo, W. R. Waldman, L. H. Innocentini-Mei, N. Durán, *J. Polym. Environ.* 18 (2010) 250-259.
- B. Li, X. Zhang, R. Su, *Polym. Degrad. Stab.* 75 (2002) 35-44.
- Z. Luo, S. Wang, X. Guo, *J. Analytical Appl. Pyrolysis* 95 (2012) 112-117.
- D. C. O. Marney, L. J. Russell, R. Mann, *Fire Mater.* 32 (2008) 357-370.
- B. A. L. Ostman, *Smoke and Soot*, (V. Babrauskas, S. J. Grayson, eds) Heat Release in Fires, Chapman & Hall, London, (1995) p. 238.
- L. V. P. Pin, Z. Wang, K. Hu, W. Fan, *Polym. Degrad. Stab.* 90 (2005) 523-534.
- V. S. Ramachandran and R. F. Feldman, *Cement Technol.* 2 (1971) 121-129.

- P. Sannigrahi, D. H. Kim, S. Jung, A. Ragauskas, *Energy Environ. Sci.* 4 (2011) 1306-1310
- D. Savy and A. Piccolo, *Biomass and Bioenergy* 62 (2014) 58-67.
- B. Schartel and T. R. Hull, *Fire Mater.* 31 (2007) 327–354.
- D. K. Shen, S. Gu, A. V. Bridgwater, *Carbohydrate Polym.* 82 (2010) 39–45.
- C. Shih-Hsuan and W. Wun-Ku, *Polymer* 39 (1998) 1951-1955.
- W. Wang, W. Zhang, S. Zhang, J. Li, *Constr. Building Mat.* 65 (2014) 151-158.
- C. L. Wedig, E. H. Jaster, K. J. Moore, *J. Agric. Food Chem.* 35 (1987) 214-218.
- N. Werther and S. Winter, *Proceedings of the 1st European Workshop Fire Safety of Green Buildings* (2015).
- R. H. White and M. A. Dietenberger, *Wood Products: Thermal Degradation and Fire Encyclopedia of Materials: Science and Technology* (ISBN: 0-08-0431526) 9712-9716.
- H. Wikberg and S. L. Maunu, *Carbohydrate Polym.* 58 (2004) 461-466.
- W. Xing, H. Yuan, P. Zhang, H. Yang, L. Song, Y. Hu, *J. Polym. Research* 234 (2013) 1-12.

Conclusions and Future Perspectives

The aim of this thesis was the exploitation of lignocellulosic biomasses as fillers or additives in polymer-based bio-composites. The work was divided into two activities, which differed in the origin of the lignocellulosic feedstock and the approach adopted for its use and valorisation. In the first activity, a lignocellulosic biowaste from biorefinery (LC) was used as filler in a microbial polyester matrix. The second activity regarded lignosulfonates (LS), by-products from pulping process, which were exploited as fire retardant additives in wood flour-based composites.

In the first activity, a chemical, physical and morphological characterization of LC was first tackled. Then, the biomass was submitted to chemical fractionation in order to isolate its main components: acid-insoluble lignin (IL) and holocellulose (HC). LC was also solvent-extracted in order to recover two solid residues, TE and W. LC and its derivatives were used as fillers in poly(3-hydroxybutyrate) (PHB) with the aim to obtain bio-composites with reduced costs and enhanced properties.

Bio-composites characterisation evidenced that the addition of LC as filler in PHB improved the viscoelastic properties of the polymer melt, increased the crystallization rate, reduced the thermal stability and improved the resistance towards soil microbial attack. In order to better correlate these effects to the activity of specific constituents of LC, PHB bio-composites filled with LC derivatives were also prepared. It was found that the enhanced rheological behavior and increased crystallization rate were mainly due to the lignin and polysaccharide components present in LC. The decrease of bio-composites thermal stability was, on the other hand, provoked by pro-degrading agents present in the parent LC and in the derivative TE, which were leached by water extraction. Alongside these interesting findings, all the bio-composites, independently from the nature of the filler, displayed an overall worsening of mechanical properties due to a poor interfacial adhesion between the phases. On the whole, however, the results of this study are quite interesting as LC and some of its derivatives can compete with commercial processing aids and nucleating agents, with the advantage of being largely available low cost by-products. The use of LC and its derivatives, indeed, can limit some of major PHB shortcomings as high costs, narrow processing window and physical aging.

In the second activity, LS from pulp and paper industry were characterized and purified through dialysis in order to remove most of carbohydrate contaminants. Pristine LS and its purified

derivative (LD) were used, alone or combined with ammonium polyphosphate (APP), as fire retardant additives for the production of wood flour particleboards. With respect to the unmodified particleboard, the samples containing mixtures of lignosulfonates and APP were characterized by improved fire performances, in terms of heat released and char formed. This finding was related to an increased charring barrier effect, probably due to a synergistic interaction between lignosulfonates and APP. This outcome emerged also from the study of the particleboards thermo-degradative properties, where a lower thermal stability and a noticeable increase of char yield were recorded. However, as with LC-filled bio-composites, the presence of the pristine and dialysed lignosulfonates additives worsened particleboards mechanical properties. Despite this shortcoming, the activity evidenced that lignosulfonates can partially substitute commercial fire retardants. Their partial replacement can provide benefits for the environment, human health and economics. As a matter of fact, the majority of flame retardants are halogenated products, so they provoke the release of toxic gases in the course of a fire. Moreover, their price, as in the case of ammonium polyphosphate is relatively high, around 5.8 €/Kg. The replacement with lignosulfonates, which are also endowed with fire retardancy properties and are largely available at the much lower price of 0.23 €/Kg, is absolutely desirable.

Overall, despite the interesting obtained results, optimization of the bio-composites preparation conditions is necessary, to justify the scale up of the processes along with the development of a life cycle assessment, aimed to evaluate the economic and environmental impact of processes and products.

In the case of the LC-filled composites, future goals should be addressed to improve the interfacial adhesion between filler and matrix, by performing chemical modifications on the lignocellulosic biomass or by using coupling agents. In this way, the compatibility between filler and matrix may be enhanced, thus resulting in improved bio-composite mechanical properties. As regards LS, the future activity will deal with the preparation of novel formulations of particleboards, in which commercial fire retardants are replaced with lignosulfonates, yet keeping unchanged the flame performance properties.

Coming to the end, this research activity was inspired by the existing literature on wood plastic composites (WPCs). Over time, the WPCs production have been scaled-up to industrial applications, and final objects are currently available in several fields as sustainable construction and automotive. On the basis of this evidence, we trust that the exploitation and valorisation of

lignocellulosic biowastes is pursuable, but a most detailed investigation is necessary in order to further address the academic and industrial interest towards this area.

List of Figures

Introduction

Figure 1: From plant to cell wall: schematic representation of inner structure.

Figure 2: Cellulose structure.

Figure 3: Typical xylan-type hemicellulose structure [Wang, 2008].

Figure 4: Lignin monolignols.

Figure 5: Potential chemical modifications carried out on lignocellulosic biomass and polymer.

Figure 6: Natural fibre-polymer composites and mechanism of interaction with coupling agent as reported by Ashori, 2008. Reprinted with permission from Elsevier.

Figure 7: Applications of lignocellulosic-based composites and films.

Chapter 1

Figure 1.1: a) SEM micrographs of AL and b) LC.

Figure 1.2: a) FTIR-ATR and b) ^{13}C CP MAS-NMR spectra of AL and LC.

Figure 1.3: TGA/DTG thermograms of AL and LC.

Chapter 2

Figure 2.1: a) Time evolution of G' and b) M_w during *Dynamic Time Sweep* test for PHB and PHB-based blends; $T = 190\text{ }^\circ\text{C}$.

Figure 2.2: a) Optical image and b) FTIR-ATR spectrum of PHB/5AL after 5600 s during *Dynamic Time Sweep* test at $190\text{ }^\circ\text{C}$.

Figure 2.3: *Dynamic Frequency Sweep* curves of PHB and PHB/30LC; $T = 190\text{ }^\circ\text{C}$, G' (full symbols), G'' (empty symbols).

Figure 2.4: Isothermal TGA at $190\text{ }^\circ\text{C}$ for PHB and PHB-based blends.

Figure 2.5: a) DSC cooling and b) second heating scans of PHB and PHB-based blends.

Figure 2.6: a) Fracture surfaces of PHB/5LC and b) PHB/30LC. Arrows indicate agglomerated particles.

Figure 2.7: a) FTIR-ATR spectrum of PHB, PHB/15LC and PHB/30LC and b) curve-fitting of the C=O peak of PHB.

Figure 2.8: SEM micrographs of a) PHB and b) PHB/30LC after 0, 10, 20 and 80 days of soil burial.

Chapter 3

Figure 3.1: SEM micrographs of a) LC, b) TE, c) W, d) IL and e) HC.

Figure 3.2: a) FTIR-ATR spectra of LC-derivatives and b) difference spectra between the derivatives and the feedstock. The curves were vertically translated.

Figure 3.3: ^{13}C CP MAS-NMR spectra of LC and its derivatives. The curves were vertically translated.

Figure 3.4: a) TGA and b) DTG curves under inert atmosphere of LC and its derivatives.

Chapter 4

Figure 4.1: a) Normalized M_w vs time for heat-treated PHB and PHB-based blends; $T=190\text{ }^\circ\text{C}$.

b) Normalized G' vs time from *Dynamic Time Sweep* measurements.

Figure 4.2: DFS plots of the viscoelastic properties vs the angular frequency for PHB and PHB-based blends: G' , G'' (a), η^* (b). Full and empty symbols refer to G' and G'' , respectively.

Figure 4.3: TGA curves under inert atmosphere of neat PHB and PHB-based blends.

Figure 4.4: DSC a) cooling and b) second heating scans of PHB and PHB-based blends. All the curves were vertically translated.

Figure 4.5: SEM micrographs of HC before and after sonication treatment.

Figure 4.6: DSC a) cooling and b) second heating DSC scans of PHB and PHB/sonicated HC bio-composites. All the second heating curves were vertically translated.

Figure 4.7: (top row) Optical photomicrographs of PHB spherulites grown at 127 °C; (bottom row) SEM images of fracture surfaces of crystallized samples.

Figure 4.8: a) Spherulite radial growth rate (G_{MO}) and b) Half-time of crystallization ($\tau_{1/2}$) as a function of crystallization temperature.

Figure 4.9: SEM micrographs of fracture surfaces of a) PHB; b) PHB/LC; c) PHB/IL and d) PHB/HC.

Chapter 5

Figure 5.1: SEM micrographs and chemical structure of calcium lignosulfonates.

Figure 5.2: Dialysis treatment and ^{13}C CP MAS-NMR spectra of LS and LD.

Figure 5.3: TGA and DTG curves of LS and LD under inert atmosphere.

Figure 5.4: Cone calorimeter equipment.

Figure 5.5: SEM micrographs of wood flour.

Figure 5.6: Appearance of some of the prepared particleboards prior to the cone calorimeter test (up row) and after combustion (bottom row).

Figure 5.7: a) HRR, b) ARHE and c) THR curves vs combustion time of lignosulfonates-modified particleboards.

Figure 5.8: Mass (%) vs combustion time of lignosulfonate-modified particleboards.

Figure 5.9: TSP vs combustion time of lignosulfonates-modified particleboards.

Figure 5.10: a) HRR, b) ARHE and c) THR curves vs time of fire-retarded particleboards.

Figure 5.11: Mass (%) vs time of fire-retarded particleboards.

Figure 5.12: TSP vs time of fire-retarded particleboards.

Figure 5.13: a) TGA and b) DTG curves of particleboards.

Figure 5.14: Flexural test.

Figure 5.15: SEM micrographs of the fracture surface of specimens after failure in the flexural tests.

List of Tables

Chapter 1

Table 1.1: Thermal parameters obtained from TGA and DSC for LC and AL.

Chapter 2

Table 2.1: Thermal parameters of PHB and PHB-based blends measured through DSC.

Table 2.2: Average values of the PHB/LC bio-composites mechanical properties measured from tensile, flexural and impact tests.

Table 2.3: Properties of the soil.

Chapter 3

Table 3.1: Signal assignment in ^{13}C CP MAS-NMR spectra of LC, IL, HC, W and TE.

Table 3.2: Average thermal data of LC and its derivatives measured through TGA.

Chapter 4

Table 4.1: Storage modulus, weight-average molecular weight and polydispersity index of PHB and PHB-based blends after 2700 s at 190 °C.

Table 4.2: Average thermal data of neat PHB and PHB-based blends measured through TGA.

Table 4.3: Main thermal parameters of PHB and PHB-based blends measured through DSC.

Table 4.4: Main thermal parameters of PHB and PHB/sonicated HC bio-composites measured through DSC.

Table 4.5: Avrami index, n determined at the indicated crystallization temperatures.

Table 4.6: Average mechanical data of neat PHB and PHB-based bio-composites measured through tensile tests.

Chapter 5

Table 5.1: Particleboard codes and compositions (wt.%).

Table 5.2: Signal assignment in ^{13}C CP MAS-NMR spectra of LS and LD.

Table 5.3: Chemical composition of the dialysate. Concentrations are expressed in [mg/mL].

Table 5.4: Average thermal data of LS and LD measured through TGA.

Table 5.5: Average results obtained from cone calorimeter characterization of particleboards.

Table 5.6: Average thermal data of particleboards measured through TGA.

Table 5.7: Main flexural properties of particleboards.

Ringraziamenti

Questa tesi di Dottorato è il frutto della caparbia e del sacrificio della sottoscritta. Il percorso che ha portato ad oggi è stato complesso e non esente da momenti di grande scoraggiamento. Tuttavia, la collaborazione e l'impegno di molti hanno permesso di giungere al termine di questo cammino. La tesi racchiude dati ottenuti grazie alla collaborazione di diversi Istituti di Ricerca. Desidero, pertanto, ringraziare chi, con diversi ruoli, ha contribuito al raggiungimento di tale traguardo.

Ringrazio il mio Tutor universitario, Professor Alessandro Piccolo, e il suo gruppo di ricercatori, in particolar modo il Dottor Davide Savy e la Dottoressa Susanna Nuzzo, per aver reso possibile questa collaborazione di ricerca e per il tempo che mi hanno dedicato.

Un ringraziamento doveroso e profondamente sentito va al gruppo di ricerca dell'Istituto per i Polimeri, Compositi e Biomateriali di Pozzuoli con il quale lavoro da quattro anni. In particolar modo ringrazio il mio Tutor aziendale, Dott. Gennaro Scarinzi, con il quale abbiamo portato avanti l'attività sperimentale. Lo ringrazio per l'estremo impegno profuso ai fini di questa tesi e alla incredibile dedizione che lo ha spesso trattenuto in Istituto fino a tarda sera. Quindi, ringrazio il Dott. Mario Malinconico per avermi aiutata a trovare soluzioni alternative quando ho avuto bisogno e ad accompagnarmi in questo cammino dandomi la possibilità e la forza per continuare. Inoltre, voglio ringraziare il Dott. Pierfrancesco Cerruti, che per me rappresenta da sempre una guida e una luce quando mi perdo in sentieri bui. Grazie alla sua grande conoscenza, molti suggerimenti si sono convertiti in risultati interessanti che sono qui discussi. Ringrazio la Dott.ssa Barbara Immirzi, con la quale sono state svolte le misure di Cromatografia a Permeazione di Gel e che, da un punto di vista umano, mi ha sempre trattato come una figlia, supportandomi e sopportandomi in molte occasioni. Grazie alla Dott.ssa Emilia Di Pace, il cui interesse per il mio lavoro ha permesso che io potessi intraprendere una collaborazione con lei. Ringrazio il Dott. Roberto Russo e le mie care amiche, Marianna e Francesca, che hanno ascoltato i miei sfoghi e che sono stati compagni di risate e battute anche nei momenti in cui avrei voluto abbandonare tutto.

Ringrazio il Professor Franco Cotana e i Dottori Mattia Gelosia, David Ingles e Gianluca Cavalaglio del Centro di Ricerca sulle Biomasse dell'Università degli Studi di Perugia con i quali ho intrapreso una viva e stimolante collaborazione, che ero sicura avrebbe portato ai frutti ottenuti.

Gli ultimi mesi di Dottorato sono stati trascorsi in Tecnalia Research & Innovation, Centro di Ricerca e Sviluppo Tecnologico, in Azpeitia nei Paesi Baschi. L'esperienza che ho vissuto è stata resa possibile grazie alla disponibilità del Dott. Javier Garcia Jaca che ringrazio. I miei ringraziamenti sono rivolti al mio Tutor, Dott. Aitor Barrio Ulanga che è sempre stato disponibile e che mi ha indirizzato ad escogitare piani alternativi quando la sorte non era dalla nostra parte. Inoltre, voglio dire grazie al Dott. Alvaro Tejado Etayo, con il quale ho collaborato su un nuovo progetto di ricerca. Parlare con lui, anche se per breve tempo, mi ha permesso di crescere e di ritrovare la passione per il lavoro. Grazie a tutto il gruppo della Divisione "Costruzione Sostenibile" e ai ragazzi che mi hanno accompagnato al lavoro tutte le mattine tra un colpo di sonno e una battuta. "Francesca os echa mucho de menos y os quiere decir gracias a todos". L'ospitalità e la gentilezza di Idoia, David, Nabila, Carol, Max e Gorka hanno fatto sì che potessi sfruttare a pieno questa esperienza e che potessi godere di momenti indimenticabili.

Giungendo alla fine desidero ringraziare Graziano per avermi aiutato con la lingua inglese, e la mia meravigliosa amica Ida e i suoi genitori per il supporto che ogni giorno sono in grado di darmi, e per il bene che mi trasmettono.

Infine, ringrazio con amore i quattro componenti della mia famiglia che rappresentano il mio punto di riferimento. Sono le radici di un albero che è spesso esposto a tempeste e che è in grado di sostenersi solo per merito loro. Grazie di tutto, ma soprattutto di trasmettermi speranza per il futuro.

Acknowledgements

This Doctoral thesis is the result of personal determination and sacrifice. The path which led me to this day was difficult and not free from moments of demoralization. However, cooperation and dedication of many have made possible for me to reach this moment. The thesis includes data obtained from the cooperation between several Research Centres. Therefore, I wish to thank who has contributed, with different roles, to the achievement of this aim.

I thank Professor Alessandro Piccolo along with his researchers group, in particular Dr. Davide Savy and Dr. Susanna Nuzzo for the time they dedicated to me.

I want to address heartfelt thanks to the research group of the Institute for Polymers, Composites and Biomaterials of Pozzuoli, with whom I have worked for four years. In particular, I thank my Tutor, Dr. Gennaro Scarinzi, with whom I have carried out the experimental activity. I thank him for the huge dedication he put in this thesis, which has often made him stay at the Institute until late in the evening. Then, I thank Dr. Mario Malinconico for having helped me discover new solutions when I needed them and who followed me in this path, giving me the opportunity to go on. Moreover, I want to thank Dr. Pierfrancesco Cerruti, who has always been my mentor and light anytime I lose myself in dark paths. A great amount of data are here discussed thanks to his suggestions. I thank Dr. Barbara Immirzi, with whom I carried out the Gel Permeation Chromatographic measurements. Humanely, she has often treated me as a daughter, supporting and bearing me. Thanks to Dr. Emilia Di Pace, whose interest for my work allowed me to start a cooperation with her. Thanks to Dr. Roberto Russo and my dear friends, Marianna and Francesca, who have patiently listened to my surges of anger and with whom I shared good laughs anytime I would have liked to abandon everything.

Also, I thank Professor Franco Cotana and Drs. Mattia Gelosia, David Ingles and Gianluca Cavalaglio of Biomass Research Centre from University of Perugia with whom I have started a fruitful cooperation, concluded with the expected results.

I spent last months of Ph.D. in Tecnalia Research & Innovation, Azpeitia (Basque Country). The experience was made possible by the availability of Dr. Javier Garcia Jaca, whom I thank. Moreover, I want to thank my Tutor, Dr. Aitor Barrio Ulanga, who was very available and who directed me towards new plans when we did not have good luck. Moreover, I want to thank Dr.

Alvaro Tejado Etayo, with whom I cooperated about a new project. Talking with him, even if for a few times, has helped me to find again my passion for the work. Thanks also go to the groups of “Sustainable Construction Division” and all the guys who have kindly carried me to work every morning. “Francesca os echa mucho de menos y os quiere decir gracias a todos”. Hospitality and kindness of Idoia, David, Nabila, Carol, Max and Gorka have helped me to enjoy this experience and unforgiveable moments.

Coming to the end, I wish to thank my English helper, Graziano, and my wonderful friend Ida and her parents for the help they provide me every day.

Finally, I thank my family with my whole heart. They represent the roots of a tree, that often is exposed to storms and that, thanks only to them, is able to sustain itself. Thanks for everything, but above all for instilling me hope for the future.